ISBN: 978-90-365-3005-7

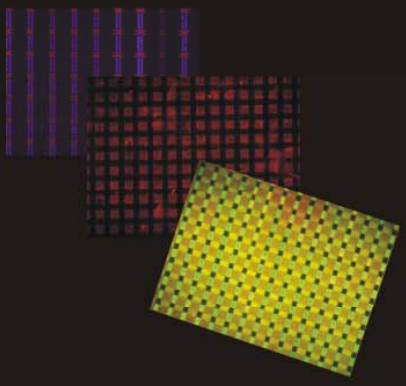

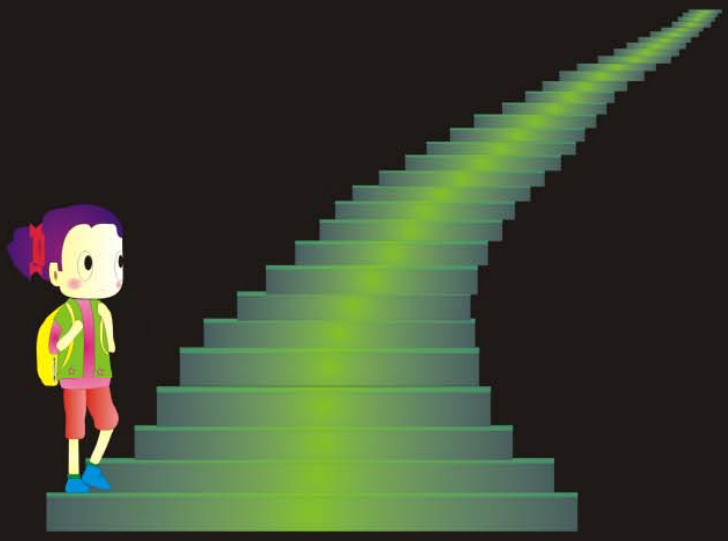

Lateral Interactions at Functional Monolayers Shu Han Hsu 2010

Lateral Interactions at Functional Monolayers

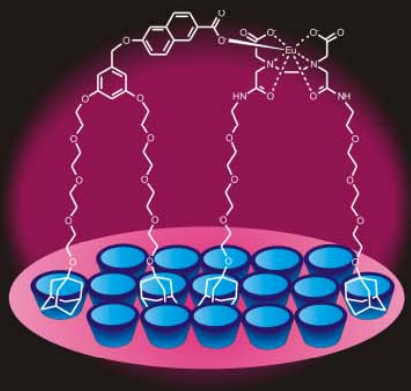

Shu Han Hsu

LATERAL INTERACTIONS

AT

FUNCTIONAL MONOLAYERS

The research has been supported by NanoNed, a national nanotechnology program coordinated by the Dutch Ministry of the Economic Affairs (Project No. TMM. 6976).

Publisher: Wöhrmann Print Services, Zutphen, The Netherlands

ISBN: 978-90-365-3005-7

LATERAL INTERACTIONS

AT

FUNCTIONAL MONOLAYERS

PROEFSCHRIFT

Ter verkrijging van
de graad van doctor aan de Universiteit Twente,
op gezag van de rector magnificus,
prof. dr. H. Brinksma,
volgens besluit van het College voor Promoties
in het openbaar te verdedigen
op donderdag 20 mei 2010 om 16.45 uur

door

Shu Han Hsu

geboren op 3 oktober 1982
te Hsinchu, Taiwan

Dit proefschrift is goedgekeurd door:

Promotoren:	prof. dr. ir. D. N. Reinhoudt
	prof. dr. ir. J. Huskens
Assistent-promotor:	dr. A. H. Velders

To my grandma, grandpa, parents and all my family

Table of Contents

Chapter 1

General Introduction

Nanotechnology is a multidisciplinary field of science and technology dealing with the fabrication, investigation, and manipulation of matter on the nanoscale. At the nanoscale level, materials show new properties compared to the bulk as witnessed by various analytical techniques applied in the nanosciences.

Nanofabrication is the discipline of nanotechnology that deals with the development of general fabrication methods for the preparation of nanostructures, patterned substrates, and of assembly methods for the anchoring of structures to the patterned areas. Parrallel to "top-down" nanofabrication techniques, (nano)structures shaped from bulk materials can be built using the "bottom-up" strategy, which is largely governed by self-assembly.

Self-assembly offers the simple and rapid creation of new structures at various length scales.[1] Complex and functional structures can be created through the assembly of small building blocks, i.e. atoms, (bio)molecules, and particles. Deeper understanding is required about the interactions that govern the assembly of building blocks at the nanoscale. Thus, supramolecular chemistry,[2] which studies assembly processes of molecules by noncovalent forces, plays a unique role in bottom-up nanofabrication.

Increasing interest in organic synthesis on solid supports is built on the growing knowledge of interfacial chemistry. The ability to control the chemical and structural properties of surfaces is crucial for the advancement of catalysis,[3] electronics,[4] chemical sensing,[5] and many other applications.[6] The availability of numerous analytical techniques capable of detecting chemical changes in films that are just a few molecules thick, have made studies of interfacial reactions a viable and important area of modern science.

Control over functional groups at the surface of solid supports (e.g. silicon oxide or metals) allows tailoring of monolayers in a predictable manner, resulting in the formation of functional, more complex nanostructures on surfaces to meet the needs for specific

applications, such as molecular sensing. Various chemical interaction strategies, e.g. covalent bonding, electrostatic interactions, hydrogen bonding, metal-ligand, and host-guest interactions have been used to chemically organize the self-assembly of molecules. Furthermore, processes between assembled molecules leading to e.g. electron or energy transfer allow exploring the fundamentals of (single) molecular behavior.

A lack of knowledge on lateral interactions in supramolecular systems at interfaces exists, which inspired the present study. This thesis targets a fundamental understanding of molecular interactions on solid supports both in covalent and noncovalent systems, by employing patterning techniques such as microcontact printing. Moreover, the understanding of molecular interactions allows us to study self-assembling systems in a systematic manner.

Chapter 2 provides a literature review regarding recent studies on lateral molecular interactions at interfaces. Particular attention is paid to the lateral chemical interactions used to direct the assembly of molecules on surfaces and molecular communication through energy or electron transfer.

Chapter 3 describes the preparation of imidazolide monolayers, amine layers activated with *N*,*N*-carbonyldiimidazole (CDI), which is used as a versatile platform for surface patterning with amino-, carboxyl- and hydroxyl-containing compounds through reactive microcontact printing. Its surface reactivity is investigated by preparing the direct and reverse fluorescent patterns using microcontact printing.

In Chapter 4, a layer of coumarin dye molecules is immobilized on imidazolide monolayers. These can act as fluorescent reporters for probing reactive μCP. Herein, patterned surfaces are prepared based on imidazolide monolayers with orthogonal functional reactivity, combining reactive alkyne and functional cyclodextrin patterns on one substrate. This allows simultaneous or consecutive functionalization through covalent and noncovalent chemistry.

Chapter 5 introduces the multivalent binding of a supramolecular complex at a multivalent host surface by combining the orthogonal cyclodextrin host-guest and lanthanide-ligand coordination interaction motifs. This system is used to monitor the molecular coordination events by sensitized Eu^{3+} luminescence. Assembly of a mixture of a guest-functionalized antenna and an Eu^{3+}-complexed ligand molecule in a patterned fashion onto a receptor surface provides efficient localized sensitized emission. The correlation between

emission and surface composition is investigated as well as the complex stoichiometry at interfaces.

Chapter 6 continues the study described in Chapter 5: the same lanthanide complex system is used to study the dependence of complex formation at the surfaces on the solution ratio of antenna and Eu^{3+}-complexed ligand under kinetic and thermodynamic control. This control is exerted by addition of a competing host in solution. The kinetics of the exchange process on the cyclodextrin monolayer are studied *in situ*. The system allows qualitative and quantitative analysis of multivalent interactions. A heterotropic multivalency model at interfaces is presented to provide insight into the nonlinear amplification process.

Chapter 7 shows a preliminary experiment for the fabrication of submicrometer-scale molecular patterns of the antenna-lanthanide complex introduced in Chapters 5 and 6. Fabrication of nanoscale patterns is achieved from supramolecular microcontact printing an antenna, and consecutive filling of the non-patterned areas with the Eu^{3+}-EDTA complex. Fluorescence and AFM measurements are used to monitor this stepwise procedure.

In Chapter 8, patterned surfaces are introduced to develop microstructures of quantum dots via supramolecular interactions. Adamantyl-terminated dendrimers are immobilized on cyclodextrin monolayers via two different methods for subsequent immobilization of cyclodextrin-functionalized quantum dots. The molecular recognition functionality of quantum dots is probed by interaction with ferrocenyl-functionalized dendrimers as well as adamantyl-functionalized lissamine rhodamine dyes. These are introduced onto the quantum dots surface by cross patterning over quantum dot patterns. Such multicomponent structures allow investigation of their photophysical properties.

References

[1] G. M. Whitesides, B. Grzybowski, *Science* **2002**, *295*, 2418.
[2] D. N. Reinhoudt, M. Crego-Calama, *Science* **2002**, *295*, 2403.
[3] J. H. Clark, D. J. Macquarrie, *Chem. Soc. Rev.* **1996**, *25*, 303.
[4] C. A. Mirkin, M. A. Ratner, *Ann. Rev. Phys. Chem.* **1992**, *43*, 719.
[5] A. J. Ricco, R. M. Crooks, G. C. Osbourn, *Acc. Chem. Res.* **1998**, *31*, 289.
[6] A. Ulman, *Chem. Rev.* **1996**, *96*, 1533.

Chapter 2

Lateral Interactions in Self-assembled Monolayers

ABSTRACT. This chapter describes the recent literature regarding lateral molecular interactions in self-assembled monolayers. The first part focuses on systems on metal surfaces, discussing the covalent and noncovalent interactions of the terminal functionality or between the molecular chains of the layer. The second part highlights the intermolecular interactions of systems on oxide surfaces. Finally, a few examples regarding electron transfer and energy transfer across the layers will be reviewed.

2.1 Introduction

Molecular self-assembly has been defined as "the spontaneous association of molecules under equilibrium conditions into stable, structurally well-defined aggregates joined by non-covalent bonds."[1] Self-assembly provides a unique paradigm to obtain complex and functional molecular architectures in a spontaneous process from small building blocks.[2, 3] Processes ranging from the noncovalent association of organic molecules in solution to the growth of semiconductor quantum dots on solid substrates have been called self-assembly.[4, 5]

Self-assembled monolayers (SAMs) are defined as ordered molecular assemblies formed by the adsorption of an adsorbate on a solid surface. Developing a comprehensive understanding of the assembly of SAMs requires considerations of both kinetic and thermodynamic factors. The process leading to the formation of SAMs involves the interplay of the metal-organic/oxide-organic headgroup and the noncovalent lateral interactions among the internal organic groups of the molecular backbone. The major forces that can be exploited are ionic, hydrogen bonds, coordinative, van der Waals, and hydrophobic interactions. The organization of the organic layers results from maximizing the attractive lateral interactions within the geometric constraints imposed by the structure of the adlayer.[6]

The brief introduction of this chapter is written from a surface perspective, with the focus on the fundamental principles governing the growth of self-assembled monolayers. This provides an overview of different self-assembled systems, focused on systems on metal and oxide surfaces.

The following parts deal with the lateral molecular interaction, or reactions on surfaces, either covalent or noncovalent. The noncovalent interactions within the monolayers can be metal-ligand, ionic, dipolar, H-bonding, and $\pi-\pi$ stretching interactions. Finally, energy and electron transfer within the monolayer are reviewed.

2.2 Self-Assembly on surfaces

Molecular nanotechnology is important for many applications because control over the position of the molecules allows the fabrication of nanostructures with new functionalities. It is strightforward that the modular design of monolayers can be employed for a broad range of applications. Self-assembled monolayers provide a convenient way to produce surfaces with

specific chemical functionalities that allow one to tune precisely the physicalchemical properties of the surface. For example, in surface coatings, the monolayers can engineer the wetting properties or inhibit corrosion by appropriate endgroups or SAMs of mixed composition. The monolayers can be active elements in sensors as well as for the specific adsorption of biomolecules. In each case the understanding of the structure and the organization of the monolayers is a prerequisite for a successful use in practical applications.[7]

2.2.1 Self-assembled monolayers

Because of the absence of chemically reactive functional groups on most substrate surfaces, an activation process is needed to create reactive sites that can initiate further grafting processes. Molecules that can be assembled on a solid support consist of a head group, a backbone and a terminal (functional) group. The terminal functional group of a monolayer is critical in its interfacial properties, the hydrophobic/hydrophilic character, adhesive characteristics, and the ability to perform chemical reactions using the pendant functional groups. The molecular backbone may exhibit a tilt angle with respect to the surface normal. The alkyl chains may be bent or exhibit gauche defects by incorporation of different functional groups into the alkyl chains. Different backbones have different degrees of freedom to describe their conformational state. Variation of the interactions in each of these regions can dramatically alter film (or monolayer) properties. The geometrical arrangement and structure of the molecules in the surface-bound layer depend on the geometry of the substrate binding sites, the strength of the substrate-head group bonds, the relative sizes of the head groups compared to the remainder of the molecule, and the intermolecular forces.

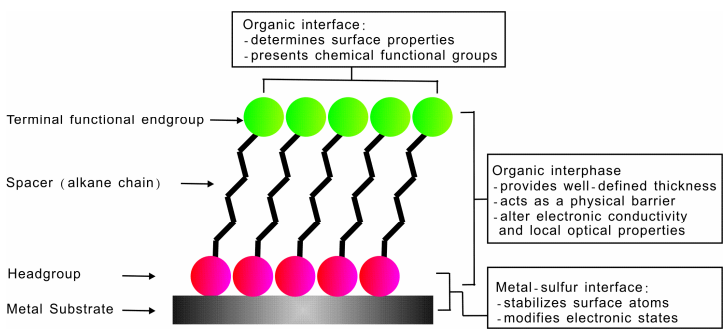

Figure 2.1 Sketch of molecules in monolayers on a metal substrate.

Substrates can have a planar surface, such as silicon oxide wafers, or curved surfaces, such as nanoparticles. Different molecules can be adsorbed onto metal or oxide surfaces to form the monolayers *via* physical interaction or chemical reaction between the adsorbates and the surface. The most common adsorbate/substrate combinations are sulfur-containing molecules on gold and alkylsilanes on oxide surfaces. Thiols on gold have become a model system for monolayer preparation,[8] because of the ease of preparation, the well-defined order and the relative inertness of the substrate. Unlike alkylsilane, which are irreversibly attached to the surface via covalent bond, the gold-thiol interaction is reversible which permits the alkanethiolates to interact with each other in order to achieve the formation of a highly compact monolayer. Alkylsilane monolayers on oxide surfaces such as SiO_2, Al/Al_2O_3, ITO, PtO, TiO_2 and ZrO_2, have some advantageous features, where the covalent nature of the assembly results in a better stability thus allowing extensive handling and further modification steps without deterioration of the monolayer.[6, 9]

2.2.2 Organization of the monolayers

The stability of the monolayers mainly results from the order of the assemblies. The nature of the chemical interaction between substrate and adsorbate, as well as the type and strength of the intermolecular interactions between the adsorbates are necessary to hold the assembly together. The balance between intermolecular and molecule-substrate interactions determines packing and orientation.

Molecules are organized in different ways on surfaces: (a) covalent attachment brought by directly linking groups of interest or via linking agents, (b) electrostatic interactions, driven by ion exchange, ion-pairing or donor-acceptor interactions, (c) hydrogen bonding, especially relvant in biological systems, (d) hydrophobic interactions leading to self-assembly of long chain fatty acid derivatives, (e) van der Waals forces involved in physisorption of molecules on solid surfaces, and (f) physical entrapment inside the pores or cavities of hosts such as cyclodextrins. Both covalent and noncovalent interactions between adsorbates and the surface can assist the formation of well ordered monolayers and allow the manipulation of molecular structures. These lateral interactions in the monolayers will be discussed in detail in this chapter.

2.3 Metal surfaces: covalent ractions

The covalent chemistries that have been widely used in organic chemistry for producing chemical bonds have also been applied to modify the physicalchemical properties of monolayers on surfaces. Metal substrates have been shown to work excellently for monolayer preparation where strong affinity between adsorbates and metal surfaces can create a dense monolayer. The proximity of adjacent chains in a dense monolayer makes it possible to perform chemical reactions between adjacent molecules. By using molecules with different terminal or internal functionalities, the resulting surface functionality and structural stability can be varied. As the functionalities of the end groups of thiols incorporated into SAMs become more complex, a better understanding of the intermolecular interactions and their effect on the stability and morphology of these systems is necessary. However, these interactions permit additional stabilizing forces that go beyond simple alkanethiols systems. Different examples of covalent reactions in a monolayer on metal surfaces will be discussed according to the interacting/ or reactive group present in the terminal functionality or in the molecular chains.

2.3.1 Covalent reactions between terminal groups on metal surfaces

Monolayers on metals containing terminal groups that are reactive or can be activated to form covalent bonds laterally are discussed first. An type of such reactions is the polymerization of surface-attached unsaturated compounds. This in-plane polymerization can enhance the stability of the monolayer.

Most examples of in-plane polymerization were performed through irradiation, for instance, the polymerization of (mercaptomethyl)styrene monolayers on silver was induced under laser irradiation. Ford *et al.* observed that all monomers were consumed during irradiation monitored in situ with surface enhanced Raman spectroscopy (Figure 2.2).[10] The vinyl stretching mode was used to follow the kinetics of the irradiation process, the signal of which disappeared during photoinitiated surface polymerization. The rate of reaction is expected to decrease as monomer is exhausted. The ability to produce a polymer of these vinyl

monolayers via laser irradiation suggests the possible application for surface patterning, where a laser writes a pattern onto a substrate forming a stable resist.

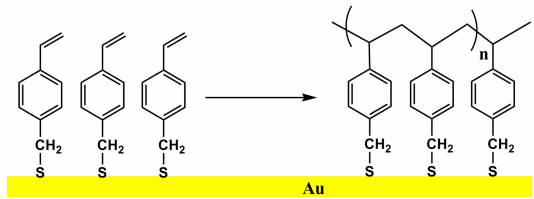

Figure 2.2 The polymerization of a SAM of (mercaptomethyl)styrene on a silver surface.[10]

Peanasky *et al.* showed what factors affect the reactivity and the resulting degree of polymerization of the monolayer. They presented spectroscopic and electrochemical data describing the structure of undec-10-ene-1-thiol monolayers on Au as a function of the γ irradiation time. The study has led to a preliminary understanding that the polymerization reaction is controlled by the distance over which the tethered monomer groups can move on the surface. In other words, the polymerization on metal surfaces is stress limited, affected by the environmental conditions.[11]

Lee *et al.* achieved in-plane enyne metathesis reactions in SAMs on gold terminating in vinyl and acetylenyl groups which can perform subsequent Diels−Alder reactions (Figure 2.3).[12] In solution, enyne metathesis processes catalyzed by ruthenium and molybdenum offer great potential for the formation of C-C bonds. By utilizing the proximity effect, the in-plane enyne metathesis of vinyl and acetylenyl groups at the surface is more favored leading to the formation of 1,3-dienes on the SAMs. In-plane enyne metathesis offers a versatile platform for the functionalization of surfaces under mild reaction conditions and with a high compatibility with functional groups.

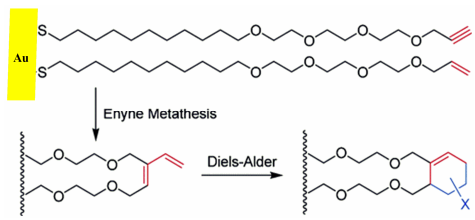

Figure 2.3 Schematic description of the in-plane enyne metathesis and Diels-Alder procedure (x = functional group).[12]

With the help of the proximity effect on the surface, many other reactions can be performed between adjacent chains in monolayers. Whitesides *et al.* demonstrated an interesting study of interchain anhydride formation in the monolayers of mercaptohexadecanoic acid (Figure 2.4).[13] They described a simple, two-step method that generates mixed SAMs of carboxylic acids and amides from a well-ordered SAM of carboxylic acids on gold. Reaction with trifluoroacetic anhydride in the presence of triethylamine leads first to the formation of a mixed anhydride intermediate, which then reacts with the adjacent carboxylate group to produce the interchain adduct. The resulting mixed SAMs contain a mixture of –COOH, and –CONHR functional groups as characterized by polarized infrared external reflectance spectroscopy, X-ray photoelectron spectroscopy, contact angle, and ellipsometry. They also demonstrated control of the wettability of the SAMs by reacting the interchain anhydride with alkylamines having different alkyl groups to manipulate interfacial physical properties.

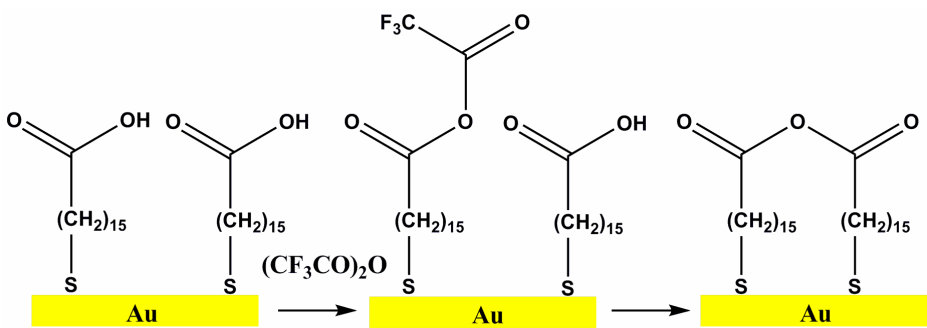

Figure 2.4 Formation of an interchain anhydride from the monolayer of mercaptohexadecanoic acid on the gold surface.[13]

Several other reactive intermediates can promote interfacial reactions to create different functionalization of the surfaces, such as the activation of a free carboxylic acid by *N*-hydroxysuccinimidyl (NHS) esters for subsequent reaction with an amine. Mark *et al.* fabricated multilayer ultrathin films composed of an amino-undecanethiol (AUT) SAM, an intermediate PAMAM dendrimer mediating layer, and a biomolecular sensing layer (BS layer) (Figure 2.5).[14] A SAM of AUT on Au was activated with bis- [sulfosuccinimidyl]suberate (BS), a noncleavable cross-linker with amino-reactive groups at both ends. The surfaces were

then exposed to a solution of G4-PAMAM dendrimers, and a second round of activation with BS was carried out in order to covalently immobilize amino-modified DNA probe to the dendrimer layer. This bioactive layer was characterized by AFM to image the G4-PAMAM dendrimer molecules immobilized on AUT-modified Au, which shows the correct mean diameter and height of the dendrimer macromolecules. Fluorescence, ellipsometry, XPS, and ATR-FTIR data provided evidence for the successful immobilization of DNA to the dendrimer-modified surfaces. The study described here demonstrates that it is feasible to synthesize stable, covalently linked dendrimer-based sensor matrixes that permit increased ligand immobilization capacity and can be used for the specific and sensitive detection of DNA-DNA interactions.

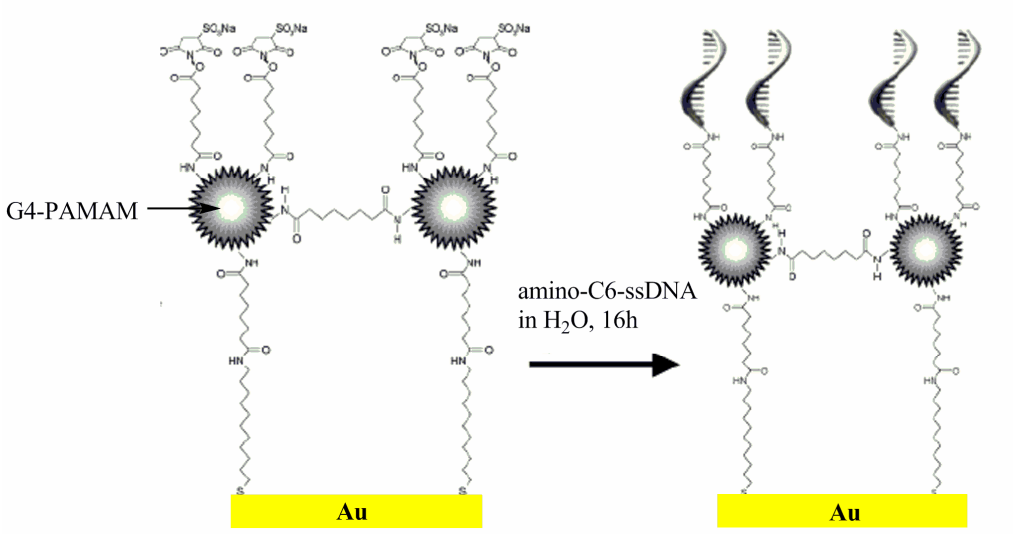

Figure 2.5 Schematic representation of the general procedure for immobilizing DNA on gold surfaces using a interconnecting monolayer of amino-terminated PAMAM dendrimer molecules as an intermediate coupling layer (Molecules not drawn to scale).[14]

Besides irradiation, interchain chemical bonds can also be formed by electrochemical polymerization of appropriate adsorbates. McCarley *et al.* observed the first electrochemical polymerization of a monolayer using a *N*-pyrroylalkanethiol on Au.[15, 16] Voltammetric waves showed that the pyrrole groups of the monolayer were converted to a conducting polymer or oligomer film on the surface. This polymer layer demonstrated enhanced stability during

competitive adsorption experiments with electroactive ferrocenyl alkanethiols, indicating that the electrochemically oxidized *N*-pyrroylalkanethiol monolayers are not readily displaced. Thus, they concluded that monolayers of *N*-pyrroylalkanethiol on Au undergo electrochemical polymerization to yield a stable poly(*N*-alkylpyrrole) film without desorption of the thiol moiety from the Au surface.

Fox *et al.* prepared monolayers of ω-anthracene-modified alkanethiols on gold, which undergo photodimerization at 350 nm irradiation (Figure 2.6a).[17] Strong surface fluorescence in this film indicated that the terminal anthracene groups are close-packed and this promotes π-π stacking and intermolecular charge transfer interactions. The photodimerization is reversible by irradiation the monolayer at 254 nm, but the photodecomposition results in a partial loss of anthracene confirmed by cyclic voltammetry. Similarly Li *et al.* showed the electron-induced cross-linking reaction of a 4′-nitro-1,1′-biphenyl-4-thiol monolayers on Au (Figure 2.6b).[18] Such intermolecular cross-linking accompanies the reduction of the nitro groups of the 4′-nitro-1,1′-biphenyl-4-thiol monolayers to amino groups, while the underlying aromatic biphenyl layer is dehydrogenated and cross-linked.

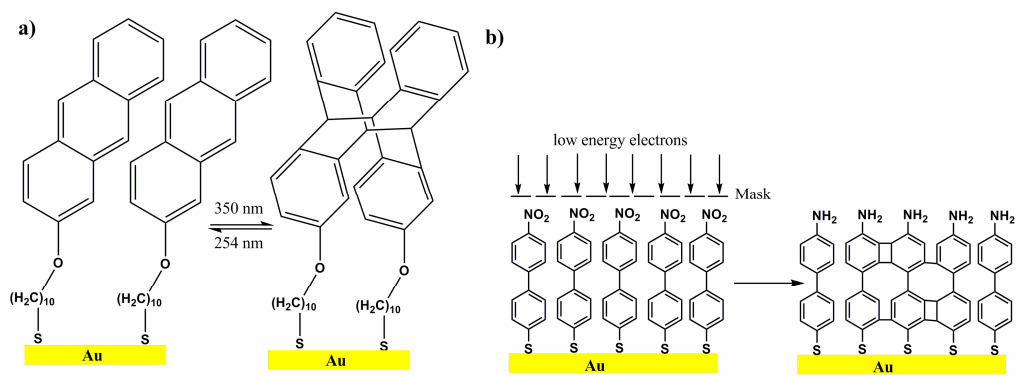

Figure 2.6 (a) The photodimerization of anthracene SAMs on the gold surface.[17] (b) The electron-induced chemical lithography and subsequently chemical reaction: an electron beam converts the terminal nitro groups of a 4′-nitro-1,1′-biphenyl-4-thiol monolayer to amino groups while the underlying aromatic layer is cross-linked.[18]

2.3.2 Covalent reactions within molecular chains on metal surfaces

The incorporation of photopolymerizable functional groups within alkyl chains of SAMs on surfaces has been intensively studied, even leading to a new polymeric platform for interfacial design. Batchelder *et al.* prepared monolayers containing diacetylenes on gold which show excellent durability and stability (Figure 2.7).[19] This monolayer contains a so-called internal molecular scaffolding, and when irradiated with UV, adjacent molecules in the monolayers are covalently connected to form a highly conjugated polymer backbone within a monolayer. The combination of FTIR and Raman spectroscopies provided direct evidence that the films form via growth of islands, in which the molecules display a high degree of local order. The resulting polymers appear to be extremely stable. Once complete, the polymer cannot be reversed by further UV-irradiation or by exposure to organic solvents. Moreover, Kim and co-workers used carboxylic acid-terminated alkanethiol diacetylene ($HS(CH_2)_{10}C{\equiv}CC{\equiv}C(CH_2)_{10}$-COOH) as a building block for preparing multilayers.[20] Infrared external reflectance spectroscopy and ellipsometry indicated multilayer formation by layer-by-layer growth, which can be polymerized under UV irradiation either after the deposition of each individual layer or after all layers are deposited. Subsequently, they made a comparison of the polymerized and unpolymerized diacetylenic SAMs with simple alkanethiol SAMs and showed that the polymerized materials are stable in aggressive solvents and at temperatures as high as 200 °C.[21] The packing quality and defects within SAMs were also examined with electrochemical methods, which showed that polymerized diacetylenic SAMs on Au are far more stable than unpolymerized ones.

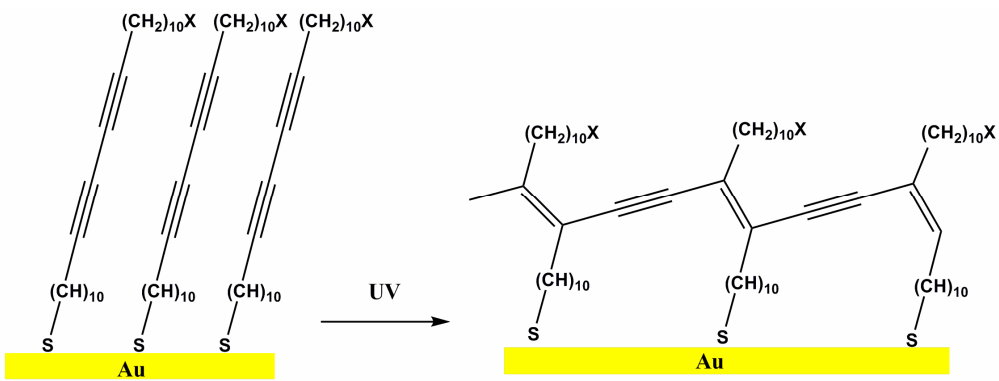

Figure 2.7 Photoinitiated polymerization of diacetylene derivatives.[20]

Mowery *et al.* fabricated SAMs of *n*-alkyl (C18) and photopolymerized polydiacetylene to investigate the impact of substrate preparation on the resulting monolayer structures.[22] With FTIR, contact angle, electrochemical methods, and AFM measurements, both the short- and long-range order of the polymerized monolayers are observed to increase substantially on evaporated gold, while the *n*-alkylthiols SAMs showed minimal structural variation under identical conditions. They also demonstrated photopolymerized diacetylene SAMs to be a versatile photoresist for fabricating spatially controlled interfacial properties within a single molecular layer.[23]

2.4 Metal surfaces: noncovalent interactions

The use of noncovalent interactions offers reversibility, error correction and therefore the potential dense packing of monolayers with high order. The focus here is on components interacting through noncovalent intermolecular forces, like metal-ligand, ionic, hydrogen bonding, π-π stretching and van der Waals interactions. The systems will be discussed according to the presence of noncovalent interactions in the terminal groups of the functionalities, followed by the interactions in the molecular chains in the monolayers on metal surfaces.

2.4.1 Noncovalent interactions between terminal groups on metal surfaces

2.4.1.1 Metal-ligand interactions

Metal-ligand coordination uses a coordinative bond, formed by the electronic interaction of organic molecules (the ligands) with a metal (ion) to be assembled into supramolecular structures. The coordinative bonds keep the systems together, which has two advantages. First, the coordination is highly directional, especially when transition metals such as copper, silver, and gold are involved. This is an advantage for the specific positioning of molecular building blocks. Secondly, the strength of coordination can be fine-tuned by changing the ligands.

The combination of molecular recognition elements and monolayers generates a powerful tool to monitor sensing processes at monolayer/solution interfaces. An early report on the construction of a transition metal complex on a flat metal surface showed that a SAM of

mercaptoundecanoic acid coordinated Cu(II) to the terminal carboxylate groups (Figure 2.8). This served as a chemical sensor that responds to analytes based on known bulk-phase intermolecular interactions with a high degree of selectivity and sensitivity. In particular, a surface layer of coordinatively unsaturated Cu(II) was demonstrated to provide selective and reversible binding sites for organophosphonates in a selective surface acoustic wave device.[24]

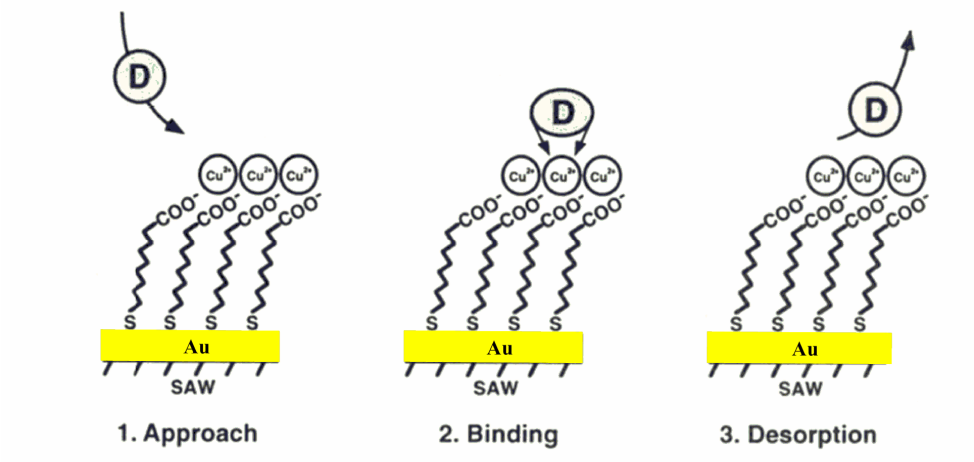

Figure 2.8 The approach of sensing an analyte using a surface layer of coordinatively unsaturated Cu(II) (D = analytes).[24]

Dutta *et al.* demonstrated a sensor for metal cations using different thiolated ligands, e.g. aminoethanethiol, mercaptopropionic acid, mercaptoundecanoic acid, mercaptopropanol, mercaptoundecanol, and cystein, as SAMs functionalized on silicon microcantilevers with gold nanostructured surfaces (Figure 2.9). Binding of metal ions (Li^+, Cs^+, Co^{2+}, Cu^{2+}, Al^{3+}, Cr^{3+}) to the active surface of a cantilever induces a surface stress that was detected as a bending of the cantilever. It was concluded that short chain-functionalized SAMs show better selectivity in sensing monovalent and trivalent metal ions than divalent ions, while the long chain thiol-coated cantilevers show better selectivity in sensing divalent cations. The shape and magnitude of the response profiles of the cantilevers were highly characteristic for the metal ions and type of modified SAMs.[25]

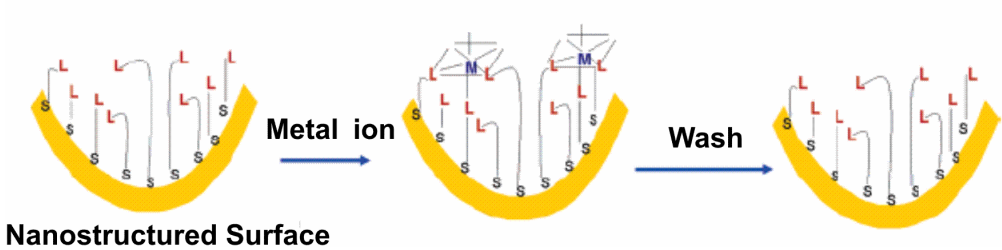

Figure 2.9 Schematic representation of SAMs of thiolated ligands with variable chain length as ion recognition phase for metal ions on nanostructured surfaces on silicon cantilevers.[25]

When the recognition take place at the interface, molecular recognition events depend mainly on the interactions between the immobilized receptors and the ions in solution, and to a lesser extent on monolayer density and packing properties. In contrast, lateral metal-ligand recognition is mainly influenced by the organization and packing of individual molecules within the monolayers. Such metal-ligand interactions result in an ion-templating effect on the surface during monolayer formation, showing high selectivity for the ion recognition.[26] Reinhoudt *et al.* [27, 28] and Port *et al.*[29] almost simultaneously reported the formation of SAMs with crown ethers as terminal groups, used as receptors to detect electrochemically inactive cations in solution. By monitoring the capacitance and charge transfer resistance of the monolayer, the association constants were determined for the interactions of various metal ions with monolayers of different crown ether adsorbates. Furthermore, it was shown that the high surface density of crown ethers leads to lateral sandwich complexation of metal ions (Figure 2.10a), which can be prevented by dilution of the crown ether monolayers with heptanethiol.[28]

Multivalent binding of a supramolecular complex at a multivalent host surface by combining the orthogonal cyclodextrin host-guest and metal ion-ethylenediamine coordination interaction motifs has also been described by our group.[30] The system employs a heterotropic divalent linker, with a cyclodextrin-complexing adamantyl group on one end and a metal-complexing unit on the other. Three building blocks were employed, the coordination motif with the ethylenediamine ligand, Cu(II) as a divalent, and Ni(II) as a potentially trivalent building block (Figure 2.10b). The binding of the complexes to a cyclodextrin monolayer was studied as a function of pH by means of surface plasma resonance (SPR) spectroscopy. Both

Ni(II) and Cu(II) ions were observed to form a divalent bisadamantyl system that coordinated to cyclodextrin monolayers. A sequential multivalent, heterotropic binding model was used to explain these divalent binding events for both complexes.

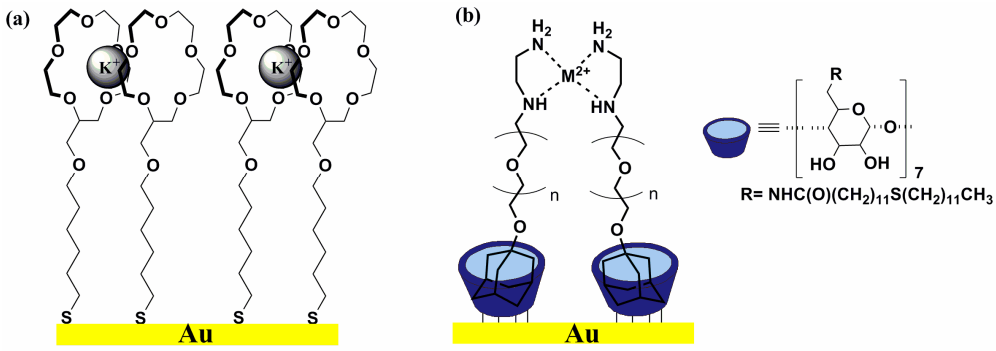

Figure 2.10 (a) Sandwich complexation of metal ions by crown ether adsorbates.[28] (b) The complex formed by adamantyl ethylenediamine derivatives supramolecularly associated with β-cyclodextrin thioether derivatives self-assembled on a gold surface (M = Cu^{2+}or Ni^{2+}).[30]

2.4.1.2 Ionic interactions

Electrostatic or ionic forces attract positive and negative charged species (ions), and this force can be used for the assembly of molecular structures. Although no chemical bonds are formed between the two components, ion-pair formation between similarly sized organic ions in solution produces stable, nondissociating adducts, especially in solvents of low dielectric constant.[31]

The electrostatic interactions in a monolayer of ionic components may lead to a variety of phenomena. Winograd *et al.* studied the penetration of thermally evaporated Au atoms in alkanethiolate SAMs on Au to control Au penetration by adjusting the interactions between terminal groups of CH_3, CO_2CH_3, CO_2H, and CO_2K SAMs on Au substrates (Figure 2.11).[32, 33] It was found that Au atoms equally well penetrate into the CH_3 and CO_2CH_3 films with the formation of smooth buried layers. For the CO_2H film, although Au atoms can still penetrate through it, mushroom like clusters are formed on Au substrates due to H-bonding between the adsorbates. In the case of CO_2K films most Au atoms form islands at the interface without penetration. They concluded that van der Waals forces and H-bonds are not strong enough to block Au atoms from going through but that ionic interactions are able to block penetration of Au atoms.

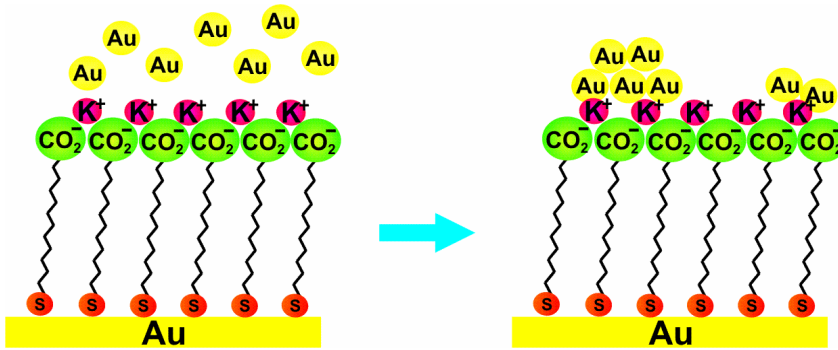

Figure 2.11 Controlling the penetration of Au atoms by modifying molecular interactions of the terminal groups with ion pairing.[32]

Ji *et al.* reported a sensing monolayer for detecting cesium ions (Cs^+) modified onto Au-coated microcantilevers (Figure 2.12a).[34] Mixed monolayers on a gold coated cantilever was prepared by adsorption of 1,3-alternate-bis(11-mercapto-1-undecanoxy)-calix[4]benzocrown-6 and decane-1-thiol. As the Cs^+ ions diffuse to the SAMs coated microcantilever accommodating the crown cavity, the bending of the cantilever was measured by monitoring the position of a reflected laser beam onto a four-quadrant photodiode. The bending response of the SAM-coated microcantilever upon Cs^+, K^+, and Na^+ complexation was compared for the same concentration of each ion (10^{-5} M), which indicated that SAM-coated microcantilevers were much more selective towards Cs^+ ions compared to K^+ and Na^+ ions. This study has shown that the concept of ion selective SAM-coated cantilevers can be applied successfully to detect trace amounts (ppb) of cesium ions in situ with remarkable sensitivity.

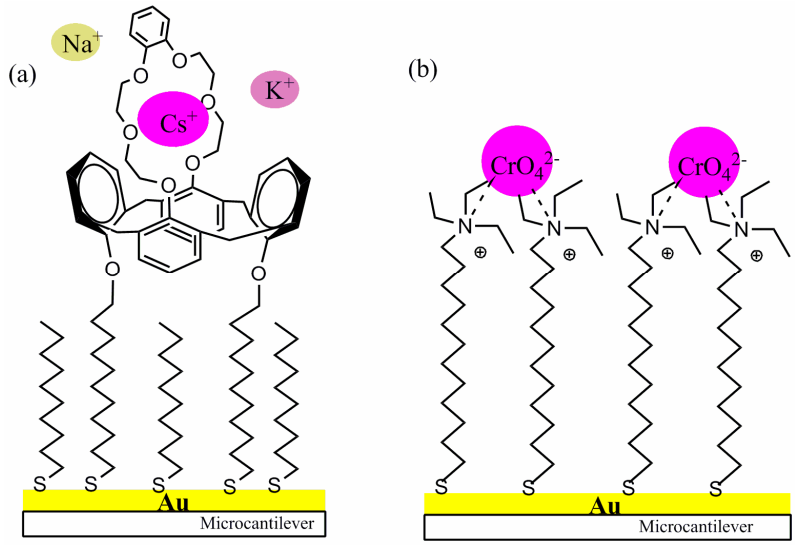

Figure 2.12 Schematic representations of the molecular structure (a) of receptor molecule 1,3-alternate-25,27-bis(11-mercapto-1-undecanoxy)-26,28-calix[4]benzocrown-6 co-absorbed with decane-1-thiol on the gold surface of a microcantilever;[34] and (b) of the self-assembled monolayer of triethyl-mercaptododecylammonium bromide on the gold surface of the microcantilever and ion pair formation with CrO_4^{2-}.[35]

Ji. *et al.* also reported other SAM-modified microcantilevers for the detection of trace amounts of CrO_4^{2-} using triethyl-mercaptododecylammonium bromide (Figure 2.12b).[35] It is known that quaternary ammonium compounds are useful ion-pair reagents for the chromatographic analysis of CrO_4^{2-}.[35] Therefore, the microcantilever undergoes bending due to adsorption of CrO_4^{2-} ions on the SAMs. A concentration of 10^{-9} M CrO_4^{2-} can be detected using this technology in a flow cell with a high selectivity over other anions (Cl^-, Br^-, CO_3^{2-} and SO_4^{2-}).

Valincius *et al.* observed that electron transfer to the ferrocenyl-terminated SAMs composed of 9-mercaptononyl-5-ferrocenylpentanoate ($Fc(CH_2)_4COO(CH_2)SH$) is promoted by highly hydrophilic ions (Cl^-, SO_4^{2-}, F^-, and $NH_2SO_3^-$ anions) (Figure 2.13a and b).[36] This suggested that the anion-induced electron transfer rate might be related to changes of the physical and chemical molecular properties as well as to the structure of the SAMs. They also suggested that ion-pairing directly influences the stability of the ferrocenyl-terminated monolayers due to increased lateral interactions.

Recently, Norman *et al*. adopted similar redox-active ferrocenyl-terminated SAMs (ferrocenylundecanethiolate) to modify a gold-coated microcantilever for observation of the redox-induced surface stress that caused the cantilever to bend (Figure 2.13c).[37] Oxidation of the ferrocenyl SAMs in perchlorate electrolyte generates compressive surface stress changes attributable to steric constraints in the closely-packed ferrocenyl-terminated SAMs. They suggested that the redox-induced deflection of a microcantilever modified with ferrocenyl-terminated SAMs is caused by a monolayer volume expansion resulting from collective reorientational motions, which is induced by the complexation of perchlorate ions to the surface-immobilized ferrocenium cations. This finding indicated that the cantilever responds to collective in-plane molecular interactions rather than reporting individual events.

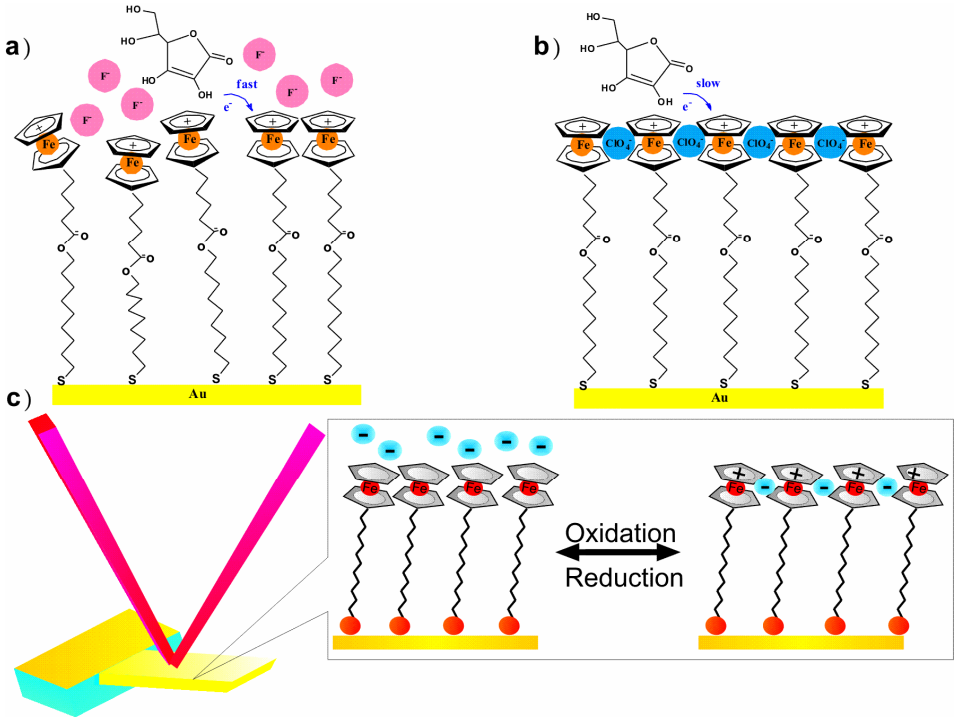

Figure 2.13 Schematic illustration of possible structural changes in the ferrocenyl-terminated SAMs upon transition from (a) hydrophilic to (b) hydrophobic anions in solution indicated by the changes of electron transfer rate; and (c) the redox-induced deflection of the ferrocenylundecanethiolate SAM-modified microcantilevers in perchlorate electrolyte solution.[37]

2.4.1.3 Hydrogen bonding interactions

Sastry *et al.* studied the kinetics of ion exchange as well as the pH-dependent cation (Cd^{2+} and Pb^{2+}) binding to self-assembled monolayers of carboxythiophenol using a quartz crystal microbalance (Figure 2.14).[38] SAMs of carboxythiophenol on Au have a surface rich on carboxylic acid functionalities which can be used to bind the Cd^{2+} and Pb^{2+} through an ion-exchange process. At low pH, the carboxylic acid groups are not expected to be ionized, and they can form hydrogen bonds with neighboring carboxylic acid groups. At high pH the carboxylic groups are deprotonated and can be used to bind the cations through an ion-exchange process. The stoichiometry of the cations to carboxylic acid can be 1:2 (cations bind as M^{2+}) or 1:1 (cations bind as $M(OH)^{+}$),[39] respectively. This study showed that the degree of exchange at high pH values is twice as large as that expected from charge neutrality considerations, indicating chemical attachment as $M(OH)^{+}$. This probably resulted from the incorporation of $Cd(OH)^{+}$ and $Pb(OH)^{+}$ instead of doubly charged cations to the carboxylic acid groups, in agreement with X-ray reflectivity measurements.[39]

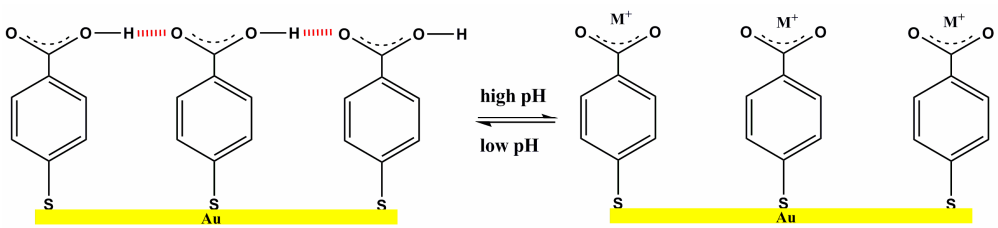

Figure 2.14 Organization of SAMs of 4-carboxythiophenol on Au at low pH, and its counterion adsorption ($M^{+} = Cd(OH)^{+}$ and $Pb(OH)^{+}$) at the surface of the SAMs at high pH.[38]

Credo *et al.* patterned a substrate for molecular assembly on a surface featuring adsorbates with recognition elements. They used moieties featuring complementary recognition to tune the current-voltage properties of the patterned region (Figure 2.15).[40] Diacyl 2,6-diaminopyridine decanethiolate (DAP) was inserted in a monolayer of decanethiolate on Au using replacement lithography by a STM tip (Figure 2.15A). Furthermore, electroactive functionalization of the monolayer was achieved through incubation in a solution of the complementary ferrocenyl-terminated uracil (Figure 2.15B). Replacement of the electroactive ferrocene-uracil was achieved by solution incubation in a nonelectroactive

dodecyl uracil (Figure 2.15C). To verify the hydrogen bond-mediated assembly process, bulk electrochemical and spectroscopic techniques were used. Therefore, these complementary hydrogen bonding molecules were used to control the electronic properties of chemically well-defined surface structures to add and remove an electroactive functionality in a molecular assembly.

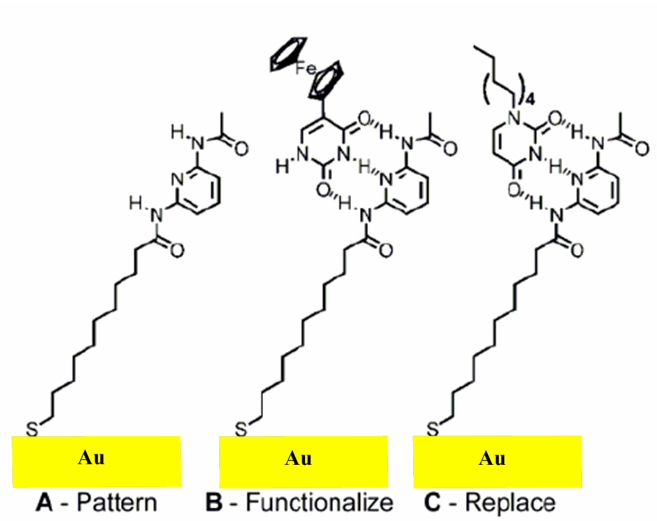

Figure 2.15 Formation of molecular assemblies. (A) Diacyl 2,6-diaminopyridine decanethiolate "binder" (DAP), (B) recognition of complementary electroactive ferrocene-uracil, (C) recognition of complementary nonelectroactive dodecyl uracil "eraser."[40]

2.4.1.4 π-π Stacking interactions

The intermolecular interactions for widely used π-conjugated molecules such as pentacene, tetracene, and oligo-phenyls are usually dominated by intermolecular π-π stretching interactions, which can be deconvoluted into long-range electrostatic forces and short-range charge transfer interactions. Because of their rich electronic and photonic properties, conjugated organic molecules are ideal candidates as probe components for the structure of monolayers that may find potential applications in optoelectronic devices.[41]

Evans *et al.* studied the effect of incorporating aromatic groups into alkanethiol SAMs to understand the interrelationships between the molecular structures of π-conjugated molecules

and their organization.[6] By using ellipsometry, wetting, FTIR, surface (contact) potential, and surface enhanced raman spectroscopy (SERS), they found that the quality of the monolayers was dependent on both the size of the dipole introduced into the film and the length of the aliphatic chain on top of the aromatic group. For well-ordered surfaces, they suggested that it is necessary that the aliphatic chain on top of the aromatic group is larger than C_8 in length, with the best results being found for C_{12}. They proposed that the length of the alkyl chain provides a strong driving force for monolayer formation by maximizing van der Waals interactions. It was concluded that a decreasing polarity introduced by the aromatic group and an increasing alkyl chain length leads to an increased film quality.

Reese *et al.* prepared SAMs of thiols bearing conjugated terminal groups and characterized the SAMs by optical ellipsometry and electrochemical measurements (Figure 2.16).[42] The thickness of the films composed of thiols **1, 2**, and **3** corresponds well to the expected thickness of monolayers in which the components are oriented almost perpendicular to the Au surface. Cyclic voltammetry measurements with $K_4Fe(CN)_6$ as the external redox agent in aqueous KCl solution on a SAM-modified gold electrode (thiols **1**, **2**, and **3**) showed that these monolayers are densely packed and that they block electron transfer between the gold and the solution electrophore. π -π Interactions between neighboring conjugated subunits of these SAMs block electron transfer between the electrode and a redox species in both aqueous and nonaqueous media more efficiently than did a monolayer of dodecanethiol. Strong π-π interactions were also observed in the emission spectra of SAMs of **2** and **3** by fluorescence spectroscopy, which are red-shifted as a result of exciton interactions between the chromophores on Au.

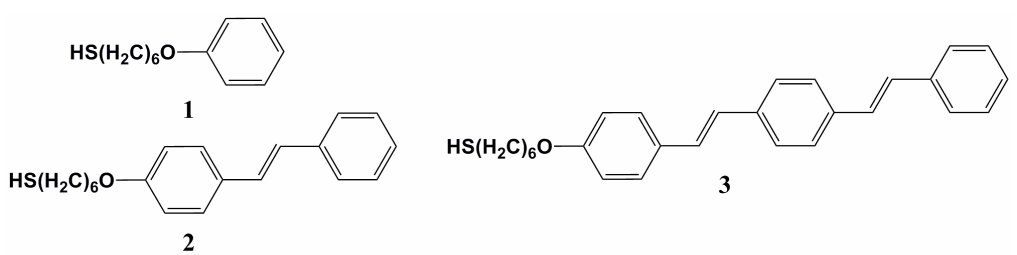

Figure 2.16 Molecular structures of thiols bearing conjugated terminal aromatic groups.[42]

2.4.1.5 Dipolar interactions

Dipolar interactions are attractive interactions between molecular entities resulted from non-uniform distributions of positive and negative charges on the various atoms. All dipole forces are anisotropic, which means that they depend on the relative orientation of the molecules. The term includes: dipole-dipole, dipole-induced dipole, and induced dipole-induced dipole forces.[43]

Heeg *et al.* studied the adsorption of alkanethiols and cyano-terminated thiols with the same chain length. Mixed monolayers of these two thiols on Au were prepared and characterized by angle resolved X-ray photoelectron spectroscopy (ARXPS) (Figure 2.17A).[44] The ARXPS signal showed that the cyano to methyl ratio is nonlinear to the volume fraction of cyano-terminated thiols in the deposited solution. This observation gave quantitative evidence that the solution composition does not dictate completely the layer composition, which showed a preferential adsorption of the methyl-terminated alkanethiol at the Au surface.

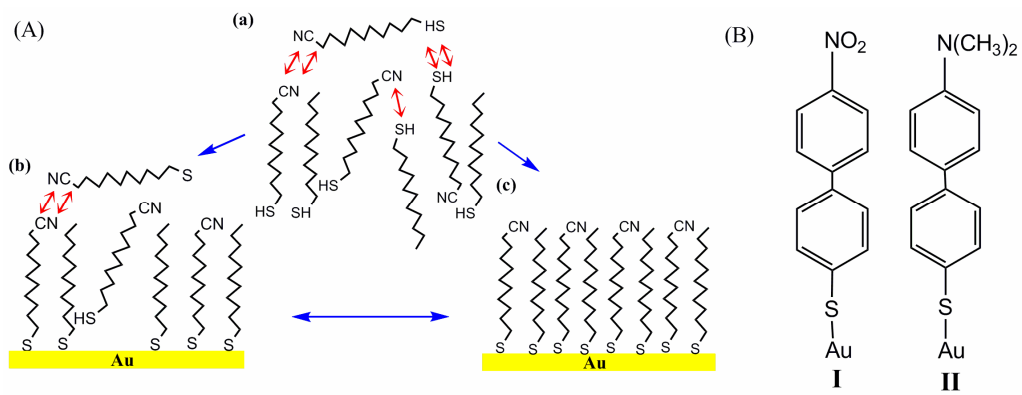

Figure 2.17 (A) Schematic drawing of the possible adsorption of alkanethiols and cyano-terminated alkanethiols to a gold surface.[44] (**a)** Random distribution of both molecules in solution (possible weak interaction between the functional groups are indicated by arrows); (**b)** disordered monolayer consisting of chemically bound alkanethiols and non-bound molecules; (**c)** perfect chemically bound self-assembled monolayer consisting of alkanethiols and ω-cyano-terminated alkanethiols. (B) 4′-substituted-4-mercaptobiphenyls with (NO_2 I) and dimethylamino(($(CH_3)_2$N II).

Similar methodologies were used by Kang *et al.* to study the competition of adsorption between two different molecules to examine the extent of dipolar interactions when the molecules have significant, large dipole moments.[45, 46] They prepared a mixed monolayer of mercaptobiphenyls substituted with nitro (NO_2) and dimethylamino ($(CH_3)_2N$) moieties (Figure 2.17B). The mercaptobiphenyls substituted with nitro groups represent molecules with a strong electron - attracting group, while the dimethylamino ($(CH_3)_2N$) group is a strong electron donor. The composition of the mixed SAMs was determined to be 1:1 by external reflection FTIR spectroscopy in agreement with a simple calculation based on the Hammett equation. Therefore, they concluded that the equilibrium 1:1 ratio of the two components in the mixed SAMs is driven by the formation of a two-dimensional assembly with zero net dipole moment.

2.4.2 Noncovalent interactions within molecular chains on metal surfaces

2.4.2.1 Hydrogen bonding interactions

Studies of alkylthiols on gold have shown that the structural properties of alkyl chains interacting through van der Waals forces determine the structure of monolayers. However, as soon as specific functional groups, e.g. hydrogen bonds, are introduced into the monolayers, the picture becomes more complicated.[47, 48] The hydrogen-bonding groups, like urea[48] and amide groups, deserve special interest because they can be easily introduced into the monolayers. The amide-containing alkanethiol is unique in that the amide functional group is buried within the monolayer, creating a system in which “layers” of interactions exist that provide increased stability to the monolayer.[47]

Clegg *et al*. prepared amide-containing alkanethiol SAMs on gold to get a detailed understanding of how the amino acid composition and structure influence electron transfer rates. Using XPS and FTIR spectroscopy, they showed that the SAMs are uniaxial, and possess densely packed methylene chains with hydrogen bonding between neighboring amide moieties. These highly ordered monolayers containing a network of lateral hydrogen bonding, cross-linking within the film that form excellent electrochemical spacers as characterized by electrochemical blocking studies and double-layer capacitance measurements. They suggested that this well-defined structure can be used for systematic investigations of long-range electron transfer through amide bonds.[49, 50]

Sek *et al*. extended the understanding of contributions of intermolecular interactions to electron transfer through monolayers of alkanethiols containing amide groups (Figure 2.18a).[51] They described long-range electron transfer to covalently attached redox-active centers (i.e., ferrocene) across two types of alkanethiolate monolayers, containing one and two amide groups in the place of selected methylene groups in the main alkyl chain. The focus is the effect of the amide location on the kinetics of mediated electron transfer. Impedance spectroscopy and chronoamperometry indicated that the deeply "buried" (i.e., located close to the electrode surface) amide groups are responsible for a significant increase of electron coupling compared to simple alkanethiol monolayers. The presence of amide bonds in the outer part of the monolayer did not affect the rate of electron transfer across the monolayer.

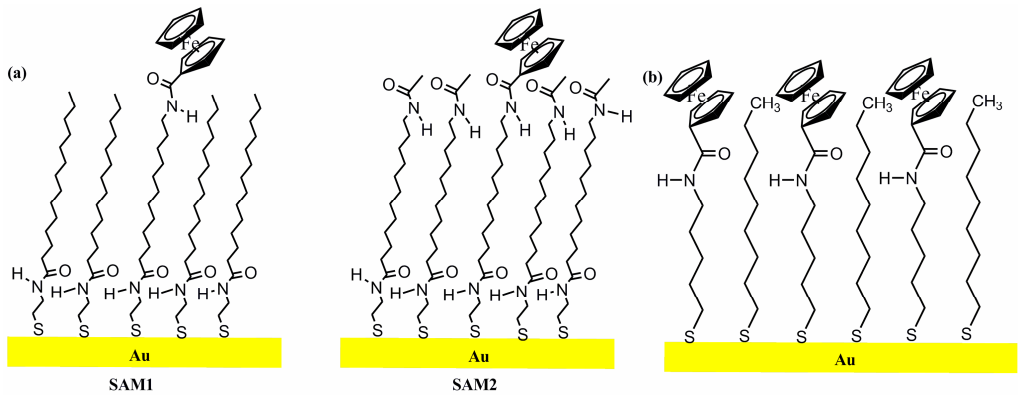

Figure 2.18 (a) Scheme of the monolayer assemblies SAM **1** possessing one plane of amide groups (internal) and SAM **2** formed by diamides in the internal and external planes.[51] (b) Schematic representation of a mixed monolayer system involving ferrocenylalkyl and alkanethiol spacers.[52]

Sabapathy *et al.* demonstrated the electrochemical behavior of coadsorbed monolayers of ferrocenylalkyl disulfides and non-electroactive unsubstituted alkanethiols on Au (Figure 2.18b).[52] Cyclic voltammetry and infrared reflection-absorption spectroscopy of the coadsorbed systems showed an unexpected negative shift in the formal potential of the ferrocenyl compounds with the amide linkages. This is attributed to disorder arising from the disruption of the hydrogen bonds within the monolayer caused by the alkanethiol "spacers",

thus making it slightly easier for the ferrocene subunits to undergo oxidation. Interchain hydrogen bonding within surface-confined layers was also probed by broadening of the amide stretch appearing around 3300 cm^{-1} in the infrared surface spectra.

Lenk *et al.* synthesized a fluorocarbon molecule for self-assembly and characterized the formation of the monolayer on Au (Figure 2.19a).[53] Both infrared and near-edge X-ray absorption (NEXAFS) showed the fluorocarbon segment to be highly oriented, with the chain axis nearly normal to the gold surface. They concluded that the amide moieties in the chain provide orientational stability through intermolecular hydrogen bonding and enhanced mechanical integrity.

Whitesides and co-workers reported the preparation and self-assembly of a series of fluorinated alkanethiols with an amide moiety on Au.[54] They investigated the susceptibility of several short chain alkanethiols self-assembled on gold toward exchange with longer chain alkanethiols. They observed that one of the amide-containing alkanethiol ($CF_3CH_2NHCOCH_2SH$) monolayers exhibited significantly enhanced stability against thermal desorption in vacuum or exchange with hexadecanethiol ($C_{16}SH$) in ethanol.

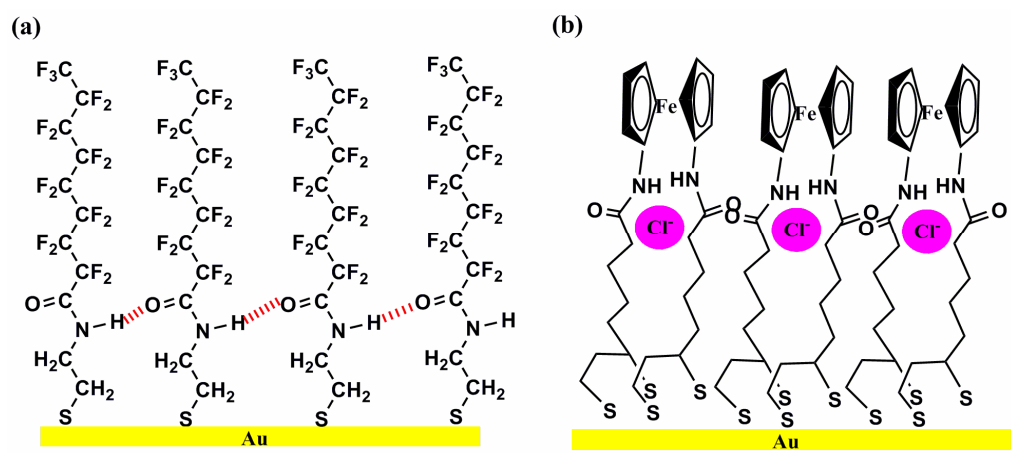

Figure 2.19 (a) Schematic diagram showing the structure of fluorinated SAMs on gold and the possible hydrogen bonding between adjacent amide groups by the red hatched bars.[53](b) Schematic drawing of anion binding within the surface-confined host, 1,1′-bis(alkyl-*N*-amido)ferrocene.[55]

By introducing amide groups, Beer *et al.* showed that monolayers of 1,1′-bis(alkyl-*N*-amido)ferrocene at Au have selective anion recognition properties that show better sensitivity than the same receptors in solution (Figure 2.19b).[55] Organic-phase diffusive voltammetry of this redox-active SAMs was studied, showing that the hydrogen-bond mediated recognition of specific anions is accompanied by a significant perturbation of the ferrocene redox potential. These surface confined receptors presented a sensing amplification, a two-fold higher cathodic shift for Cl^-, Br^-, and $H_2PO_4^-$, which is associated with surface pre-organization of the host recognition units.

Deoxyribonucleic acid (DNA) is the ultimate example, which uses lateral hydrogen bonding to match complementary single strands.[56, 57] DNA immobilization is a fundamental methodology for the construction of DNA biosensors and DNA-based nanodevices, and DNA-based self-assembly provides a way for "bottom-up" assembly.[58, 59]

There are several examples that use hybridization of complementary DNAs with immobilized single strand DNAs for sensing purposes.[60] Willner and co-workers prepared a three-component oligonucleotide/DNA layered assembly on a Au electrode that acts as a specific biosensor for the analysis of the Tay-Sachs mutant[61] by means of impedance spectroscopy (Figure 2.20).[62] Impedance measurements showed the corresponding response to TS-mutant binding to the immobilized oligonucleotide, upon the formation of a double-stranded DNA oligonucleotide complex at the electrode. In order to amplify the formation of DNA complex (with the analyte), the resulting double strand DNA was interacted with a biotinylated oligonucleotide, which is complementary to a residual sequence of the analyte DNA. As the secondary DNA is labeled by biotin, the subsequent reaction with avidin resulted in a superstructure that blocks the interface, therefore increasing the electron transfer resistance which is the signal for detecting the mutant.

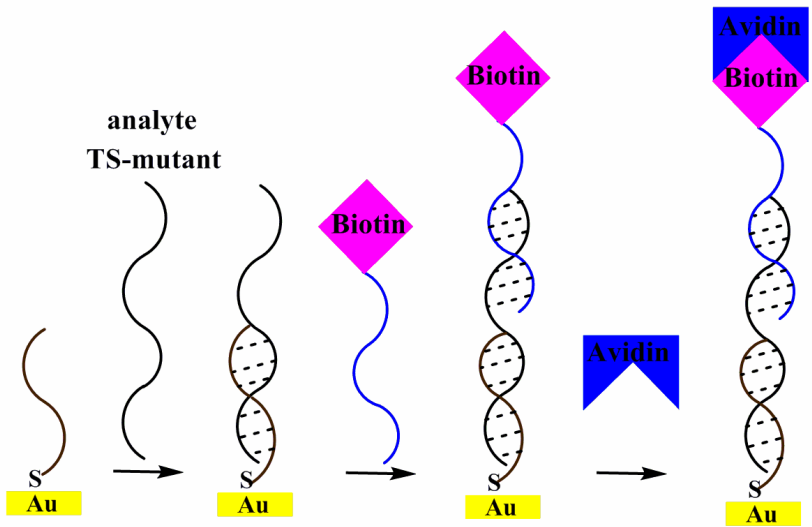

Figure 2.20 Amplified detection of complementary binding of single stranded DNA (TS-mutant) to a DNA-immobilized SAM on Au.[62]

Steel *et al.* have developed an electrochemical method to quantify the surface density of DNA immobilized on gold.[63] The surface density of DNA, the number of nucleotide phosphate residues, was calculated from the amount of cationic redox marker measured at the electrode surface. DNA was immobilized on gold by forming mixed monolayers of thiol-modified, single-stranded oligonucleotide and 6-mercapto-1-hexanol. Using chronocoulometry, they determined the saturated amount of charge-compensating redox markers in the DNA monolayer, which is proportional to the number of phosphate residues, and thereby the surface density of DNA, giving a value of $(1\text{-}10)\times10^{12}$ molecules/cm^2. This method permits quantitative determination of both single- and double-stranded DNA at electrodes.

2.4.2.2 π-π Stacking interactions

Matile *et al.* described multicomponent zipper assemblies of rigid-rod π -stacked architectures composed of p-oligophenyl rods (POP) and naphthalenediimide (NDI) stacks on conducting surfaces. NDI chromophores attached to rigid-rod scaffolds (POP-NDI) are assembled step-by-step to build mutually interdigitating π stacks along interdigitating rigid-rod scaffolds, which serve as hole and electron transporting pathways. By steady-state-fluorescence spectroscopy

and cyclic voltammery, this zipper assembly (POP-NDI) demonstrated higher photocurrent due to the directional flow of electrons along coaxial n/p heterojunctions (Figure 2.21).[64, 65] These supramolecular 3D assemblies were designed to access cascade n/p-heterojunctions with directionality in the current-voltage curves. Oligophenylethynyl (OPE) scaffolds were introduced to explore the importance of topological matching for zipper architectures and to determine the compatibility of the zipper assembly of the cascade heterojunctions. Excellent organization of OPE-NDI zipper architectures was confirmed in AFM images and by the observed bathochromic absorption of OPE in the action spectrum. This implies a co-planar orientation of phenyl groups leading to higher charge mobility. With the fact that the observed photocurrent was much higher upon OPE-NDI excitation than upon POP-NDI excitation, they concluded that the highly ordered and oriented supramolecular organization is essential for electron or hole transport to or from active sites.

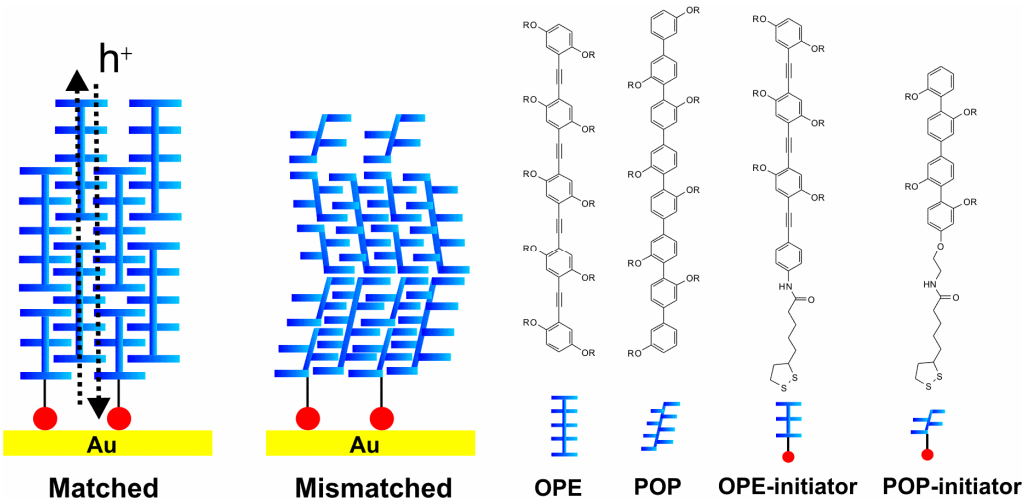

Figure 2.21 Schematic representation of matched and mismatched zipper assembly of OPE-NDI and POP-NDI propagators and initiators on Au (R = NDI group).[65]

2.4.2.3 Dipolar interactions

Normally, the alkyl chains of SAMs are stabilized through lateral van der Waals interactions, capable of forming close-packing overlayers.[66, 67] In order to understand the effect of

intermolecular electrostatic interactions within the monolayer plane on the packing and ordering, Ulman *et al.* incorporated sulfone groups (SO_2) into the alkyl chains (Figure 2.22).[6] One could assume that electrostatic interactions between functional groups such as SO_2 groups introduce a well-defined orientation of dipole moments. By contact angle measurement, disorder in the monolayer was observed, possibly resulting either from intramolecular electrostatic interactions (repulsive forces) between the sulfone groups or from intermolecular interactions between sulfone groups of neighboring chains. These in-plane dipoles have a profound effect on the molecular tilt, i.e. the molecules tilt in one direction only. Evidence from FTIR indicates that this molecular tilt is the result of strong $SO_2 \cdots SO_2$ electrostatic interaction that promotes the formation of a plane of dipoles within the assembly.[6]

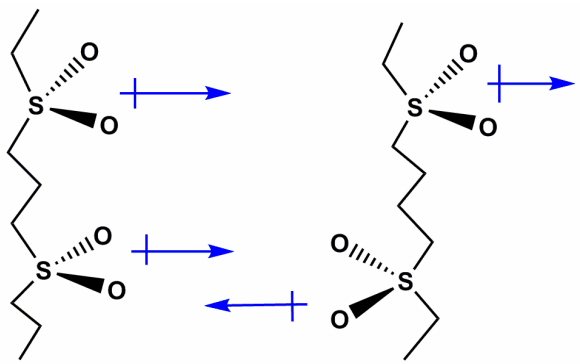

Figure 2.22 A scheme showing two sulfone groups in an alkyl chain.[6]

2.5 Oxide surfaces: covalent reactions

In previous chapters, different intermolecular interactions in the functionalized monolayers focused on adsorbates immobilized on gold surfaces. The thiol-based monolayers are relatively unstable both thermally and chemically, therefore restricting the conditions that can be employed for subsequent synthetic modifications of these monolayers, as well as limiting the chemistry that can be used. Covalent attachment *via* a siloxane linkage onto an oxide surface can overcome the problems mentioned above. In this part the important role of intermolecular interactions in monolayers on oxide surfaces will be discussed.

2.5.1 Covalent reactions between terminal groups on oxide surfaces

Fryxell *et al.* constructed a monolayer of an alkyltrichlorosilane on a silica surface to determine the reactivity of the siloxane groups. By XPS measurements, the monolayers on a scrupulously dried silica surface showed a lower density surface coverage, which might be due to little or no adsorbed water to affect cross-linking, leaving only the silanols on the oxide surface to react with the chlorosilanes in a solution (Figure 2.23). They proposed a hypothesis that those monolayers might be expected to have considerably more conformational mobility and permeability than the dense, highly rigid monolayers prepared from hydrated substrates. In spite of the similarity between the two related systems, there is apparently a significant kinetic difference in the chemical behavior of these closely related monolayer types.[68]

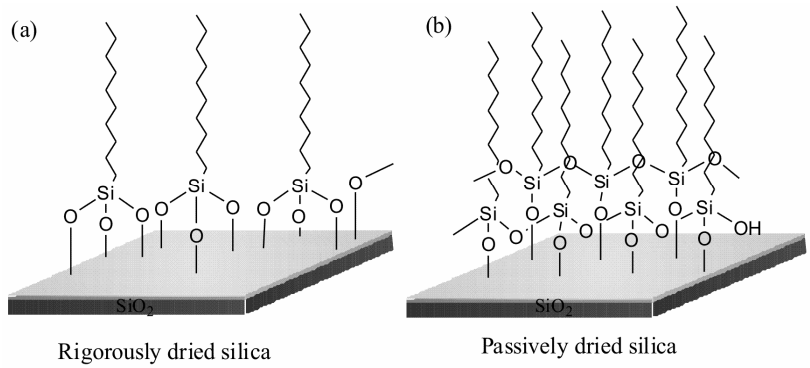

Figure 2.23 Schematic of SAMs formation on (a) rigorously dried and (b) hydrated substrates.[68]

Soja *et al.* prepared a mixed monolayer of octanoic acid (OA) and 16-mercaptohexadecanoic acid (MHDA) on TiO_2 and observed the evolution of a dimerization-induced chelate effect (Figure 2.24). For a range of solution compositions, IR spectroscopy showed that the mol fraction of MHDA within the mixed monolayer exceeds that in solution. The fraction of MHDA increased with time, while the sum of the surface coverages of MHDA and OA remained constant. They presented a mechanism in which the formation of disulfide bonds between neighboring MHDA thiol groups leads to increased coverage of MHDA on the TiO_2 surface. This illustrates that covalent interactions between surfactant functional groups can dramatically influence the composition and adsorption-desorption equilibria of mixed monolayers.[69]

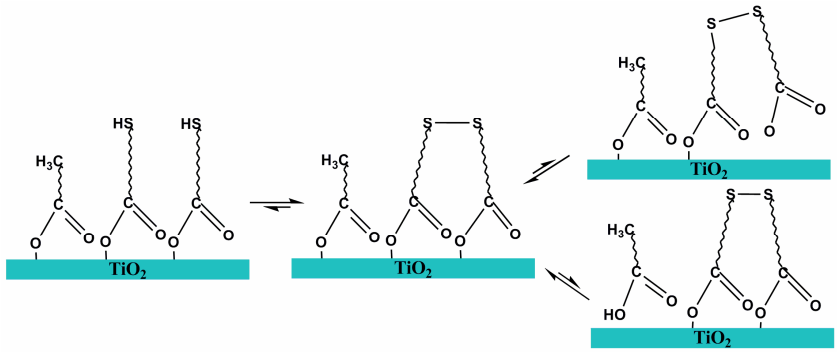

Figure 2.24 Schematic representation of the time-dependent increase of the 16-mercaptohexadecanoic acid (MHDA) surface coverage resulting from disulfide formation between the thiol groups of surface-adsorbed MHDA molecules on a TiO_2 film.[69]

2.6 Oxide surfaces: noncovalent interactions

2.6.1 Noncovalent interactions between terminal groups on oxide surfaces

2.6.1.1 Metal-ligand interactions

Li *et al.* have prepared a number of ruthenium and osmium metal carbonyl complexes on the substrates coated with ligand monolayers of (3-cyanopropyl)trichlorosilane on the oxide surface (Figure 2.25).[70] With polarized variable-angle attenuated total internal reflection infrared spectroscopy, they found that both the ruthenium and osmium first yielded a trinuclear species, $M_3(CO)_{10}(\mu\text{-}CO)L$, with an edge bridging CO and then rearranged into a more stable mononuclear species, $M(CO)_2L$, (M= Ru, Os). They demonstrated that polarized variable-angle attenuated total internal reflection is a valuable tool for analyzing surface-bound monolayers, by which not only information on the molecular structure, but also on the molecular orientation can be obtained.

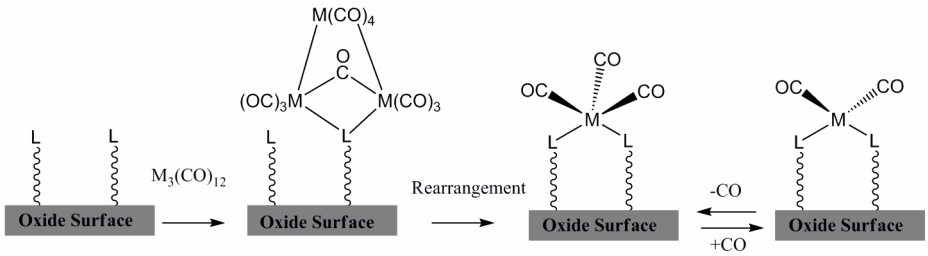

Figure 2.25 Formation of surface-bound $M(CO)_2L$ with multiple steps (M = Ru and Os, L = $NC(CH_2)_3Si$-).[70]

2.6.1.2 π-π Stacking interactions

Nam *et al.* have synthesized an organotrimethoxysilane containing a 1-cyano-1,2-bis(biphenyl)-ethylene (CNMBE) moiety, which provides a strong π-π intermolecular interaction (Figure 2.26). A SAM of well-ordered structure was readily obtained by a one-pot grafting reaction of CNMBE on an oxidized silicon substrate under mild conditions. Densely packed SAMs of CNMBE were observed by ATR-FTIR, AFM, and contact angle measurements. The introduced bis(biphenyl) moiety and urea linkage into the organosilane were expected to induce an efficient and dense grafting onto the surface by strong intermolecular π-π interaction and hydrogen bonding. This might counterbalance the disassembling molecular motion by a long and flexible spacer. The observed fluorescence emission spectrum clearly shifts to longer wavelengths which shows that bis(biphenyl)-ethylene aggregation is a main driving force for the monolayer formation and enables the fabrication of a well-ordered monolayer by a one-pot grafting reaction.[71]

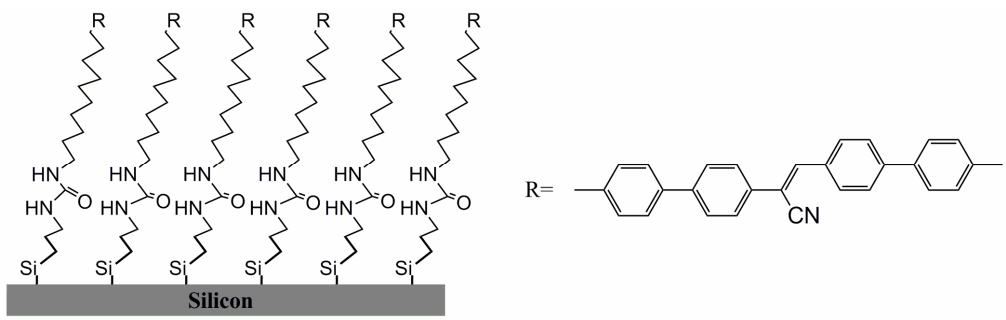

Figure 2.26 Monolayers of organosilanes containing a 1-cyano-1,2-bis(biphenyl)-ethylene moiety and its solid state thin films on quartz substrates under irradiation at 365 nm.[71]

2.7 Lateral electron/and energy transfer

The efficiency and complexity of electron and energy transfer reactions in natural photosynthesis have led many chemists to design donor-acceptor-linked systems that mimic these multistep ET/EN processes. It is clear that good electronic coupling and a low

reorganization energy are required for the charge transport in the surface-confined molecular layer to occur rapidly.[72] Knowledge of electron transfer between adsorbed molecules and a metal electrode was immensely advanced by introducing redox molecules into monolayers.[73, 74] Systems with electron and energy transfer will be discussed following the complexity of the layers/monolayers from simple to more complex structures.

Hapiot *et al.* chose *n*-type Si(111) substrates covalently modified with an oxidizable ferrocene-terminated alkyl monolayer to prepare a conducting monolayer on nonconducting surfaces.[75] They used scanning electrochemical microscopy (SECM) to probe the electroactive ferrocene monolayers using ferrocene/ferrocenium ($FeCp_2$) redox couples that display a more positive standard potential than the grafted ferrocene on the silicon surface. SECM probes the surface locally from the solution side with the dissolved redox mediator. A Pt ultramicroelectrode (UME) tip approaching a ferrocene monolayer displayed a clear positive feedback and the occurrence of continuous electron transfer between the electrogenerated ferrocenium species produced at the UME and the interface (Figure 2.27a). It was concluded that the thin ferrocenyl monolayer behaves like a purely conducting material with very fast electron communication between immobilized ferrocenyl headgroups in a 2D-like charge-transport mechanism.

Hapiot *et al.* used a redox-active ferrocenyl-terminated dendrimer to explore the relation of electronic communication.[76] To improve the stability of such systems, a negatively charged interface was prepared by electrochemical reduction of an aryl carboxylic diazonium salt, which produces active aryl radicals covalently attached to a carbon surface, leading to an arylcarboxylic multilayer. After soaking the modified electrode in a KOH solution, the resulting carboxylated surface behaved as an almost blocking insulating interface, which allows the immobilization of dendrimers of different generations. Different electron-transfer rate constants (K_{el}) were observed for different generations and this revealed the variation in communication between dendrimers. When comparing G1 and G2, G1-adsorbed at the surface displayed the largest K_{el} for a given mediator, which suggested that charge transfer inside or between two G2 dendrimers is less efficient. A clear conclusion could not be drawn as the structural organization of the dendrimers inside the layer could also interfere with the intrinsic properties of a redox dendrimer (Figure 2.27b).

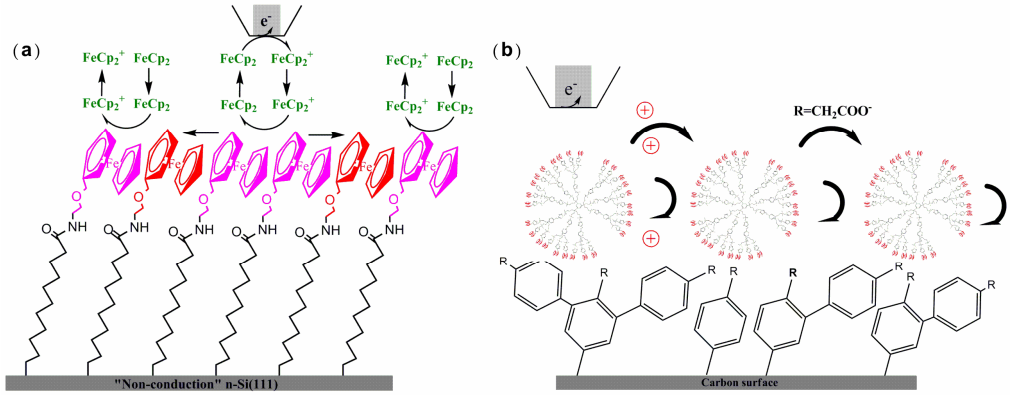

Figure 2.27 Process involved in the SECM measurements of electron transfer between an electroactive (a) ferrocene monolayer,[75] (b) dendrimers bound to an insulating surface and a mediator in solution.[76]

Yokota *et al.* designed an electroactive tetrathiafulvalene thiol ($TTFC_{11}H_{22}SH$) to pursue an intermolecular electronic coupling, which is embedded in an *n*-alkanethiol SAM matrix as islands (Figure 2.28).[77] This system is a good candidate for revealing whether intermolecular interactions affect the conductance measurements by STM, because TTF derivatives possess one of the strongest intermolecular interactions. The intermolecular coupling can be tuned by alteration of the oxidation state. They observed by STM the height difference between different islands of TTF on Au illustrating a positive correlation between the apparent height of the island, island size and the intermolecular conduction path. They proposed two mechanisms to explain the intermolecular conduction paths. The first possibility is an electrochemical exchange reaction between neighboring TTF backbones. The second possibility is an intermolecular coupling (i.e., hopping or band formation). Overall, on the basis of the strong intermolecular electronic coupling of TTF molecules, an efficient intermolecular conduction path is created within monolayers.

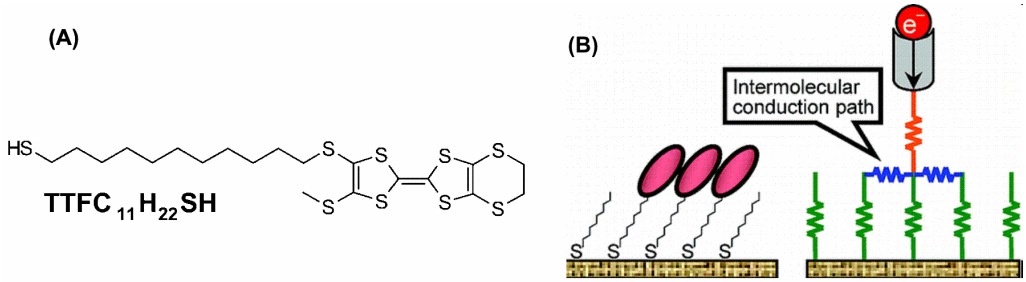

Figure 2.28 (A) Molecular structure of $TTFC_{11}H_{22}SH$. (B) Schematic model of a $TTFC_{11}H_{22}SH$ island embedded in alkanethiol SAMs (left) and the intermolecular conduction paths upon STM measurement (right). The blue, orange, and green resistances represent intermolecular paths, and STM tip-molecule path, and alkyl-chain paths, respectively.[77]

Electron transfer through peptides, such as helices, has attracted much attention.[78-80] Takeda *et al.* prepared SAMs of helical peptides on Au to study the effects of the monolayer structure, i.e. constituting amino acids, molecular orientation and molecular packing, on long-range electron transfer through the helical peptides (Figure 2.29).[81] Different lengths of helical peptides were prepared having a thiophenyl linker at the *N*-terminus for immobilization on Au and a redox active ferrocene moiety as an electron-transfer probe at the C-terminus. The logarithms of the standard rate constants obtained by electrochemical measurements showed a linear relationship with the direct distances between the ferrocene moiety and gold. Some data deviated from this linear relationship, which could be explained by the differences in molecular packing evaluated from the monolayer capacitance measurements. They concluded that an electron is transferred along a few molecules along the surface normal so that the vertical orientation or the increase of the interchain backbone separation slows down the electron transfer. With a closely packed monolayer, the electron transfer is suppressed because vibrational modes are restricted. They proposed different models for the observed effects on the basis of either electron tunneling or sequential hopping.

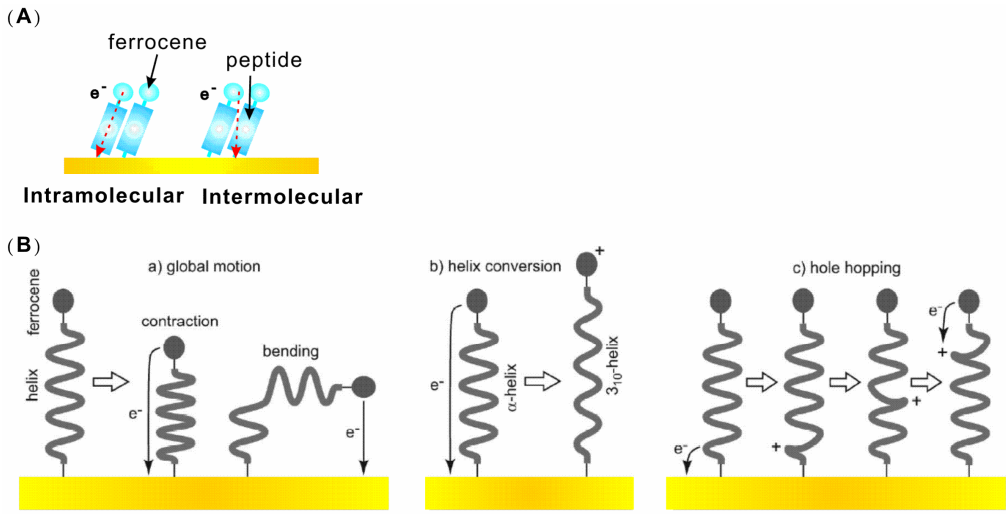

Figure 2.29 Schematic illustrations of (A) intramolecular electron transfer and intermolecular electron transfer through the helical peptide monolayers and (B) proposed mechanisms for the molecular dynamics effect on the electron transfer, (a) global motion-gated electron tunneling, (b) electron tunneling coupled with helix conversion from α-helix to 3_{10}-helix, and (c) hole hopping among the amide groups assisted by a local backbone motion.[81]

Grätzel *et al*. reported the rapid ambipolar cross-surface charge transfer within monolayers of Ru complexes anchored on the surface of mesoscopic oxide films (TiO_2) (Figure 2.30).[82] Cyclic voltammetric, spectroelectrochemical, and impedance measurements were applied to determine the percolation threshold and rate for hole transfer across the surface. They proposed that the Ru complex with high charge percolation rates could arise from a relatively low energy barrier for electron exchange and an enhanced electronic coupling between the NCS-groups. Charge propagation within the Ru complex confined monolayer proceeds by thermally activated electron hopping between adjacent molecules. Therefore, good spatial overlap of the adjacent molecular orbitals and low reorganization energy are required to achieve high percolation rates. They demonstrated the ability of the bipyridyl ligands of the Ru complexes to conduct electrons along the surface and reveal the important role played by the NCS groups in enhancing the hole transport within the monolayers.

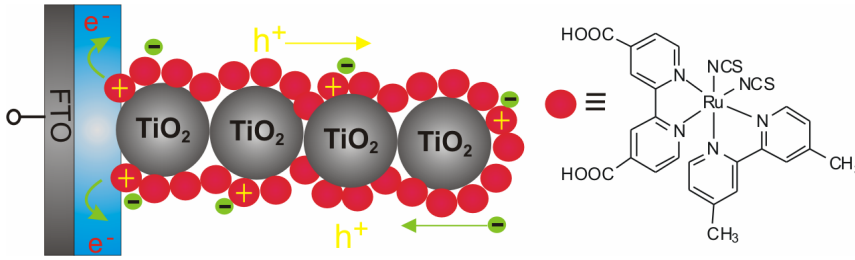

Figure 2.30 Schematic model showing the cross surface charge percolation through the redox active monolayer adsorbed on mesoscopic oxide films, which is deposited on a conducting glass substrate.[82]

The fact that all fossil fuel sources are finite makes solar energy conversion and photocurrent generation a topic of utmost importance. The way to convert light into electrons can be defined as the consequence of light absorption by a chromophore. Imahori *et al.* prepared mixed monolayers of boron-dipyrrin thiols (antenna system, molecule B in Figure 2.31) and porphyrin thiols (energy acceptor, molecule P in Figure 2.31) to examine the photoinduced electron transfer from the boron-dipyrrin to the porphyrin on the gold surface (Figure 2.31).[83, 84] The occurrence of photoinduced energy transfer from the singlet excited state of the boron-dipyrrin moiety to the porphyrin moiety in mixed SAMs of B and P thiols on the Au electrode was successfully confirmed by steady-state fluorescence spectroscopy. Thus, their system not only mimics light-harvesting and charge separation processes in photosynthesis but also acts as an efficient light-to-current converter in molecular devices.

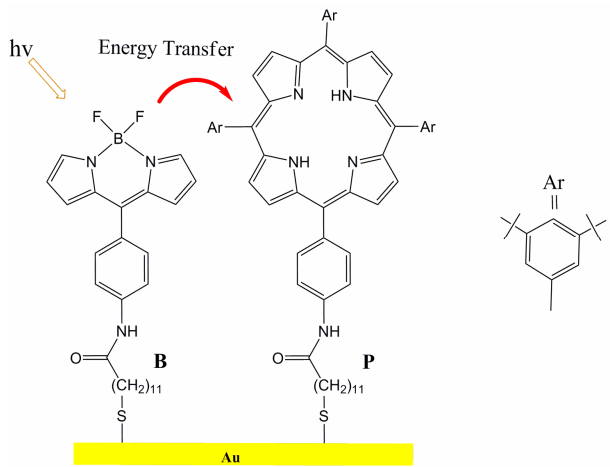

Figure 2.31 Photoinduced energy transfer at gold electrode modified with monolayers of boron dipyrrin thiol (B) and porphyrin alkanethiol (P).[83, 84]

Hamers *et al.* studied the role of photoelectron ejection during the photochemical grafting of n-alkenes onto a carbon surface (Figure 2.32).[85] 1-Alkenes carrying various terminal functional groups (-NHCOCF$_3$, -NHCOO(*tert*-butyl), -COOCH$_3$, -CH$_3$) were grafted from neat liquids using 254 nm light. These layers were characterized using X-ray photoelectron spectroscopy and infrared reflectance absorption spectroscopy. Pronounced differences in reactivity were observed between the molecules: trifluoroacetamide-terminated alkenes were grafted the fastest and yielded self-terminating layers after 4 h irradiation. This acts as the best electron acceptor and has the highest reactivity. They demonstrated that photoejection of electrons from the solid into the acceptor levels of the alkenes initiates the functionalization reaction and controls the overall rate. Finally, a low reactivity moiety, 10-*N*-Boc-amino-dec-1-ene, was introduced to react and form dense monolayers by seeding a carbon surface with small amounts of a good electron acceptor, such as the trifluoroacetamide moiety. This study provides important new mechanistic insights into the use of ultraviolet light to initiate grafting of alkenes onto surfaces.

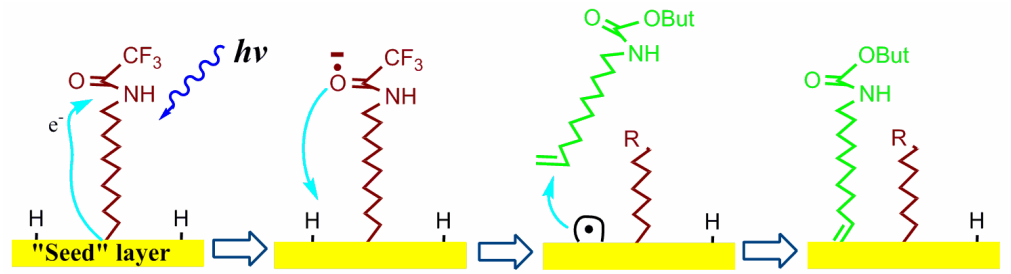

Figure 2.32 Proposed mechanism for the grafting of trifluoroacetic acid protected 10-aminodec-1-ene on amorphous carbon as the seed layers in the grafting of molecules with low reactivity such as 10-*N*-Boc-amino-dec-1-ene.[85]

2.8 Conclusions

In this chapter, some examples of lateral molecular reactions and interactions at surfaces have been discussed, both covalent and noncovalent. It shows that self-assembly using molecular interactions enables the creation of 2D and 3D nanostructures from small building blocks. However, beyond the fundamental interest, the lateral interactions within monolayers have

hardly been addressed. It still requires more effort to fully explain its potential to the fabrication of devices that target specific applications. These will be of great benefit for the development of novel technologies, especially for the fabrication of materials with characteristic length scales of 1-100 nm. The exploration of molecular lateral interactions would be a way to achieve an ultimate level of control in assembling matters for applications in the nanodevices. This thesis describes the versatility of the combined molecular interactions, covalent and noncovalent, in creating functional nano-/microstructures at the interface.

2.9 References

[1] G. M. Whitesides, B. Grzybowski, *Science* **2002**, *295*, 2418.
[2] J. M. Lehn, *Proc. Natl. Acad.Sci. U.S.A.* **2002**, *99*, 4763.
[3] J. M. Lehn, *Chem. Soc. Rev.* **2007**, *36*, 151.
[4] P. Douglas, J. F. Stoddart, *Angew. Chem. Int. Ed.* **1996**, *35*, 1154.
[5] J. Aizenberg, A. J. Black, G. M. Whitesides, *Nature* **1999**, *398*, 495.
[6] S. D. Evans, E. Urankar, A. Ulman, N. Ferris, *J. Am. Chem. Soc.* **1991**, *113*, 4121.
[7] B. Pignataro, *J. Mater. Chem.* **2009**, *19*, 3338.
[8] R. G. Nuzzo, L. H. Dubois, D. L. Allara, *J. Am. Chem. Soc.* **1990**, *112*, 558.
[9] J. C. Love, L. A. Estroff, J. K. Kriebel, R. G. Nuzzo, G. M. Whitesides, *Chem. Rev.* **2005**, *105*, 1103.
[10] J. F. Ford, T. J. Vickers, C. K. Mann, J. B. Schlenoff, *Langmuir* **1996**, *12*, 1944.
[11] J. S. Peanasky, R. L. Mccarley, *Langmuir* **1998**, *14*, 113.
[12] J. K. Lee, Y. S. Chi, J. S. Lee, Y.-G. Kim, Y. H. Jung, E. Oh, S.-B. Ko, H.-j. Jung, P.-S. Kang, I. S. Choi, *Langmuir* **2005**, *21*, 10311.
[13] L. Yan, C. Marzolin, A. Terfort, G. M. Whitesides, *Langmuir* **1997**, *13*, 6704.
[14] S. S. Mark, N. Sandhyarani, C. C. Zhu, C. Campagnolo, C. A. Batt, *Langmuir* **2004**, *20*, 6808.
[15] R. J. Willicut, R. L. Mccarley, *Adv. Mater.* **1995**, *7*, 759.
[16] R. J. Willicut, R. L. Mccarley, *J. Am. Chem. Soc.* **1994**, *116*, 10823.
[17] M. A. Fox, M. D. Wooten, *Langmuir* **1997**, *13*, 7099.
[18] Q. He, Y. Tian, A. Kuller, M. Grunze, A. Golzhauser, J. B. Li, *J. Nanosci. Nanotechnol.* **2006**, *6*, 1838.
[19] D. N. Batchelder, S. D. Evans, T. L. Freeman, L. Haussling, H. Ringsdorf, H. Wolf, *J. Am. Chem. Soc.* **1994**, *116*, 1050.
[20] T. S. Kim, R. M. Crooks, M. Tsen, L. Sun, *J. Am. Chem. Soc.* **1995**, *117*, 3963.
[21] T. Kim, Q. Ye, L. Sun, K. C. Chan, R. M. Crooks, *Langmuir* **1996**, *12*, 6065.
[22] M. D. Mowery, H. Menzel, M. Cai, C. E. Evans, *Langmuir* **1998**, *14*, 5594.
[23] M. D. Mowery, A. C. Smith, C. E. Evans, *Langmuir* **2000**, *16*, 5998.
[24] L. J. Kepley, R. M. Crooks, A. J. Ricco, *Anal. Chem.* **1992**, *64*, 3191.
[25] P. Dutta, P. J. Chapman, P. G. Datskos, M. J. Sepaniak, *Anal. Chem.* **2005**, *77*, 6601.
[26] K. Bandyopadhyay, L. H. Shu, H. Y. Liu, L. Echegoyen, *Langmuir* **2000**, *16*, 2706.
[27] S. Flink, F. C. J. M. van Veggel, D. N. Reinhoudt, *J. Phys. Chem. B.* **1999**, *103*, 6515.

[28] S. Flink, B. A. Boukamp, A. van den Berg, F.C.J.M van Veggel, D. N. Reinhoudt, *J. Am. Chem. Soc.* **1998**, *120*, 4652.
[29] A. J. Moore, L. M. Goldenberg, M. R. Bryce, M. C. Petty, A. P. Monkman, C. Marenco, J. Yarwood, M. J. Joyce, S. N. Port, *Adv. Mater.* **1998**, *10*, 395.
[30] O. Crespo-Biel, C. W. Lim, B. J. Ravoo, D. N. Reinhoudt, J. Huskens, *J. Am. Chem. Soc.* **2006**, *128*, 17024.
[31] P. I. Nagy, K. Takacs-Novak, *J. Am. Chem. Soc.* **2000**, *122*, 6583.
[32] Z. H. Zhu, T. A. Daniel, M. Maitani, O. M. Cabarcos, D. L. Allara, N. Winograd, *J. Am. Chem. Soc.* **2006**, *128*, 13710.
[33] Z. Zhu, B. C. Haynie, N. Winograd, *Appl. Surf. Sci.* **2004**, *231*, 318.
[34] H. F. Ji, R. Dabestani, G. M. Brown, P. F. Britt, *Chem. Commun.* **2000**, 457.
[35] H. F. Ji, T. Thundat, R. Dabestani, G. M. Brown, P. F. Britt, P. V. Bonnesen, *Anal. Chem.* **2001**, *73*, 1572.
[36] G. Valincius, G. Niaura, B. Kazakeviciene, Z. Talaikyte, M. Kazemekaite, E. Butkus, V. Razumas, *Langmuir* **2004**, *20*, 6631.
[37] L. L. Norman, A. Badia, *J. Am. Chem. Soc.* **2009**, *131*, 2328.
[38] M. Sastry, V. Patil, K. S. Mayya, *J. Phys. Chem. B.* **1997**, *101*, 1167.
[39] F. Leveiller, C. Bohm, D. Jacquemain, H. Mohwald, L. Leiserowitz, K. Kjaer, J. Alsnielsen, *Langmuir* **1994**, *10*, 819.
[40] G. M. Credo, A. K. Boal, K. Das, T. H. Galow, V. M. Rotello, D. L. Feldheim, C. B. Gorman, *J. Am. Chem. Soc.* **2002**, *124*, 9036.
[41] A. Doron, M. Portnoy, M. LionDagan, E. Katz, I. Willner, *J. Am. Chem. Soc.* **1996**, *118*, 8937.
[42] S. Reese, M. A. Fox, *J. Phys. Chem. B.* **1998**, *102*, 9820.
[43] Y. Shnidman, A. Ulman, J. E. Eilers, *Langmuir* **1993**, *9*, 1071.
[44] J. Heeg, U. Schubert, F. Kuchenmeister, *Fresenius. J. Anal. Chem.* **1999**, *365*, 272.
[45] J. F. Kang, A. Ulman, S. Liao, R. Jordan, *Langmuir* **1999**, *15*, 2095.
[46] J. F. Kang, A. Ulman, R. Jordan, D. G. Kurth, *Langmuir* **1999**, *15*, 5555.
[47] R. Valiokas, M. Ostblom, S. Svedhem, S. C. T. Svensson, B. Liedberg, *J. Phys. Chem. B.* **2002**, *106*, 10401.
[48] J. H. Kim, H. S. Shin, S. B. Kim, T. Hasegawa, *Langmuir* **2004**, *20*, 1674.
[49] R. S. Clegg, S. M. Reed, J. E. Hutchison, *J. Am. Chem. Soc.* **1998**, *120*, 2486.
[50] R. S. Clegg, J. E. Hutchison, *Langmuir* **1996**, *12*, 5239.
[51] S. Sek, B. Palys, R. Bilewicz, *J. Phys. Chem. B.* **2002**, *106*, 5907.
[52] R. C. Sabapathy, S. Bhattacharyya, M. C. Leavy, W. E. Cleland, C. L. Hussey, *Langmuir* **1998**, *14*, 124.
[53] T. J. Lenk, V. M. Hallmark, C. L. Hoffmann, J. F. Rabolt, D. G. Castner, C. Erdelen, H. Ringsdorf, *Langmuir* **1994**, *10*, 4610.
[54] S. W. Tamchang, H. A. Biebuyck, G. M. Whitesides, N. Jeon, R. G. Nuzzo, *Langmuir* **1995**, *11*, 4371.
[55] P. D. Beer, J. J. Davis, D. A. Drillsma-Milgrom, F. Szemes, *Chem. Commun.* **2002**, 1716.
[56] N. L. Rosi, C. A. Mirkin, *Chem. Rev.* **2005**, *105*, 1547.
[57] B. Samori, G. Zuccheri, *Angew. Chem. Int. Ed.* **2005**, *44*, 1166.

[58] D. Reishus, B. Shaw, Y. Brun, N. Chelyapov, L. Adleman, *J. Am. Chem. Soc.* **2005**, *127*, 17590.
[59] E. Winfree, F. Liu, L. A. Wenzler, N. C. Seeman, *Nature* **1998**, *394*, 539.
[60] J. Fritz, M. K. Baller, H. P. Lang, H. Rothuizen, P. Vettiger, E. Meyer, H. J. Guntherodt, C. Gerber, J. K. Gimzewski, *Science* **2000**, *288*, 316.
[61] C. R. Scriver, A. L. Beaudet, W. S. Sly, D. Valle, B. Childs, K. W. Kinzler, B. Vogelstein, *The Metabolic and Molecular Bases of Inherited Disease, Vol. 2, pp. 2839-2879,* **1995**.
[62] A. Bardea, F. Patolsky, A. Dagan, I. Willner, *Chem. Commun.* **1999**, 21.
[63] A. B. Steel, T. M. Herne, M. J. Tarlov, *Anal. Chem.* **1998**, *70*, 4670.
[64] A. Sisson, L., N. Sakai, N. Banerji, A. Fürstenberg, E. Vauthey, S. Matile, *Angew. Chem. Int. Ed.* **2008**, *47*, 3727.
[65] R. Bhosale, A. Perez-Velasco, V. Ravikumar, R. S. K Kishore, O. Kel, A. Gomez-Casado, P. Jonkheijm, J. Huskens, P. Maroni, M. Borkovec, T. Sawada, E. Vauthey, N. Sakai, S. Matile, *Angew. Chem. Int. Ed.* **2009**, *48*, 6461.
[66] R. S. Clegg, S. M. Reed, R. K. Smith, B. L. Barron, J. A. Rear, J. E. Hutchison, *Langmuir* **1999**, *15*, 8876.
[67] C. J. Vanoss, M. K. Chaudhury, R. J. Good, *Chem. Rev.* **1988**, *88*, 927.
[68] G. E. Fryxell, P. C. Rieke, L. L. Wood, M. H. Engelhard, R. E. Williford, G. L. Graff, A. A. Campbell, R. J. Wiacek, L. Lee, A. Halverson, *Langmuir* **1996**, *12*, 5064.
[69] G. R. Soja, J. R. Mann, D. F. Watson, *Langmuir* **2008**, *24*, 5249.
[70] D. Q. Li, L. W. Moore, B. I. Swanson, *Langmuir* **1994**, *10*, 1177.
[71] H. Nam, M. Granier, B. Boury, S. Y. Park, *Langmuir* **2006**, *22*, 7132.
[72] D. M. Adams, L. Brus, C. E. D. Chidsey, S. Creager, C. Creutz, C. R. Kagan, P. V. Kamat, M. Lieberman, S. Lindsay, R. A. Marcus, R. M. Metzger, M. E. Michel-Beyerle, J. R. Miller, M. D. Newton, D. R. Rolison, O. Sankey, K. S. Schanze, J. Yardley, X. Zhu, *J. Phys. Chem. B.* **2003**, *107*, 6668.
[73] H. O. Finklea, D. D. Hanshew, *J. Am. Chem. Soc.* **2002**, *114*, 3173.
[74] C. E. D. Chidsey, *Science* **1991**, *251*, 919.
[75] F. Hauquier, J. Ghilane, B. Fabre, P. Hapiot, *J. Am. Chem. Soc.* **2008**, *130*, 2748.
[76] A. Wang, C. t. Ornelas, D. Astruc, P. Hapiot, *J. Am. Chem. Soc.* **2009**, *131*, 6652.
[77] Y. Yokota, K. Fukui, T. Enoki, M. Hara, *J. Am. Chem. Soc.* **2007**, *129*, 6571.
[78] A. Paul, R. M. Watson, P. Lund, Y. Xing, K. Burke, Y. He, E. Borguet, C. Achim, D. H. Waldeck, *J. Phys. Chem. C.* **2008**, *112*, 7233.
[79] A. Paul, S. Bezer, R. Venkatramani, L. Kocsis, E. Wierzbinski, A. Balaeff, S. Keinan, D. N. Beratan, C. Achim, D. H. Waldeck, *J. Am. Chem. Soc.* **2009**, *131*, 6498.
[80] Y. Arikuma, K. Takeda, T. Morita, M. Ohmae, S. Kimura, *J. Phys. Chem. B.* **2009**, *113*, 6256.
[81] K. Takeda, T. Morita, S. Kimura, *J. Phys. Chem. B.* **2008**, *112*, 12840.
[82] Q. Wang, S. M. Zakeeruddin, M. K. Nazeeruddin, R. Humphry-Baker, M. Gratzel, *J. Am. Chem. Soc.* **2006**, *128*, 4446.
[83] H. Imahori, H. Norieda, H. Yamada, Y. Nishimura, I. Yamazaki, Y. Sakata, S. Fukuzumi, *J. Am. Chem. Soc.* **2001**, *123*, 100.
[84] H. Imahori, Y. Mori, Y. Matano, *J. Photoch. Photobio. C.* **2003**, *4*, 51.
[85] P. E. Colavita, B. Sun, K. Y. Tse, R. J. Hamers, *J. Am. Chem. Soc.* **2007**, *129*, 13554.

Chapter 3

Imidazolide Monolayers for Reactive Microcontact Printing*

ABSTRACT. Imidazolide monolayers prepared from the reaction of amino SAMs with *N,N*-carbonyldiimidazole (CDI) are used as a versatile platform for surface patterning with amino-, carboxyl- and hydroxyl-functionalized compounds through reactive microcontact printing. To demonstrate the surface reactivity of imidazolide monolayers, direct and inverse fluorescent patterns have been prepared.

---

*Parts of this chapter have been published in: Shu-Han Hsu, David N. Reinhoudt, Jurriaan Huskens and Aldrik H. Velders, Imidazolide monolayers for reactive microcontact printing, *J. Mater. Chem.* **2008**, *18*, 4959–4963

3.1 Introduction

Reactive microcontact printing (μCP) is a method to generate surface patterns on homogeneous self-assembled monolayers (SAMs) via covalent bond formation. Whitesides *et al.* have utilized such an approach for patterning reactive carboxylic anhydride SAMs[1] or pentafluorophenyl ester SAMs[2] resulting in amide formation. Huck *et al.* synthesized peptides by printing *N*-protected amino acids onto amino SAMs.[3] Our group demonstrated imine formation through the μCP of amines on aldehyde SAMs[4, 5] and triazole formation by the Sharpless ‘‘click’’ chemistry without a Cu catalyst by printing acetylenes onto azido SAMs.[5] However, there are only few methods available for the modification of SAMs on a surface after their assembly. A reactive *N,N*-carbonyldiimidazole (CDI)-activated amino monolayer can anchor amino-, carboxyl- or alcohol-containing molecules onto a surface by urea, amide, and carbamate formation, respectively, through μCP. This allows preparation of patterned SAMs in a fast and simple way over large areas, and with a large variety in chemistry, on the same substrate.

CDI is highly reactive and widely used to activate amino, carboxyl, or alcohol groups to form different carbonyl imidazole intermediates which can react further for different bond formations. [6-10] Keizer *et al.* and Rannard *et al.* reported high selectivities for the reaction of imidazole intermediates in the consecutive reaction with amines or hydroxy compounds, which can be explained by an asymmetric reactivity of CDI.[8, 9, 11, 12] Apart from as activating agent,[10, 13, 14] the immobilization of CDI on surfaces has not been investigated for surface patterning by reactive μCP.

A new activated SAM use CDI for constructing binary-component SAMs of different bond formations by μCP. This reactive μCP provides a method to afford direct patterns, as well as reverse patterns, where the surface reactivity of the non-reacted imidazolide monolayer can be studied by back-filling with a second type of molecule (Figure 3.1).

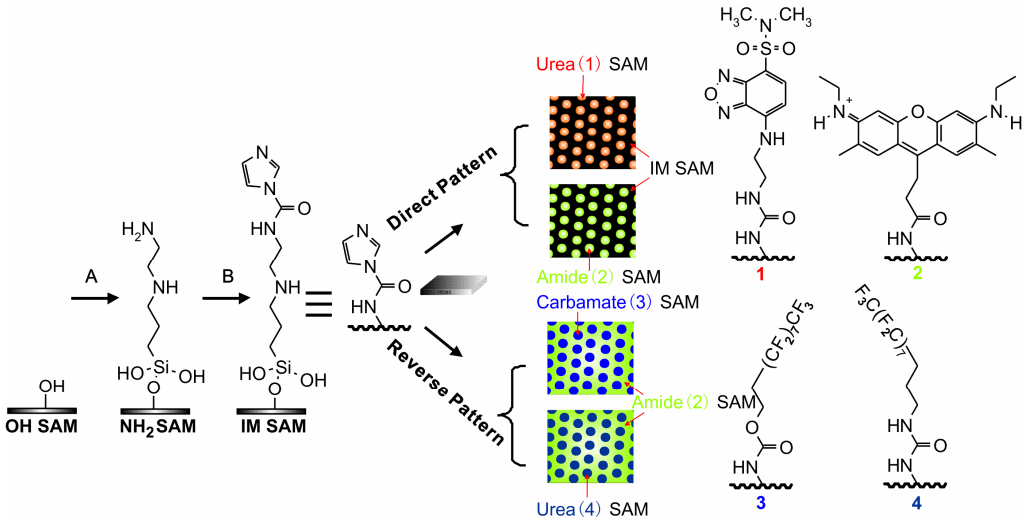

Figure 3.1 Schematic representation of the procedure for imidazolide SAM (IM SAM) preparation: A) TPEDA, B) CDI in THF. Direct patterns were prepared by printing 4-(2-aminoethylamino)-7-(*N*,*N*-dimethylsulfamoyl)benzofurazan (ADF) (**1**) and Atto520 (**2**) onto an IM SAM; reverse patterns were prepared by first printing, 1*H*,1*H*,2*H*,2*H*-heptadecafluorodecanol (HPFO) (**3**) or heptadecafluoroundecylamine (HPFA) (**4**) onto an IM SAM followed by Atto520 incubation.

3.2 Results and discussion

Formation of imidazolide SAMs. Silicon oxide or glass substrates (1 cm × 1 cm, activated with piranha solution) were functionalized with an amino-terminated monolayer prepared with *N*-([3-(trimethoxysilyl) propyl]ethylenediamine) (TPEDA) (Figure 3.1 NH_2 SAM). The amino SAMs were converted into imidazolide SAMs (IM SAM) by reaction with CDI in THF at room temperature under a nitrogen atmosphere. It is critical to maintain anhydrous conditions during the reaction with CDI since the reagent decomposes almost instantly on contact with water.[15]

Table 3.1 Advancing θ_a (º) and receding θ_r (º) water contact angles, atomic ratios of C and N from XPS of SAMs shown in Figure 3.1.

SAMs	θ_a(°)	θ_r(°)	C:N (XPS)	C:N (calcd)
NH_2 SAM	68 ± 2	55 ± 2	2.7 ± 0.2	2.5
IM SAM	52 ± 2	27 ± 1	2.5 ± 0.2	2.3

Water contact angle measurements show an advancing contact angle of 68° and a small hysteresis (13°) for the NH_2 SAM suggesting that the SAM is well packed.[16] For the IM SAM, a clear change in the polarity of the surface is observed as witnessed by the drop in advancing contact angle to 52°. The hysteresis is relatively large (25°), and might be the result of surface imperfections. Further evidence for the formation of imidazolide groups on the IM SAM stems from the peaks at 287.8 and 288.9 eV in the XPS C1s spectrum, which are characteristic for the N–C(O)–N carbon and N–C–N of the imidazolide intermediate (Figure 3.2).

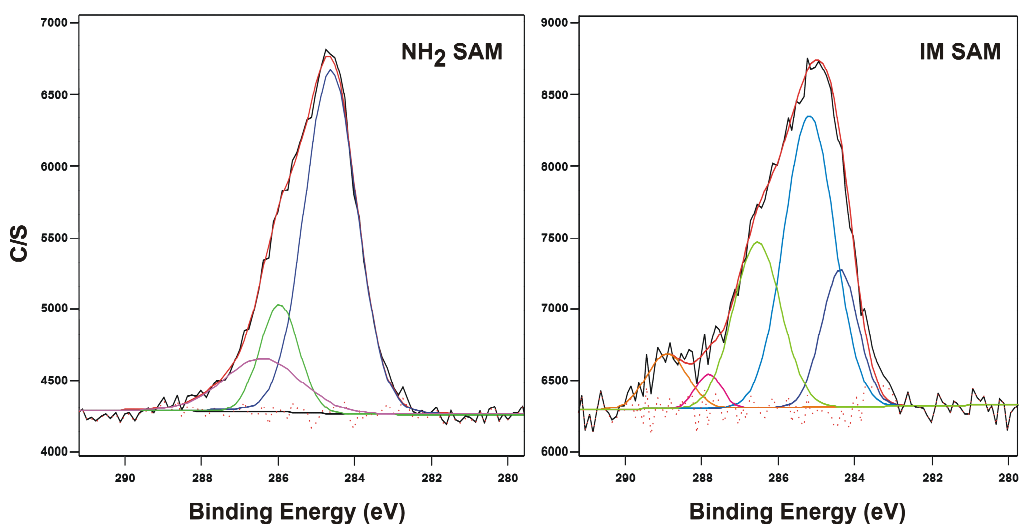

Figure 3.2 X-ray photoelectron spectra of C_{1s} for NH_2 SAM and IM SAMs on silicon oxide. The IM SAM spectrum shows two new peaks at 287.8 and 288.9 eV relatively to the NH_2 SAM spectrum.

FTIR analysis (Figure 3.3) of NH_2 SAM reveals a broad band between 3000 cm^{-1} and 3500 cm^{-1} and two bands at 2943 cm^{-1} and 2851 cm^{-1} that can be assigned to the stretching of the amino group (and possibly some adsorbed water) and to the symmetric CH_2 and asymmetric CH_2 stretching vibrations, respectively. After exposure of the NH_2 SAM to CDI, a new peak appears at 3025 cm^{-1}, typical for the aromatic carbon–hydrogen stretching vibration of the imidazolide intermediate, providing evidence for the formation of an imidazolide-terminated monolayer (IM SAM). Further, a SAM derived from IM SAM incubated with 1*H*,1*H*,2*H*,2*H*-heptadecafluorodecanol (HPFO SAM) shows typical C–F stretchings[17] at 1377 cm^{-1} and 1261 cm^{-1} besides a strong CH_2 stretching. The loss of the aromatic carbon–hydrogen stretching vibration at 3025 cm^{-1} indicates the successful covalent attachment of the HPFO to the imidazolide monolayer.

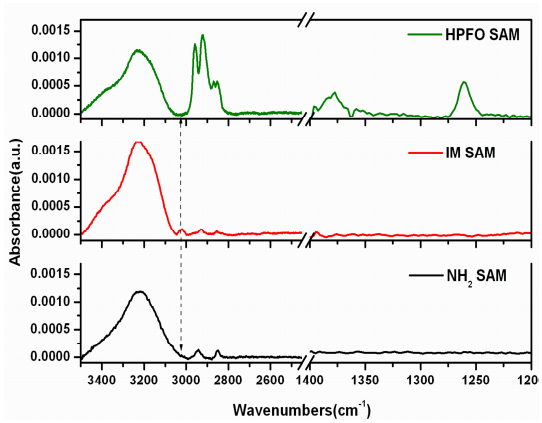

Figure 3.3 FTIR spectra of NH_2 SAM, IM SAM and HPFO SAM.

Patterning of SAMs by microcontact printing. In order to study the surface reactivity of the IM SAM, μCP was used to obtain surface patterns with fluorescent molecules. Two methods were applied to obtain patterns: (Figure 3.1): (i) the surface patterns were prepared by printing 4-(2-aminoethylamino)-7-(*N,N*-dimethylsulfamoyl)-benzofurazan (ADF) (Fluka) or Atto520 (Fluka) onto an IM SAM yielding urea and amide formation, respectively, (direct pattern); (ii) the surfaces were first patterned by printing the non-fluorescent heptadecafluoroundecylamine (HPFA) or 1*H*,1*H*,2*H*,2*H*-heptadecafluorodecanol (HPFO) followed by back-filling the

remaining reactive imidazolide-functionalized area with Atto520 (reverse pattern). The latter binary component SAMs are composed of urea (HPFA) – amide (Atto520) or carbamate (HPFO) – amide (Atto520) patterns.

In the first, direct patterning protocol, ADF was microcontact printed as 100 µm dots separated by 20 µm on NH_2 and IM SAMs. The PDMS stamp was oxidized with oxygen plasma for 1 min in order to increase the wettability and improve the spreading of the polar ink on the stamp. Directly after oxidation, the stamp was inked with ADF (1 mM), dried with nitrogen and brought into conformal contact with the SAMs on glass slides. Different printing times were applied ranging from 5 - 40 min. The substrates were vigorously rinsed and sonicated in MilliQ for 10 min directly after printing. When IM SAMs were used, the fluorescence patterns were clearly visible with fluorescence microscopy after 5 min printing. The intensity of the patterns printed with IM SAMs increased in time and leveled off after 20 min. Instead, the intensity profiles of the NH_2 SAMs showed consistent relatively weak patterns, which might come from the physisorption of ADF. The results indicate the successful covalent immobilization of ADF on the IM SAMs (Figure 3.4 A,B,C,D) compared with the NH_2 SAMs (Figure 3.4 E,F,G,H).

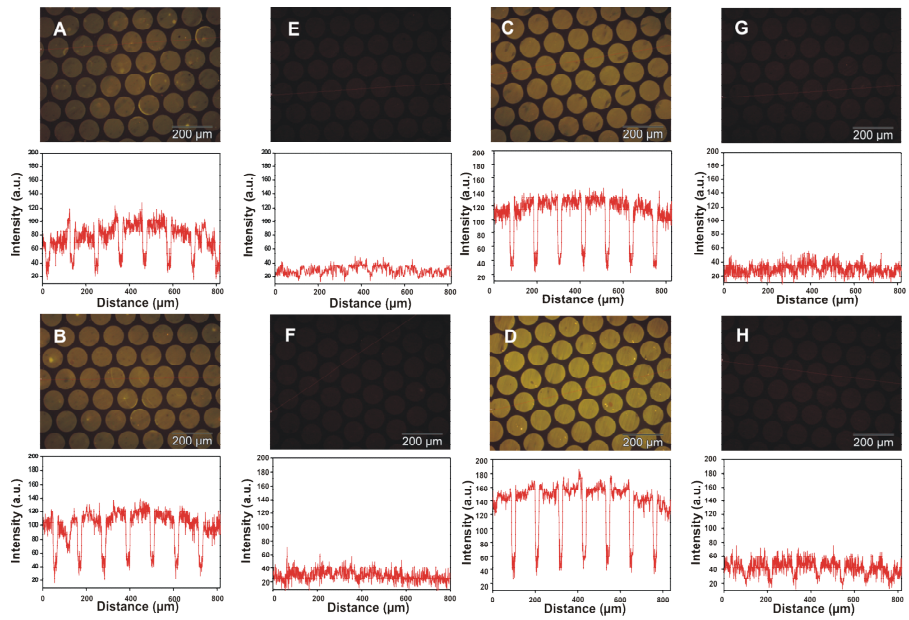

Figure 3.4 Fluorescence microscopy images (884 µm x 666 µm) of 100 µm ADF printed dots onto IM (A,B,C,D) and NH_2 SAMs (E,F,G,H) for 5 min, 10 min, 15 min, and 20 min.

A kinetic study of both the urethane and the amide formation (see Figure 3.5) shows the intensity profile of Atto520 printed patterns to level off after 1 h, which is relatively slow compared to ADF printing which reaches the maximum profile intensitiy after 20 min. Compared to amino groups, carboxylic acids react more slowly with CDI. A possible reaction mechanism for the amide formation on the surface is the attack on the carbonyl carbon of the imidazolide by the oxygen of the acid, followed by the liberation of carbon dioxide, similar to the acyl imidazole formation from carboxylic acids with CDI.[15, 18-20] Therefore, a longer printing time was applied for the amide formation by µCP with Atto520 (1 mM). The stamp was removed after 1 h and the substrates were rinsed with an acetate buffer (pH ~ 6.3) to remove any physisorbed material. The high degree of immobilization of Atto520 is shown from the higher intensity profile on the IM SAM compared to the NH_2 SAM (Figure 3.6).

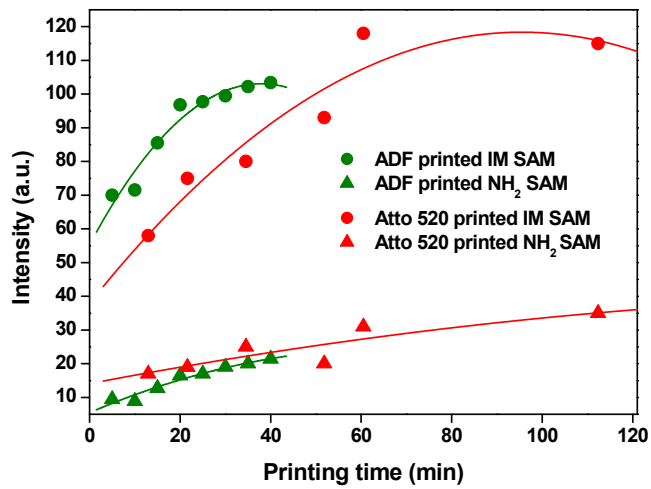

Figure 3.5 Reaction rate of ADF and Atto520 printed onto IM SAM and NH_2 SAM.

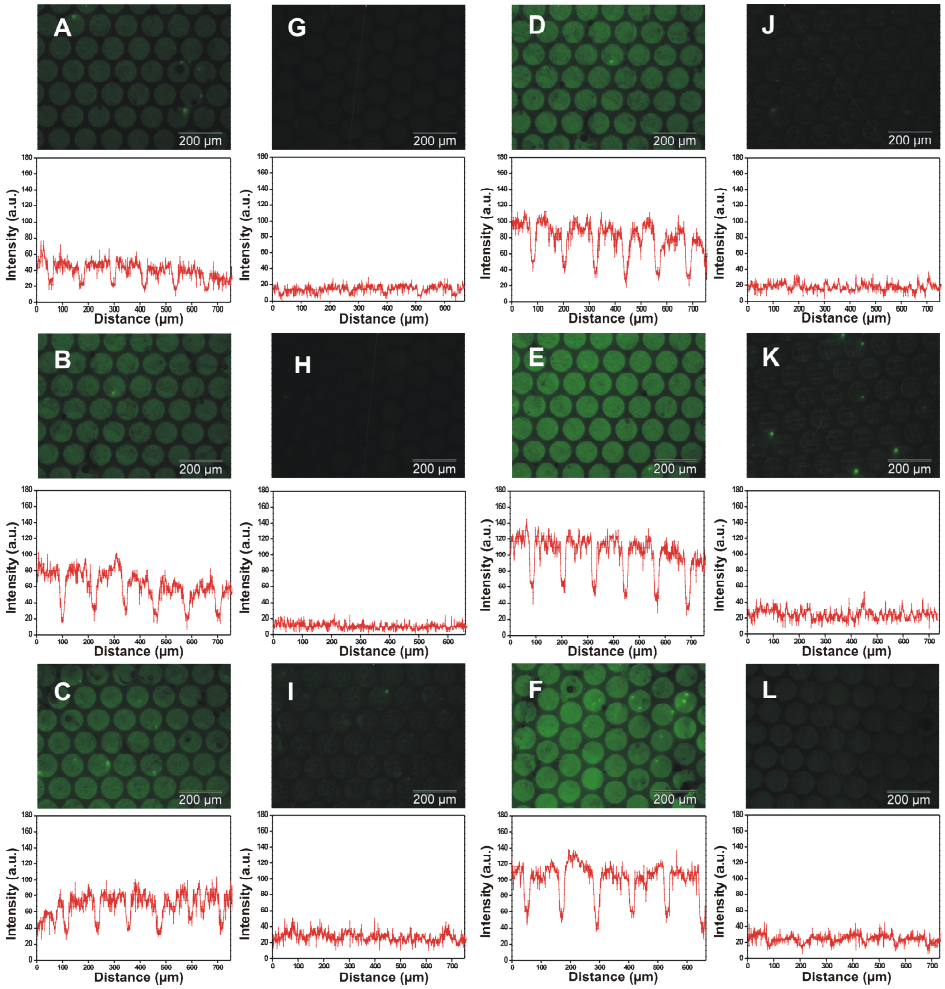

Figure 3.6 Fluorescence microscopy images (884 µm x 666 µm) of 100 µm Atto520 printed dots onto IM (A,B,C,D,E,F) and NH_2 SAMs (G,H,I,J,K,L) for 5 min, 15 min, 30 min, 50 min, 1 h and 2 h.

Physisorption likely occurs via electrostatic interaction. It is in fact possible to have such interactions between the NH_2 SAM and the printed amino- and carboxylic acid-containing molecules. Instead, for the IM SAM, the lack of charge in the imidazolide group can reduce the non-specific adsorption effects with the printing molecules.[10] In this case, the specific covalent attachment of the introduced molecules on the reactive support (IM SAM) is required for efficient and stable profile formation. In addition, a reference molecule was synthesized with a boc-protected amino group, i.e. boc-ADF, which appears

unable to form stable profiles by µCP on the IM SAM , which demonstrate the specific reaction of the amino-containing ADF molecules with the IM SAM, (see Figure 3.7).

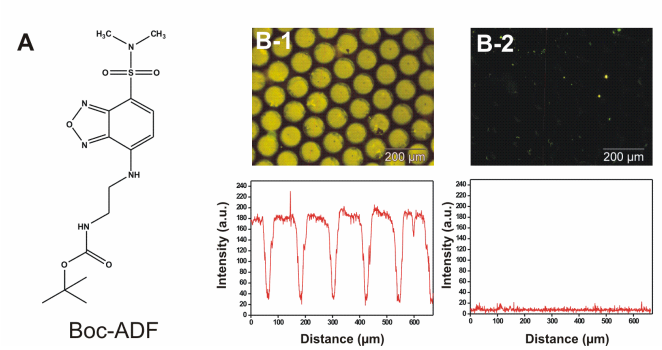

Figure 3.7 Fluorescence microscopy image (884 µm x 666 µm) of Boc-ADF (1 mM in acetonitrile) printed 100 µm diameter dots onto IM SAM for 20 min before (A) and after (B) MilliQ rinsing.

In order to evaluate the reactivity of the IM SAM in the non-printed areas after the printing and washing procedure, reverse patterns were prepared on NH_2 and IM SAMs. To this purpose, the non-fluorescent HPFA or HPFO was printed on an IM SAM for 1 h and the remaining imidazolide-terminated areas were back-filled from solution with Atto520 overnight (Figure 3.8)**.**

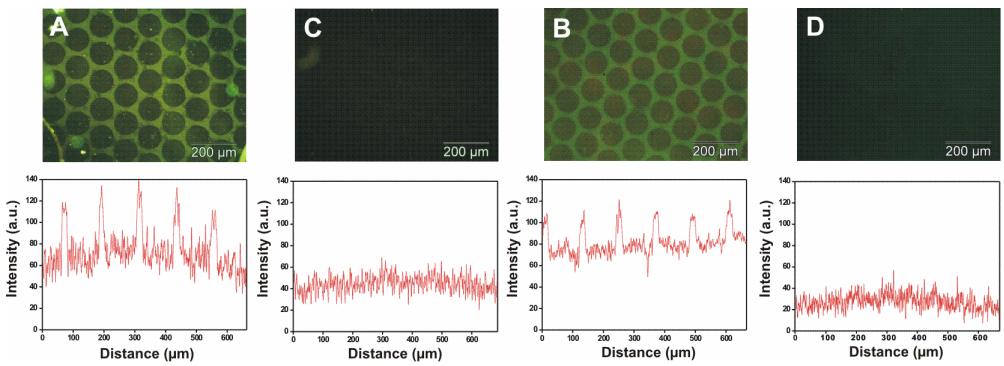

Figure 3.8 HPFA (A,C) and HPFO (B,D) (10 mM) were printed in 100 µm dots onto IM (A,B) and NH_2 SAMs (D,E) for 1 h. The remaining areas were back-filled with a 0.1 mM solution of Atto520.

HPFA and HPFO were chosen for their better water-repelling properties compared to regular alkyl-chain molecules. Rinsing and sonication with acetate buffer for 10 min were applied as described above. The intensity plots show the covalent binding of Atto520 in the non-contacted IM SAM areas as expected, but to a lesser extent also in the contacted HPFA/HPFO SAM areas. From these results, one can conclude that the imidazolide groups on the HPFA or HPFO printed areas have not all fully reacted, or that the Atto520 molecules are included in between the long fluorocarbon chains. The profile of the reverse patterns still shows the success of surface modification of the non-printed area of the IM SAM with the fluorescent dyes. It is also possible to functionalize the non-printed area by featureless stamp μCP instead of back-filling from solution, which is currently under further investigation.

3.3 Conclusions

In conclusion, using CDI, a new reactive SAM was successfully prepared and characterized by contact angle measurements, X-ray photoelectron spectroscopy, and grazing-angle infrared spectroscopy. Moreover, the reactivity of the imidazolide SAM was studied through the reaction with amino-, carboxyl-, and alcohol-containing molecules to form, respectively, the selective urea, amide, and carbamate covalent bonds by μCP. Also, the reverse pattern experiments provide the evidence of the remaining surface activity of imidazolide SAM for further introducing molecules on the same surface.

A wide variety of reactions are known with the imidazolide group: besides the good reactivity with amino-, carboxyl- and alcohol groups, the imidazole functionalities, for example, also react with thiols to form thiolcarbamates.[18] Herein, the same approaches for carboxylic acid or alcohol activation are under investigation to form different imidazolide-activated monolayers. This method constitutes a powerful strategy to provide specific coupling of a variety of functional groups with simultaneous protection from nonspecific adsorption on surface due to the lack of a charge of the introduced imidazolide SAM.[10] The imidazolide SAMs presented in this chapter serve as useful “platforms” which can be utilized to anchor a variety of functional groups by microcontact printing and open a broad window for surface patterning.

3.4 Experimental

Materials. The following materials and chemicals were used as received without further purification: *N*-([3-(trimethoxysilyl)propyl]ethylenediamine) 97% (TPEDA) (Aldrich), *N,N*-carbonyldiimidazole (CDI) (Aldrich), poly(dimethylsiloxane) (PDMS) (Dow Corning), 4-(2-aminoethylamino)-7-(*N*,*N*-dimethylsulfamoyl)benzofurazan (ADF) (Fluka), Atto520 (Fluka), Heptadecafluoroundecylamine (HPFA) (Fluka), and 1*H*,1*H*,2*H*,2*H*-heptadecafluorodecanol (HPFO) (ABCR). All other solvents used were HPLC grade purchased from either Aldrich or Sigma. MilliQ with a resistivity higher than 18 MΩ·cm was used in all experiments.

Synthesis of Boc-ADF. 4-(2-Aminoethylamino)-7-(*N*,*N*-dimethylsulfamoyl)benzofurazan (25 mg, 0.0876 mmol) was dissolved in 25 ml of water/chloroform (50:50 v/v) in the presence of sodium hydroxide (5.25 mg, 0.0131 mmol). After stirring for 15 min, di-*tert*-butyl dicarbonate (Boc_2O) (19.12 mg, 0.0876 mmol) was added at 0 ºC, and the reaction mixture was allowed to stand overnight at room temperature. The reaction was extracted with 4 x 50 ml of chloroform. The organic layer was dried over $MgSO_4$ and the solvent was evaporated under reduced pressure. The residue was purified by column chromatography (SiO_2, dichlomethane/methanol = 98:2) to give the desired product in 63% yield as a yellow powder (15.75 mg).^{1}H NMR (300 MHz, $CDCl_3$, 20 ºC,TMS) δ: 7.83 (d, J = 7.8 Hz, 1H), 6.06 (d, J = 7.8 Hz, 1H), 3.43 (m, 2H, CH_2), 3.12 (m, 2H, CH_2), 2.79 (s, 6H, CH_3), 1.39 (s, 9H, CH_3) ppm.

Substrate and monolayer preparation. Single-side and double-side polished silicon substrates (100), p-doped 2 x 2 cm silicon substrates, quartz, and microscope glass slides were used for monolayer preparation. The substrates were oxidized with piranha solution for 15 min (concentrated H_2SO_4 and 33% aqueous H_2O_2 in a 3:1 ratio; Caution: piranha should be handled carefully) and rinsed with MilliQ. After drying with a nitrogen stream, the substrates were used immediately for providing a freshly hydroxyl-terminated surface. The substrates were enclosed in a low vacuum chamber desiccator with 0.1 ml of TPEDA, continually pumping for 2 min to create a full atmosphere of vapor phase TPEDA. After overnight incubation, the slides were rinsed with ethanol and dichloromethane to remove any excess of silanes and subsequently dried with a nitrogen stream. The amino-

terminated substrates were incubated with a saturated CDI solution in freshly distilled THF in a nitrogen box overnight. After imidazolide monolayer formation, the substrates were removed from the nitrogen box, rinsed with distilled THF, and followed by drying with nitrogen. All samples were freshly prepared and used immediately after drying. HPFO SAM was prepared by incubation of the IM SAM with 2.5 mM 1*H*,1*H*,2*H*,2*H*-heptadecafluorodecanol in THF overnight.

Microcontact printing. Stamps were prepared by casting a 10:1 (v/v) mixture of poly(dimethylsiloxane) and curing agent (Sylgard 184, Dow Corning) against a silicon master. After overnight curing at 60 ºC, the stamps were oxidized by oxygen plasma for 1 min and subsequently inked by dropping an aqueous adsorbate solution onto the stamp. For the ink prepared with acetonitrile, the stamps were used without oxidization. Before printing, the stamps were dried in a stream of nitrogen. The stamps were brought into conformal contact with the substrate by applying 30 g force. The stamps were changed for each new printing step and the same inking procedure was repeated. The stamp was inked with a solution of ADF (1 mM in MilliQ), Atto520 (1mM in MilliQ) for 5 min, dried under a nitrogen flow, and brought into conformal contact with the imidazolide-terminated glass slides. After stamp removal, the substrates printed with ADF were rinsed with a copious volume of water, sonicated in MilliQ water for 10 min, blown dry with nitrogen and imaged with fluorescence microscopy. For the substrates printed with Atto520, the surface was rinsed with the acetate buffer (pH~6.3) and sonicated for 10 min. A stamp was inked with a solution of HPFA and HPFO for 30 s, dried under a nitrogen flow, and brought into conformal contact with the imidazolide-terminated glass slides for 1 h. After 1 h, the stamp was removed and the substrate rinsed with a copious volume of dichloromethane and blown dry with nitrogen. The remaining area was incubated with 0.1 mM Atto520 prepared in MilliQ water overnight. The samples were sonicated in the acetate buffer for 10 min before imaging with fluorescence microscopy.

Fluorescence microscopy. Fluorescence microscopy images were taken using an Olympus inverted research microscope IX71 equipped with a mercury burner U-RFL-T as light source and a digital Olympus DR70 camera for image acquisition. Blue excitation

(450 nm ≤ λ_{ex} ≤ 480 nm) and green emission (λ_{em} ≥ 515 nm) was filtered using a U-MWB Olympus filter cube. Green excitation (510 nm ≤ λ_{ex} ≤ 550 nm) and red emission (λ_{em} ≥ 590 nm) was filtered using a U-MWG Olympus filter cube. All fluorescence microscopy images were acquired in air.

Contact angle measurements. Contact angles were measured with Millipore water (18.2 MΩ·cm) on a Krüss G10 Contact Angle Measuring Instrument, equipped with a CCD camera. Advancing and receding angles (θ_{adv} and θ_{rec}) were determined automatically during growth and shrinkage of the droplet by a drop shape analysis software.

XPS. XPS spectra were obtained on a Physical Electronics Quantera Scanning X-ray Multiprobe instrument, equipped with a monochromatic $Al_{K\alpha}$ X-ray source operated at 1486.6 eV and 26.18 W. Spectra were referenced to the main C 1s peak set at 284.0 eV. The X-ray beam size was 100 μm and the data were collected from surface areas of 100 μm x 300 μm with a pass energy of 224 eV and a step energy of 0.8 eV for survey scans and 0.4 eV for high resolution scans. For quantitative analysis, the sensitivity factors used to correct the number of counts under each peak were: C 1s, 1.00; N 1s, 1.59. The measurement was collected after 25 cycles scanning.

FTIR. Transmission FTIR spectra (spectral resolution of 8 cm^{-1}, 1024 scans) were obtained using a BIO-RAD FTS575C FTIR spectrometer equipped with a nitrogen-cooled cryogenic mercury telluride detector. Background spectra were obtained by scanning a clean silicon substrate.

3.5 Acknowledgements

The authors are grateful to Gerard A. M. Kip for XPS and to Dr Laura Puig for making valuable comments.

3.6 References

[1] N. Horan, L. Yan, H. Isobe, G. M. Whitesides, D. Kahne, *Proc. Natl. Acad. Sci. U.S A.* **1999**, *96*, 11782.

[2] J. Lahiri, E. Ostuni, G. M. Whitesides, *Langmuir* **1999**, *15*, 2055.

[3] T. P. Sullivan, M. L. van Poll, P. Y. W. Dankers, W. T. S. Huck, *Angew. Chem. Int. Ed.* **2004**, *43*, 4190.

[4] D. I. Rozkiewicz, B. J. Ravoo, D. N. Reinhoudt, *Langmuir* **2005**, *21*, 6337.

[5] D. I. Rozkiewicz, D. Janczewski, W. Verboom, B. J. Ravoo, D. N. Reinhoudt, *Angew. Chem. Int Ed.* **2006**, *45*, 5292.

[6] A. Nefzi, R. A. Mimna, R. A. Houghten, *J. Comb. Chem.* **2002**, *4*, 542.

[7] M. D. McReynolds, K. T. Sprott, P. R. Hanson, *Org. Lett.* **2002**, *4*, 4673.

[8] S. P. Rannard, N. J. Davis, *J. Am. Chem. Soc.* **2000**, *122*, 11729.

[9] S. P. Rannard, N. J. Davis, *Org. Lett.* **2000**, *2*, 2117.

[10] I. N. Aretaki, P. Koulouridakis, N. Kallithrakas-Kontos, *Anal. Chim. Acta* **2006**, *562*, 252.

[11] H. M. Keizer, R. P. Sijbesma, E. W. Meijer, *Eur. J. Org. Chem.* **2004**, 2553.

[12] S. P. Rannard, N. J. Davis, *Org. Lett.* **1999**, *1*, 933.

[13] S. Pathak, A. K. Singh, J. R. McElhanon, P. M. Dentinger, *Langmuir* **2004**, *20*, 6075.

[14] T. Bocking, K. A. Kilian, T. Hanley, S. Ilyas, K. Gaus, M. Gal, J. J. Gooding, *Langmuir* **2005**, *21*, 10522.

[15] R. Paul, G. W. Anderson, *J. Am. Chem. Soc.* **1960**, *82*, 4596.

[16] L. Basabe-Desmonts, J. Beld, R. S. Zimmerman, J. Hernando, P. Mela, M. F. G. Parajo, N. F. van Hulst, A. van den Berg, D. N. Reinhoudt, M. Crego-Calama, *J. Am. Chem. Soc.* **2004**, *126*, 7293.

[17] T. Auletta, B. Dordi, A. Mulder, A. Sartori, S. Onclin, C. M. Bruinink, M. Peter, C. A. Nijhuis, H. Beijleveld, H. Schonherr, G. J. Vancso, A. Casnati, R. Ungaro, B. J. Ravoo, J. Huskens, D. N. Reinhoudt, *Angew. Chem. Int. Ed.* **2004**, *43*, 369.

[18] J. A. Grzyb, M. Shen, C. Yoshina-Ishii, W. Chi, R. S. Brown, R. A. Batey, *Tetrahedron* **2005**, *61*, 7153.

[19] P. J. Dunn, W. Hoffmann, Y. Kang, J. C. Mitchell, M. J. Snowden, *Org. Process Res. Dev.* **2005**, *9*, 956.

[20] R. H. Liu, L. E. Orgel, *Orig. Life Evol. Biosph.* **1998**, *28*, 47.

Chapter 4

Reporter Surfaces for Orthogonal Covalent and Noncovalent Immobilization

ABSTRACT. Fluorescent reporter surfaces were prepared using alkyne-terminated coumarins and consecutively functionalized by reactive microcontact printing azido-β-cyclodextrin. The resulting surface allows orthogonal covalent and supramolecular "host-guest" functionalization, and its specificity as well as selectivity were demonstrated by sequential and one-step printing procedures.

---

*Parts of this chapter have been submitted in: Arántzazu González-Campo, Shu-Han Hsu, Laura Puig, Jurriaan Huskens, David N. Reinhoudt, Aldrik H. Velders

4.1 Introduction

The concept of orthogonal self-assembly as the selective immobilization of multicomponent systems on heterogeneous substrates was first introduced by Wrighton and Whitesides.[1-3] For many interface applications, orthogonality is a prerequisite and different strategies have been reported to prepare patterned surfaces with orthogonal modification or functionalities. Photolithography has widely been used to pattern surfaces for subsequent orthogonal self-assembly of particles, polymers, and carbohydrates,[4-6] and Gleason *et al*. made patterned orthogonal nanodomains with amine and acetylene groups using capillary force lithography.[7] Soft lithography techniques like μCP[8-10] can be used to covalently couple molecules onto reactive or preactived surfaces, e.g. via amide,[11-14] imine,[15] urethane or carbamate[11-14] bond formation. Cu(I)-catalyzed Huisgen 1,3-dipolar cycloaddition of azide and alkynes, so-called "click chemistry",[16] has also been applied for surface modification [17] and for reactive μCP.[18, 19] An illustrative example of a functional surface allowing reversible interactions is the so-called molecular printboard,[20-22] a monolayer of β-cyclodextrins (β-CD), which has been used to immobilize small molecules, dendrimers, particles and biomolecules from solution,[23-26] and by supramolecular μCP.[27,28] A surface with orthogonal functionalities was reported, patterning heptakisazido-β-cyclodextrin (N_3-βCD) on surface-immobilized alkyne-terminated coumarins by μCP. The resulting orthogonal surface provides selectivity and specificity by allowing covalent bond formation on the alkyne-terminated patterns, and supramolecular, host-guest, interactions on the β-CD patterns. Both modalities can be addressed independently, from solution as well as through μCP.

The fluorescence properties of coumarin derivatives are influenced by substitutions at the 3- and 7-positions.[29, 30] Ellman *et al.*[31] and Yao *et al*.[32] have used this property to prepare coumarin-based fluorogenic microarrays for detection of hydrolytic enzymes, where a fluorescent coumarin is produced after a bond breakage. Here surface-immobilized coumarins were used as fluorescent reporters for probing reactive μCP, showing a fluorescent "fingerprint" of patterned monolayers after "click printing".

A patterned surface with orthogonal functional reactivities is demonstrated, combining reactive alkyne and functional cyclodextrin patterns on one surface, allowing simultaneous or consecutive reactive and/or supramolecular microcontact printing (μCP) functionalization, through covalent and noncovalent chemistry.

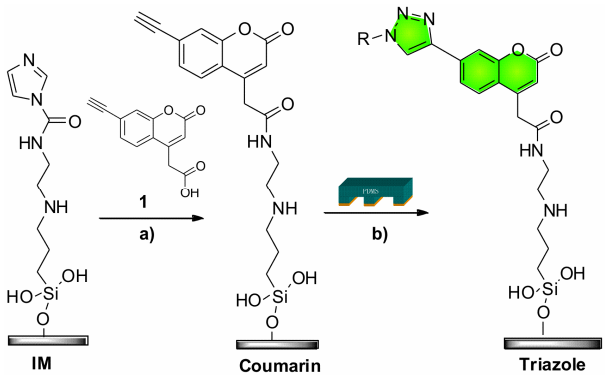

Scheme 4.1 Schematic representation of the triazole monolayer formation. a) Incubation of the IM monolayer with a solution of coumarin profluorogenic probe 1 in dry THF for 36 h. b) Click chemistry with azide-modified derivatives (N_3-R) by μCP with and without Cu^I catalyst.

4.2 Results and discussion

Preparation of triazole monolayer with decylazide. To probe the reactive μCP, fluorescent reporting alkyne-coumarin monolayers were prepared from a bifunctional profluorogenic probe **1** (Scheme 4.1) that shows an increase of the fluorescence quantum yield of 27% upon the triazole ring formation.

Coumarin-terminated monolayers were prepared by incubating imidazolide monolayers [11] in a solution of coumarin **1** in THF (1 mM) for 36 h at room temperature (Scheme 4.1). The surface reactivity of the coumarin monolayer as well as its utilization as reporter surface for reactive μCP, was proven using alkyl azides preparing full triazole monolayer surfaces in presence and absence of the Cu^I catalyst (Scheme 4.1).

Table 4.1 Atomic ratios of C and N from XPS of the monolayers (without Cu^I).

Monolayer	$C/N_{(XPS)}$	$C/N_{(calc)}$
NH_2	2.7 ± 0.2	2.5
IM	2.3 ± 0.2	2.25
coumarin	9.5 ± 0.5	9
Triazole	6.2 ± 0.4	5

Without Cu^{I} catalyst, non-oxidized stamps were inked with a solution of decylazide (18 mM in acetonitrile) for 10 min, dried under nitrogen flow and brought into conformal contact with the coumarin monolayer with a load of 30 g for 1 or 4 h. After stamp removal, the substrates were rinsed with a copious volume of acetonitrile and ethanol, and blown dry with nitrogen. Monolayer formation was monitored by XPS, FT-IR analysis, and fluorescence microscopy.

The XPS analysis showed a marked increase in the C1s spectrum after the incubation of the IM monolayers with **1**, which indicates the formation of a coumarin monolayer and the subsequent triazole monolayer. Further evidence for the formation of the coumarin monolayers stems from the clear peaks at 289 eV in the XPS C1s spectrum, which are consistent with the carbamates N-C(=O)-O and the aromatic O-C=O carbons. The C/N ratio of the IM monolayer and coumarin monolayer found by XPS is in agreement with the chemical composition (Table 4.1). After the cycloaddition reaction a decrease of the C/N ratio was observed resulting from the triazole ring formation.

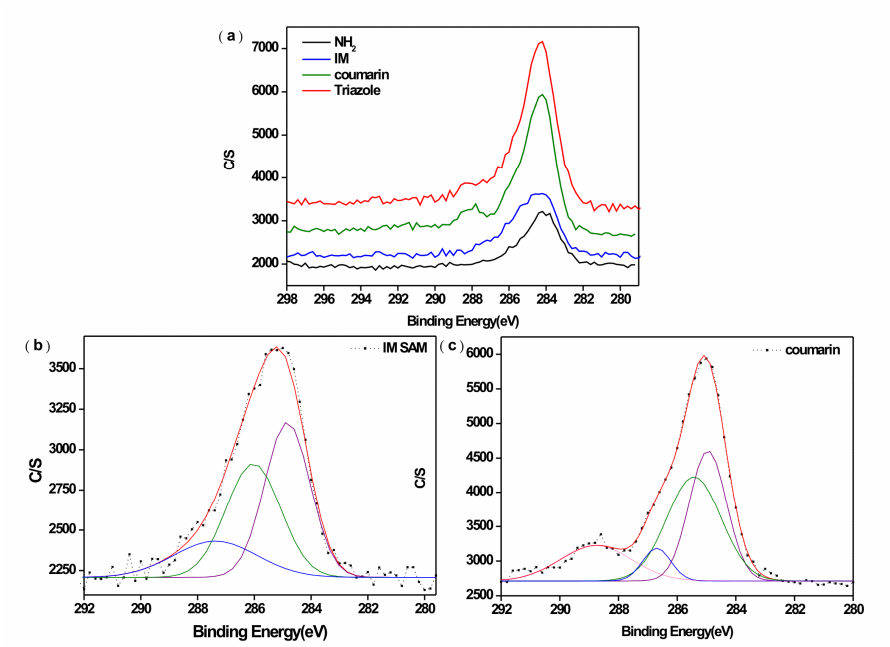

Figure 4.1 X-Ray photoelectron spectra of (a) C1s for NH_2, IM, coumarin and triazole monolayers on silicon oxide (after printing for 4 h without Cu^{I}); and the resolved C1s spectra of (b) IM monolayer and (c) coumarin monolayer.

The disappearance of the typical aromatic carbon-hydrogen stretching vibration at 3025 cm^{-1} of the IM monolayer as well as the appearance of new bands at 3317, 3000, and 2050 cm^{-1} are attributed to the H-C≡C, C_{Ar}-H and C≡C stretching modes, respectively, which provides the evidence for the formation of the coumarin monolayer. After 1 hr printing the presence of the peaks at 3317 and 2050 cm^{-1} indicate an incomplete cycloaddition. After 4 hr printing the absence of those bands and the appearance of new bands at around 3100 cm^{-1} indicate a higher conversion of the alkyne group to triazole (Figure 4.2).

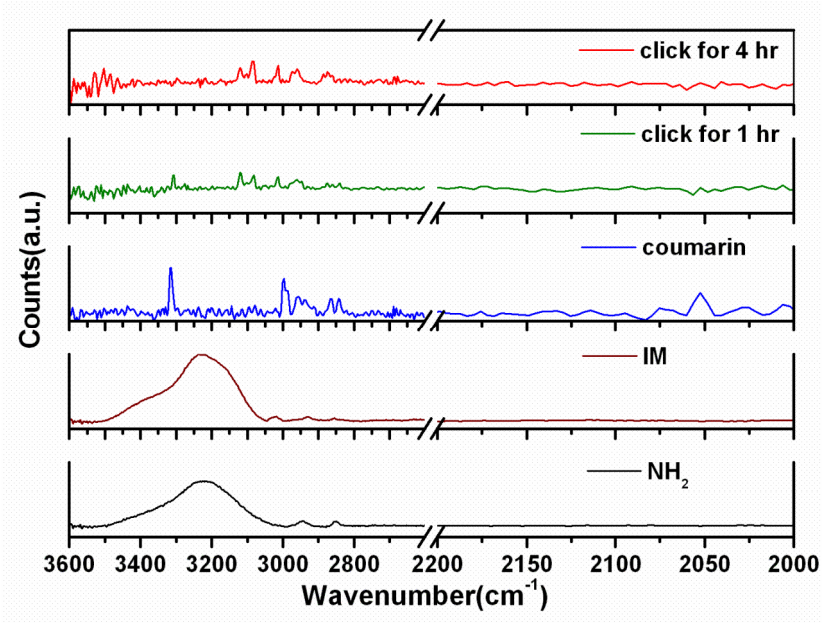

Figure 4.2 FT-IR spectra of NH_2, IM, coumarin, and triazole monolayers after printing for 1 and 4 h without Cu^I.

With the Cu^I reagent-stamping method[18], non-oxidized stamps were inked with a solution of decylazide (18 mM in acetrontrile), one drop of a solution of $Cu(OAc)_2$ (1 mM) in EtOH, and one drop of a solution of ascorbic acid (1 mM) in EtOH for 10 min. The stamp was dried under nitrogen flow and brought into conformal contact with the coumarin monolayer with a load of 30 g for 4 h.

Upon either "click" printing without Cu^I catalyst or using reagent-stamping method [18], the formation of fluorescent patterns were clearly visible with fluorescence microscopy,

proving the success of the reaction and the formation of the triazole monolayer (Figure 4.3). However, the intensity profile of the patterns showed a different increase of the fluorescence intensity when the printing was applied in the presence or absence of the Cu^{I} catalyst for 4 h. This difference reveals a different degree of conversion, which is in agreement with previously published studies.[18]

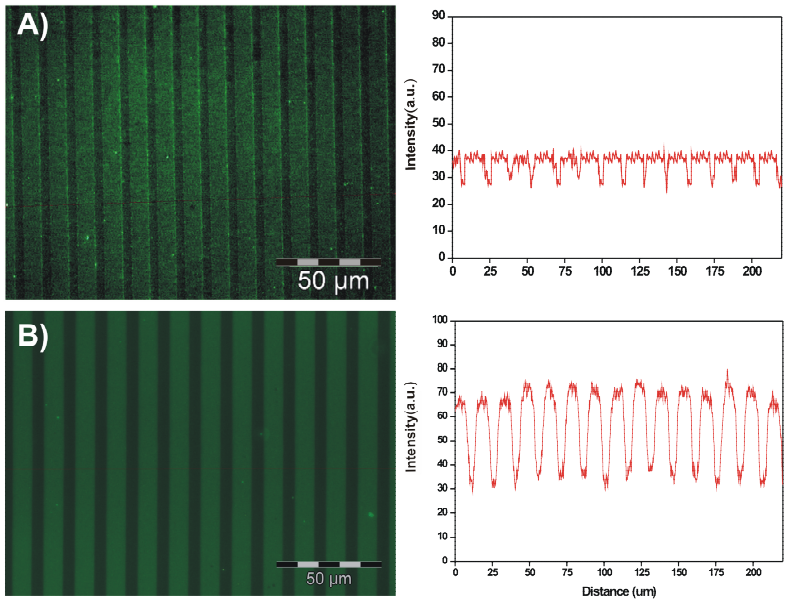

Figure 4.3 Fluorescence microscopy images of 10 µm lines of decylazide printed onto coumarin monolayers for 4 h using a UV excitation light (UV filter, 300 nm ≤ λ_{ex} ≤ 400 nm; λ_{em} ≥ 420 nm): A) µCP without Cu^{I} catalyst and B) reagent-stamping with Cu^{I} catalyst.

Preparation of the orthogonal surface by patterned alkyne-βCD surface. Orthogonal surfaces combining patterned areas for covalent and noncovalent functionalization, were prepared by µCP of N_3-βCD (**2**) through the "click" reaction on the coumarin monolayer (Scheme 4.2). The reaction was monitored by the fluorescent intensity enhancement of the coumarin monolayer upon the triazole formation, which proves the formation of covalently immobilized β-CD patterns (Figure 4.4A).

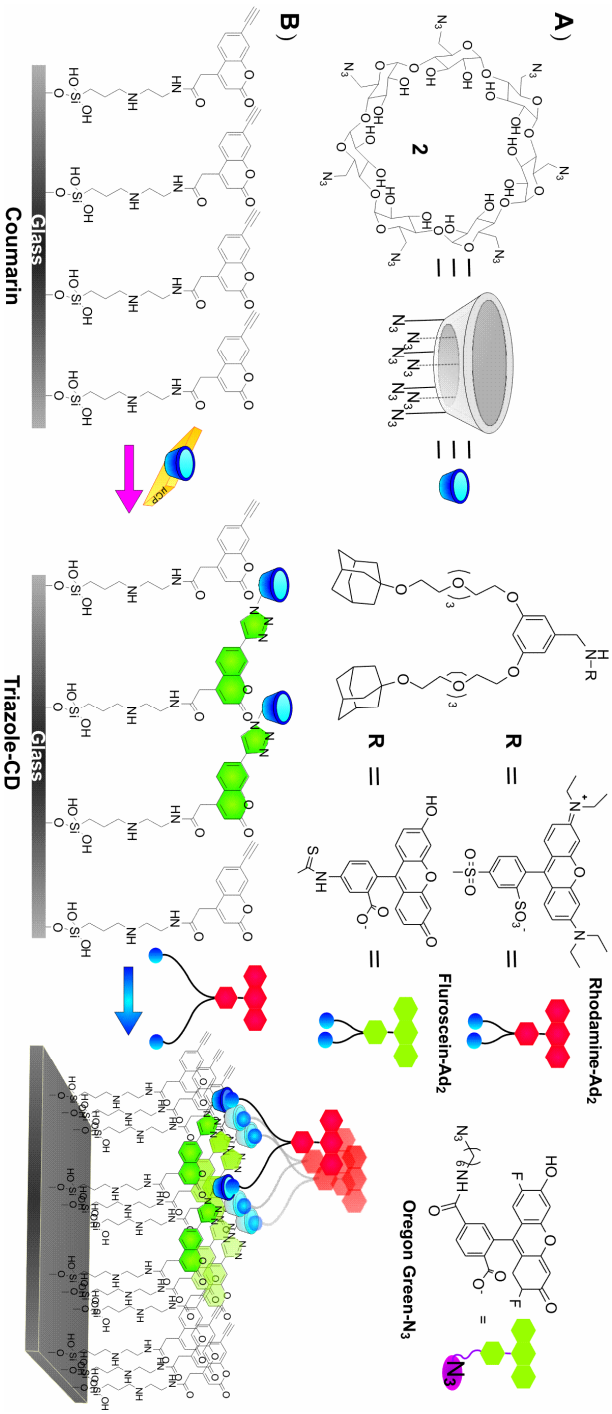

Scheme 4.2 A) Chemical structures of heptakis-azido-β-cyclodextrins (N_3-βCD) (**2**). B) Schematic procedure of orthogonal surface functionalization by printing **2** on reporting alkyne-coumarin monolayers and filling the printed β-CD patterns with rhodamine-Ad_2. Pink and blue arrows indicate covalent bond formation and supramolecular interactions, respectively.

To further confirm the presence of the β-CD patterns, the obtained substrates were incubated with an aqueous solution of lissamine rhodamine-labeled divalent adamantyl guest (rhodamine-Ad_2). After intense rinsing and sonication with a mixture of $EtOH/H_2O$, the adamantyl guest molecules were only observed in the β-CD patterns bound *via* divalent host-guest interactions (Figure 4.4B), demonstrating the availability of the immobilized β-CD and the site-specificity of the alkyne-βCD surface.[26]

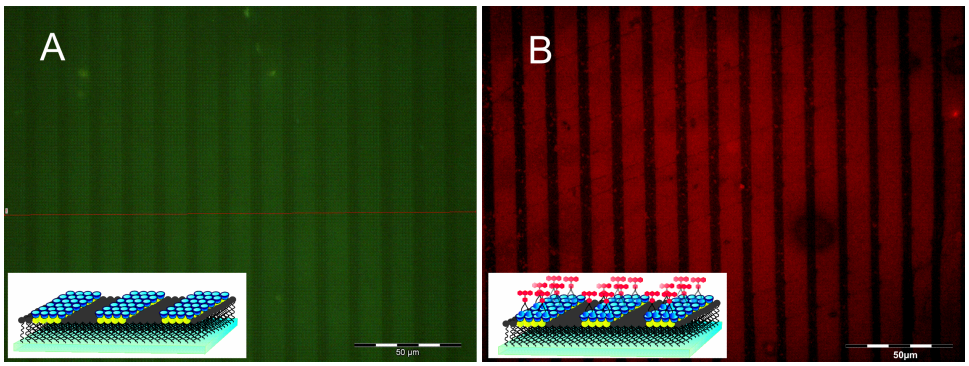

Figure 4.4 Fluorescence microscopy images of a patterned alkyne-βCD monolayer by printing N_3-βCD onto a coumarin monolayer taken with UV excitation (Scheme 4.3B) (A), and after filling the β-CD patterns of the alkyne-βCD monolayer with Rhodamine-Ad_2 using green excitation (Scheme 4.3C) (B). Scale bars represent 50 µm.

The alkyne-βCD surface described above allows several consecutive and/or simultaneous (printing and/or solution) steps to further orthogonally functionalize the patterned surface, exploiting the possibility to use covalent and/or noncovalent immobilization on the same surface. For demonstrating the surface's specificity and selectivity we have used azide-functionalized dyes and dye-labeled diadamantyl guests (Scheme 4.2). As proof of principle, three different printing protocols were performed. In the first one, a dye-labeled divalent adamantyl guest was first printed by supramolecular µCP on the alkyne-βCD surface, followed by a solution step in which the non-patterned, *viz.* empty, β-CD areas were filled with a differently colored dye (Scheme 4.3 images D and E). Secondly, a one-step functionalization was performed by cross-printing a mixture of azide-functionalized dye (Oregon Green-N_3) and a dye functionalized with adamantyl groups (rhodamine-Ad_2) (Scheme 4.3 images F and G). Last, the remaining alkyne-coumarin patterns on the alkyne-βCD surface are still functional as

was proven by cross-printing an azide-functionalized dye (Oregon Green-N_3), on the alkyne-βCD surface (Scheme 4.3 image H). For recording the multiple dye-functionalized surfaces obtained with these two protocols, different filter settings were used, as indicated in Scheme 4.3.

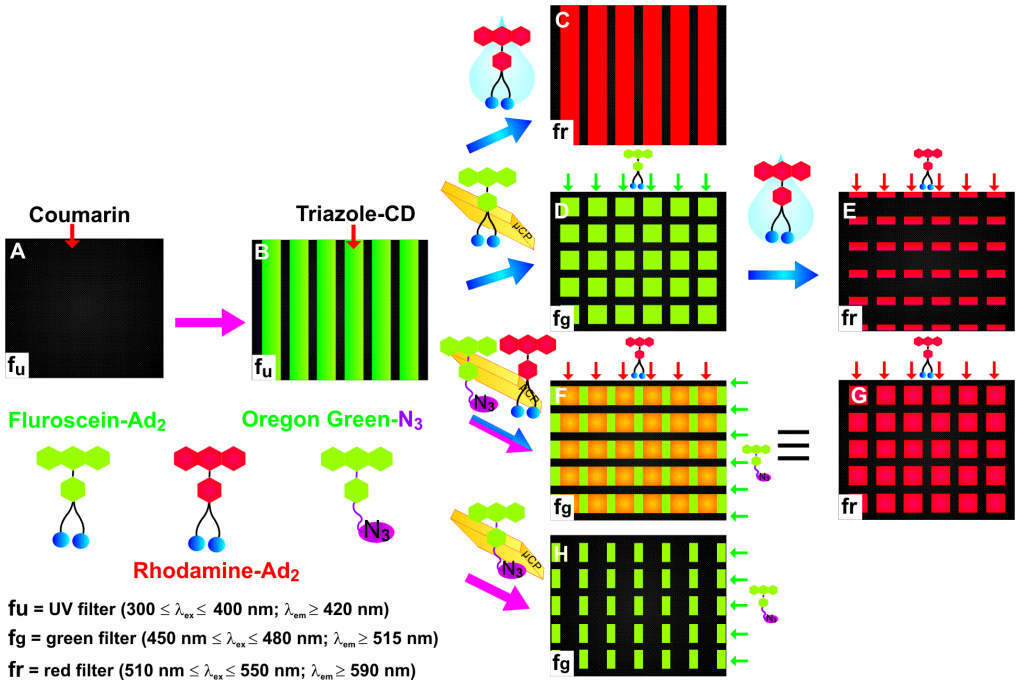

Scheme 4.3 Schematic procedure for multiple functionalization of orthogonally patterned alkyne-βCD surfaces and representation of the corresponding expected fluorescence images depending on the filter of the microscope used. A) Full coumarin monolayer using a UV excitation (UV filter, 300 nm ≤ λ_{ex} ≤ 400 nm; λ_{em} ≥ 420 nm); B) Patterned alkyne-βCD using UV excitation (UV filter); C) β-CD patterns filled with lissamine rhodamine-labeled divalent adamantyl guest (rhodamine-Ad_2) using green excitation (red filter, 510 nm ≤ λ_{ex} ≤ 550 nm; λ_{em} ≥ 590 nm); D) Cross-printed with a fluorescein-labeled divalent adamantyl guest (fluorescein-Ad_2) on the alkyne-βCD surfaces using blue excitation (green filter, 450 nm ≤ λ_{ex} ≤ 480 nm; λ_{em} ≥ 515 nm); E) Introduction of a second fluorescent dye by incubation the sample, D, with rhodamine-Ad_2 using green excitation (red filter); F) One cross-printing step of a mixture of rhodamine-Ad_2 and Oregon Green-N_3 using blue excitation (green filter); G) One cross printing step using green excitation (red filter); H) Cross-printed with Oregon Green-N_3 using blue excitation (green filter). Pink and blue arrows indicate covalent bond formation and supramolecular interactions, respectively.

First, once the coumarin monolayer was patterned by reactive μCP with N_3-βCD to form an alkyne-βCD surface with β-CD-lines of 10 μm wide and separated by 5 μm, following the procedure depicted in Scheme 4.3 images D and E, a second stamp, previously inked with an aqueous solution of fluorescein-labeled divalent adamantyl guest (fluorescein-Ad_2), was brought into contact with the surface, with the pattern perpendicular to the β-CD lines. The fluorescence image (Figure 4.5A), taken with blue excitation ($\lambda_{em} \geq 515$ nm), shows fluorescent 10 x 10 μm squares on the β-CD patterns as a result of the efficient supramolecular μCP. To examine the remaining reactivity of the β-CD patterns after the μCP, a second fluorescent guest was introduced on the surface by incubation of the substrate with a solution of rhodamine-Ad_2.[25, 27, 28] The fluorescence images (Figure 4.5B), taken with green excitation ($\lambda_{em} \geq 590$ nm), confirm the immobilization of the second guest. In fact, 5 x 10 μm fluorescent squares are observed, showing a good selectivity and directionality over the printed β-CD patterns through the availability of β-CD binding sites before and after the supramolecular μCP.

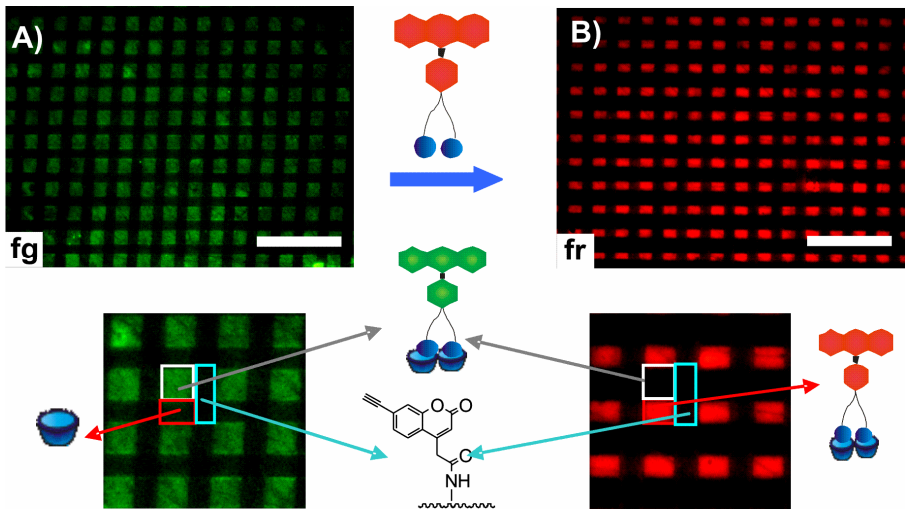

Figure 4.5 Fluorescence microscopy images of orthogonally functionalized patterned alkyne-βCD surfaces following the process shown in Scheme 4.3D and E. (A) after cross-printing fluorescein-Ad_2 onto the patterned alkyne-βCD taken with blue excitation (green filter, $\lambda_{em} \geq 515$ nm) and (B) after filling the remaining reactive β-CD patterns by incubation with rhodamine-Ad_2 taken with green excitation (red filter, $\lambda_{em} \geq 590$ nm). Each scale bar represents 50 μm.

In a second proof of concept experiment, the selectivity and specificity of the alkyne-βCD surfaces were addressed by a one step functionalization, according to the procedure

described in Scheme 4.3 images F and G. For the two-component site-selective immobilization a stamp was inked with an equimolar mixture of rhodamine-Ad_2 and Oregon Green-N_3 in EtOH and brought into contact with the alkyne-βCD surface, with the pattern perpendicular to the β-CD lines. The consecutively recorded fluorescence microscopy images show that the Oregon Green-N_3 and rhodamine-Ad_2 are selectively immobilized on the alkyne and β-CD patterns, respectively (Figure 4.6). When the fluorescence microscopy image was taken with blue excitation , $\lambda_{em} \geq 515$ nm, green fluorescent 10 x 5 μm squares on the alkyne patterns, and brownish 10 x 10 μm squares on the β-CD patterns are observed due to the different emission wavelengths of the Oregon Green-N_3 and rhodamine-Ad_2 dyes, respectively (Figure 4.6A). On the other hand, when the same area was imaged with green excitation light, $\lambda_{em} \geq 590$ nm, only the 10 x 10 μm squares corresponding to the immobilized rhodamine-Ad_2 on the β-CD patterns are observed (Figure 4.6B). The different color and size of the fluorescent squares unambiguously and directly demonstrate the high site-specificity and selectivity of the alkyne-βCD surface. The resulting surface shows repeating 15 x 15 μm squares in which four differently functionalized areas are present, free β-CD (5 x 10 μm) and Rhodamine-Ad_2 filled β-CD (10 x 10 μm), as well as alkyne-coumarin (5 x 5 μm) and "click"-immobilized Oregon Green (10 x 5 μm) areas (Figure 4.6C).

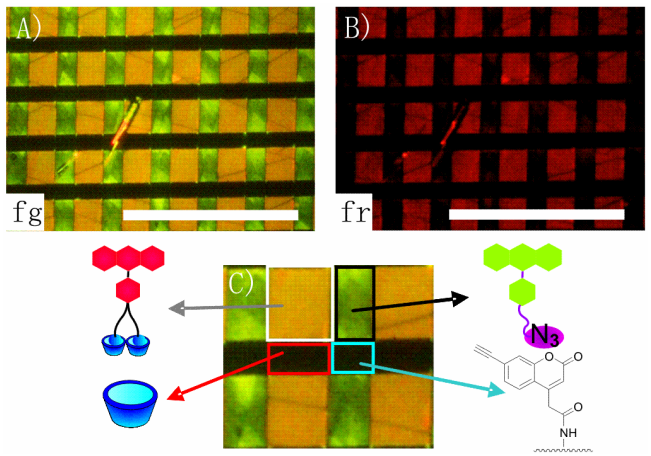

Figure 4.6 Fluorescence microscopy images of one step functionalization of orthogonally patterned coumarin-CD surfaces by printing a mixture of Oregon Green-N_3 and rhodamine-Ad_2 following the process shown in Scheme 4.3 images F and G. (A) taken with blue excitation (green filter, $\lambda_{em} \geq 515$ nm), (B) taken with green excitation (red filter, $\lambda_{em} \geq 590$ nm) and (C) overview of the four differently functionalized areas. Scale bars represent 50 μm.

The remaining alkyne-coumarin patterns on the alkyne-βCD surface are still functional as was proven by cross-printing an azide-functionalized dye, Oregon Green-N_3, on the alkyne-βCD surface by reactive μCP (Figure 4.7, Scheme 4.3H). The fluorescent microscopy images show green fluorescent 10 x 5 μm areas, only where alkynes were present. Moreover, the dark 10 μm wide lines separating the fluorescent 10 x 5 μm patterns prove the β-CD stripes to be free of reactive alkyne groups.

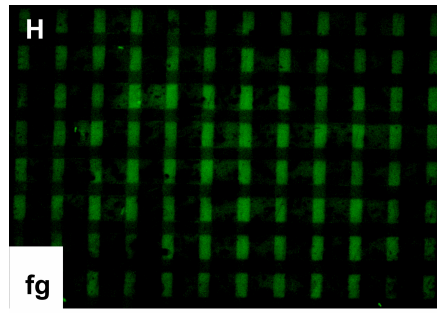

Figure 4.7 Fluorescence image of orthogonally functionalized patterned alkyne-βCD surface after cross printing Oregon Green-N_3 taken with blue excitation (Scheme 4.3H).

4.3 Conclusions

In conclusion, it is demonstrated that orthogonal surfaces can be prepared combining alkyne and cyclodextrin patterns on the same surface for further covalent or noncovalent functionalization. The utilization of an alkyne-modified coumarin as profluorogenic probe allowed the immobilization of N_3-CD and monitoring of the "click" μCP. The selectivity and specificity of the orthogonally functionalized alkyne-βCD surface have been demonstrated by sequential and one-step printing procedures with different azide and bis-adamantyl-functionalized dyes. Printing of a mixture of orthogonal, reactive dyes allowed patterned tetra-functionalized surfaces in a one-step printing procedure, with full control on the chemical functionality of the patterns. We are currently investigating the applicability of the orthogonal 'printed-printboard' surface as a platform for boundary or lateral reactions. The concept of orthogonal covalent-noncovalent surfaces is obviously not limited to alkyne and β-cyclodextrin patterns, and combinations of other patterned functional moieties can be imagined, e.g. functional groups allowing reversible covalent chemistry next to patterns with supramolecular guest properties.

4.4 Experimental

Materials The following materials and chemicals were used as received without further purification: *N*-([3-(trimethoxysilyl)propyl]ethylenediamine) 97% (TPEDA) (Aldrich), *N*,*N*-carbonyldiimidazole (CDI) (Aldrich), 7-hydroxycoumarine-4-acetic acid (Aldrich), 2,2,2-trifluoroethanol (Aldrich), *N*-phenylbis(trifluoromethanesulfonimide) (Aldrich), Dichlorobis(triphenylphosphine)-palladium (Aldrich), (trimethylsilyl)acetylene (Aldrich), Tetrabutylammonium fluoride (Fluka), Sodium ascorbate, (Aldrich), Copper(II) sulphate (Aldrich), Copper(II) acetate (Aldrich), poly(dimethylsiloxane) (PDMS) (Dow Corning), Oregon Green-N_3 (Invitrogen-Molecular Probes). Others solvents used were HPLC grade purchased from Sigma-Aldrich. MilliQ (MQ) with a resistivity higher than 18 MΩ·cm was used in all experiments. Decylazide, N_3-βCD (**2**), lissamine rhodamine-labeled divalent adamantyl guest (rhodamine-Ad_2)[26] and fluorescein-labeled divalent adamantyl guest (fluorescein-Ad_2) were prepared according previously published procedures.

Instrumentation

Contact angle measurements. Contact angles were measured with Millipore water (18.2 MΩ·cm) on a Krüss G10 Contact Angle Measuring Instrument, equipped with a CCD camera. Advancing and receding angles (θ_{adv} and θ_{rec}) were automatically determined during growth and shrinkage of the droplet by a drop shape analysis software.

Fluorescence microscopy. Fluorescence microscopy images were taken using an Olympus inverted microscope IX71 equipped with a mercury burner U-RFL-T as light source and a digital Olympus DR70 camera for image acquisition. UV excitation (300 nm ≤ λ_{ex} ≤ 400 nm) and long pass emission (λ_{em} ≥ 420 nm) was filtered using a UMWB filter cube (UV filter). Blue excitation (450 nm ≤ λ_{ex} ≤ 480 nm) and green emission (λ_{em} ≥ 515 nm) was filtered using a U-MWB filter cube (Green filter). Green excitation (510 nm ≤ λ_{ex} ≤ 550 nm) and red emission (λ_{em} ≥ 590 nm) was filtered using a U-MWG filter cube (red filter).

XPS. XPS spectra were obtained on a Physical Electronics Quantera Scanning X-ray Multiprobe instrument, equipped with a monochromatic $Al_{K\alpha}$ X-ray source operated at 1486.6 eV and 26.18 W. Spectra were referenced to the main C 1s peak set at 284.0 eV. The X-ray

beam size was 100 μm and the data were collected from surface areas of 100 μm x 300 μm with a pass energy of 224 eV and a step energy of 0.8 eV for survey scans and 0.4 eV for high resolution scans. For quantitative analysis, the sensitivity factors used to correct the number of counts under each peak were: C 1s, 1.00; N 1s, 1.59. The measurement was collected after 25 cycles scanning.

FTIR. Transmission FTIR spectra (spectral resolution of 8 cm^{-1}, 1024 scans) were obtained using a BIO-RAD FTS575C FTIR spectrometer equipped with a nitrogen-cooled cryogenic mercury telluride detector. Background spectra were obtained by scanning a clean silicon substrate.

Substrate and monolayer preparation. Single-side and double-side polished silicon substrates (2 x 2 cm) silicon substrates and microscope glass slides were used for monolayer preparation. The substrates were oxidized with piranha solution for 15 min (concentrated H_2SO_4 and 33% aqueous H_2O_2 in a 3:1 ratio; Caution: piranha should be handled carefully) and rinsed with MilliQ water (MQ). After drying with nitrogen stream, the substrates were used immediately for providing a freshly hydroxyl-terminated surface to form a silane monolayer. The substrates were enclosed in a low vacuum chamber desiccator with 0.1 ml of TPEDA, continually pumping for 2 min to fully create vapor phase of a TPEDA atmosphere. After overnight incubation, the slides were rinsed with ethanol, and dichloromethane to remove any excess of silanes, and subsequently dried with a nitrogen stream. The amino-terminated substrates were incubated with a saturated CDI solution in freshly distilled THF under nitrogen for 4 h. After imidazolide monolayer formation (IM monolayer), the substrates were rinsed with distilled THF, followed by nitrogen drying. All samples were freshly prepared and used immediately after drying. The coumarin monolayer was prepared by incubation of the IM monolayer with a 1 mM solution of coumarin **1** in THF for 36 h at room temperature under nitrogen.

Microcontact printing. Stamps (with or without features) were prepared by casting a 10:1 (v/v) mixture of poly(dimethylsiloxane) and curing agent (Sylgard 184, Dow Corning) against a silicon master. After overnight curing at 60 ºC, when was necessary the stamps were oxidized

by oxygen plasma for 1 min before use and subsequently inked by dropping an adsorbate solution onto the stamp for certain times.

4.5 Acknowledgements

Dr. Arántzazu González-Campo is acknowledged for the synthesis and characterization of the coumarin derivative; and we are grateful to Dr. Laura Puig for the original idea of this project and the design of the coumarin derivative.

4.6 References

[1] J. J. Hickman, P. E. Laibinis, D. I. Auerbach, C. F. Zou, T. J. Gardner, G. M. Whitesides, M. S. Wrighton, *Langmuir* **1992**, *8*, 357.
[2] P. E. Laibinis, J. J. Hickman, M. S. Wrighton, G. M. Whitesides, *Science* **1989**, *245*, 845.
[3] T. J. Gardner, C. D. Frisbie, M. S. Wrighton, *J. Am. Chem. Soc.* **1995**, *117*, 6927.
[4] A. del Campo, D. Boos, H. W. Spiess, U. Jonas, *Angew. Chem. Int. Ed.* **2005**, *44*, 4707.
[5] H. Xu, R. Hong, T. X. Lu, O. Uzun, V. M. Rotello, *J. Am. Chem. Soc.* **2006**, *128*, 3162.
[6] H. Sato, Y. Miura, N. Saito, K. Kobayashi, O. Takai, *Biomacromolecules* **2007**, *8*, 753.
[7] S. G. Im, K. W. Bong, B. S. Kim, S. H. Baxamusa, P. T. Hammond, P. S. Doyle, K. K. Gleason, *J. Am. Chem. Soc.* **2008**, *130*, 14424.
[8] Y. N. Xia, G. M. Whitesides, *Angew. Chem. Int. Ed.* **1998**, *37*, 551.
[9] A. Kumar, G. M. Whitesides, *Appl. Phys. Lett.* **1993**, *63*, 2002.
[10] A. Perl, D. N. Reinhoudt, J. Huskens, *Adv. Mater.* **2009**, *21*, 2257.
[11] S. H. Hsu, D. N. Reinhoudt, J. Huskens, A. H. Velders, *J. Mater. Chem.* **2008**, *18*, 4959.
[12] T. P. Sullivan, M. L. van Poll, P. Y. W. Dankers, W. T. S. Huck, *Angew. Chem. Int. Ed.* **2004**, *43*, 4190.
[13] L. Yan, W. T. S. Huck, X. M. Zhao, G. M. Whitesides, *Langmuir* **1999**, *15*, 1208.
[14] L. Yan, X. M. Zhao, G. M. Whitesides, *J. Am. Chem. Soc.* **1998**, *120*, 6179.
[15] D. I. Rozkiewicz, Y. Kraan, M. W. T. Werten, F. A. de Wolf, V. Subramaniam, B. J. Ravoo, D. N. Reinhoudt, *Chem. Eur. J.* **2006**, *12*, 6290.
[16] H. C. Kolb, M. G. Finn, K. B. Sharpless, *Angew. Chem. Int. Ed.* **2001**, *40*, 2004.
[17] L. Nebhani, C. Barner-Kowollik, *Adv. Mater.* **2009**, *21*, 3442.
[18] J. M. Spruell, B. A. Sheriff, D. I. Rozkiewicz, W. R. Dichtel, R. D. Rohde, D. N. Reinhoudt, J. F. Stoddart, J. R. Heath, *Angew. Chem. Int. Ed.* **2008**, *47*, 9927.
[19] D. I. Rozkiewicz, D. Janczewski, W. Verboom, B. J. Ravoo, D. N. Reinhoudt, *Angew. Chem. Int. Ed.* **2006**, *45*, 5292.
[20] M. J. W. Ludden, D. N. Reinhoudt, J. Huskens, *Chem. Soc. Rev.* **2006**, *35*, 1122.
[21] S. Onclin, A. Mulder, J. Huskens, B. J. Ravoo, D. N. Reinhoudt, *Langmuir* **2004**, *20*, 5460.

[22] J. Huskens, M. A. Deij, D. N. Reinhoudt, *Angew. Chem. Int. Ed.* **2002**, *41*, 4467.
[23] X. Y. Ling, I. Y. Phang, W. Maijenburg, H. Schonherr, D. N. Reinhoudt, G. J. Vancso, J. Huskens, *Angew. Chem. Int. Ed.* **2009**, *48*, 983.
[24] M. J. W. Ludden, A. Mulder, R. Tampe, D. N. Reinhoudt, J. Huskens, *Angew. Chem. Int. Ed.* **2007**, *46*, 4104.
[25] S. Onclin, J. Huskens, B. J. Ravoo, D. N. Reinhoudt, *Small* **2005**, *1*, 852.
[26] A. Mulder, S. Onclin, M. Peter, J. P. Hoogenboom, H. Beijleveld, J. ter Maat, M. F. Garcia-Parajo, B. J. Ravoo, J. Huskens, N. F. van Hulst, D. N. Reinhoudt, *Small* **2005**, *1*, 242.
[27] C. M. Bruinink, C. A. Nijhuis, M. Peter, B. Dordi, O. Crespo-Biel, T. Auletta, A. Mulder, H. Schonherr, G. J. Vancso, J. Huskens, D. N. Reinhoudt, *Chem. Eur. J.* **2005**, *11*, 3988.
[28] T. Auletta, B. Dordi, A. Mulder, A. Sartori, S. Onclin, C. M. Bruinink, M. Peter, C. A. Nijhuis, H. Beijleveld, H. Schonherr, G. J. Vancso, A. Casnati, R. Ungaro, B. J. Ravoo, J. Huskens, D. N. Reinhoudt, *Angew. Chem. Int. Ed.* **2004**, *43*, 369.
[29] Z. Zhou, C. J. Fahrni, *J. Am. Chem. Soc.* **2004**, *126*, 8862.
[30] K. Sivakumar, F. Xie, B. M. Cash, S. Long, H. N. Barnhill, Q. Wang, *Org. Lett.* **2004**, *6*, 4603.
[31] C. M. Salisbury, D. J. Maly, J. A. Ellman, *J. Am. Chem. Soc.* **2002**, *124*, 14868.
[32] Q. Zhu, M. Uttamchandani, D. B. Li, M. L. Lesaicherre, S. Q. Yao, *Org. Lett.* **2003**, *5*, 1257.

Chapter 5

Expression of Sensitized Eu^{3+} Luminescence at a Multivalent Interface*

ABSTRACT. Assembly of a mixture of a guest-functionalized antennae and Eu^{3+}-complexed ligand molecules in a patterned fashion onto a receptor surface provides efficient localized sensitized emission. Coordination of a carboxylate group of the antenna to the Eu^{3+} center and noncovalent anchoring of both components to the receptor surface were prerequisites for efficient energy transfer. A Job plot at the surface confirmed that coordination of the antenna to the Eu^{3+} center occurs in a 1:1 fashion. The efficiency of this intramolecular binding process is promoted by the high effective concentration of both complementary moieties at the surface. The system constitutes therefore an example of supramolecular expression of a complex consisting of several different building blocks which signals its own correct formation.

---

*Parts of this chapter have been published in: Shu-Han Hsu, M. Deniz Yilmaz, Christian Blum, Vinod Subramaniam, David N. Reinhoudt, Aldrik H. Velders, and Jurriaan Huskens, *J. Am. Chem. Soc.* **2009**, *131*, 12567-12569.

5.1 Introduction

Self-assembly provides a unique paradigm to obtain complex and functional molecular architectures in a spontaneous process from small building blocks.[1-8] Self-assembly at surfaces is particularly appealing since the inherent immobilization allows characterization by single molecule techniques[9] and its potential embedding in a device structure. It has only been recently recognized that surfaces, in particular those functionalized with molecular recognition units, the so-called molecular printboards, offer additional benefits regarding control over molecular orientation, footprint, stability of binding, and suppression of nonspecific interactions.[10, 11] These properties are given by the fact that molecules and complexes can be bound to such surfaces via multivalent interactions, which are governed by the principle of effective molarity.[11] When complexity is increased,[12] i.e. when going from one to more interaction motifs, new emerging properties can be expected. It has been shown before that the use of building blocks with orthogonal interaction motifs that self-assemble on molecular printboards can lead to the selective formation of one type of complex (from a large number of potential complexes) consisting of more than two different building blocks,[13, 14] and control over supramolecular aggregation of receptor-functionalized vesicles.[15] Here we show, for the first time, the spontaneous formation of such a complex that signals its own correct assembly, by expressing sensitized lanthanide luminescence. The focus is on addressing the exact stoichiometry of the complex and its signaling properties.

The trivalent cations of several lanthanides and their complexes with organic ligands are known to exhibit characteristic emission line shapes, relatively long luminescence lifetimes, and a strong sensitivity towards quenching by high frequency, e.g. O-H, oscillators.[16] Because of their sharp, narrow absorption peaks and low absorption coefficients, lanthanide ions are usually excited via energy transfer from an excited organic chromophore (the antenna or sensitizer), that has a much higher absorption coefficient.[17] The energy transfer process is strongly distance dependent and limits the practical lanthanide-antenna distance to <5 Å.[18] Photophysical properties of lanthanide complexes in solution have been extensively studied. In a supramolecular example, an EDTA-based ligand with β-cyclodextrin (β-CD) binding sites showed sensitized Eu^{3+} emission by noncovalent capture of an organic sensitizer.[19] The immobilization and photophysical properties of lanthanide complexes on surfaces have not

been investigated, except for some recent examples in which a Eu^{3+} complex was bound to a particle surface,[20] especially for sensor applications.[21-23]

Here, antenna-sensitized Eu^{3+} luminescence was employed based on host-guest interactions on the molecular printboard, which allows qualitative and quantitative studies of the complexation of four different building blocks (Figure 5.1): an EDTA-based ligand for binding a Eu^{3+} ion and the receptor surface, the Eu^{3+} ion, a naphthalene-based antenna molecule with receptor-binding moieties and with a carboxylate group for coordination to the Eu^{3+} ion, and a *β*-CD monolayer which functions as the receptor surface. The EDTA ligand and the antenna molecule are equipped with adamantyl groups (Ad) for noncovalent anchoring to the *β*-CD monolayer. The *β*-CD monolayer is used to immobilize both the sensitizer and the Eu^{3+} complex, thus enforcing close proximity of the molecules and facilitating sensitized lanthanide luminescence owing to efficient energy transfer (Figure 5.1b).

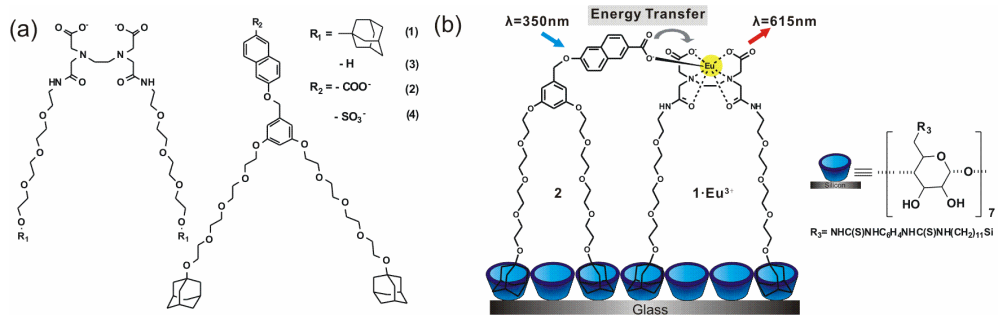

Figure 5.1 (a) EDTA-based ligands with (**1**) and without (**3**) adamantyl (Ad) moieties, and carboxylate- (**2**) or sulfonate- (**4**) modified naphthalene derivatives with Ad groups. (b) Molecular structure of the target complex on a *β*-CD SAM schematically showing sensitized Eu^{3+} luminescence.

Microcontact printing (*μ*CP) onto *β*-CD monolayers, resulting in host-guest complex formation, was used to generate surface patterns of a complex on the receptor surface. Two methods were applied to immobilize the complex onto the surface (Scheme 5.1): (i) the surfaces were patterned by printing an equimolar ratio of **1**·Eu^{3+} and **2** onto the *β*-CD SAM (**i_a**), followed by backfilling the nonprinted area with **1**·Eu^{3+}, which was used as an internal reference (**i_b**); (ii) the surfaces were patterned by printing different ratios of **1** and **2** (**ii_a**), followed by solution immersion in aqueous $EuCl_3$ (**ii_b**). The solution immersion steps (**i_b** and **ii_b**) were performed in the absence of *β*-CD in solution in order to prevent exchange of **2** by **1**·Eu^{3+} (**i_b**) and desorption of **1** and **2** (**ii_b**).[18]

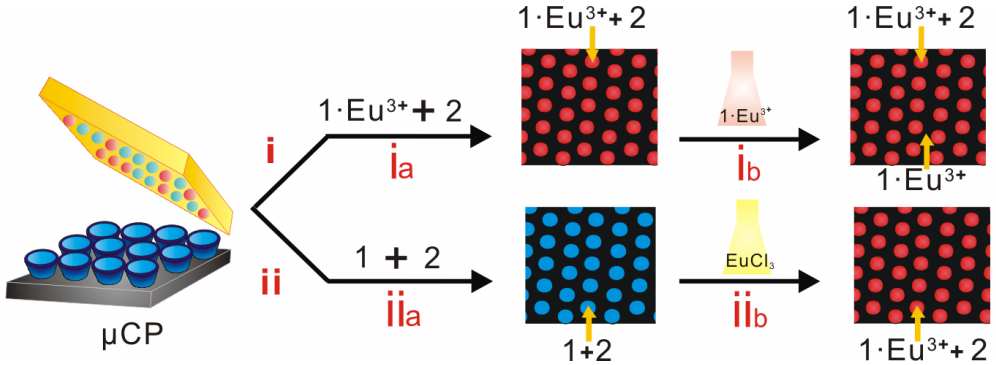

Scheme 5.1 Schematic representation of two immobilization procedures (**i** and **ii**) of the Ad ligands **1** and **2** without ($\mathbf{i}_a$, $\mathbf{ii}_a$) or with ($\mathbf{i}_b$, $\mathbf{ii}_b$) a solution step for backfilling with **1**·Eu^{3+} in the nonprinted area ($\mathbf{i}_b$) or complexation of **1** with Eu^{3+} ($\mathbf{ii}_b$).

5.2 Results and discussion

As an initial indication for energy transfer at the molecular printboard patterned using method **i**, red emission measured using filter **R**[24] only appeared in the areas where both **1**·Eu^{3+} and **2** are present (Figure 5.2a), in contrast to the background that only contained **1**·Eu^{3+}. This demonstrates qualitatively the occurrence of sensitized Eu^{3+} luminescence.

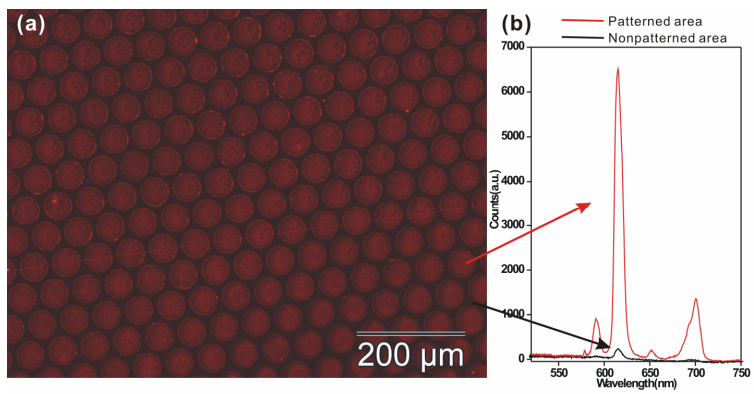

Figure 5.2 (a) Fluorescence microscopy image (left, using filter **R**[24]) of 50 μm dots on a β-CD monolayer obtained by μCP of an equimolar ratio of **1**·Eu^{3+} and **2** for 30 min (step $\mathbf{i}_a$) and subsequent incubation in a solution with **1**·Eu^{3+} for 30 min (step $\mathbf{i}_b$). (b) Local emission spectra from the patterned and nonpatterned areas, both illustrating the enhanced Eu^{3+} emission in the patterned areas.

In contrast, when using **4**, a naphthalene moiety bearing a sulfonate group instead of the carboxylate in **2,** no sensitized Eu^{3+} luminescence was observed (Figure 5.3A and B). Since the sulfonate group is not basic enough to bind a lanthanide ion, this shows that direct coordination of the carboxylate of **2** to the Eu^{3+} center is involved to obtain efficient energy transfer. A similar observation was made in solution.[19] Moreover, when an EDTA-based complex without the adamantyl functionalities was used, **3**·Eu^{3+}, no sensitization of the Eu^{3+} luminescence was observed (Figure 5.3C and D). This control experiment shows that direct coordination of the carboxylate is too weak to immobilize **3**·Eu^{3+} on surface-bound **2**, and has to be assisted by anchoring of both ligands on the receptor surface in order to have the high effective concentration[9, 10] promote the direct coordination, leading to efficient energy transfer.

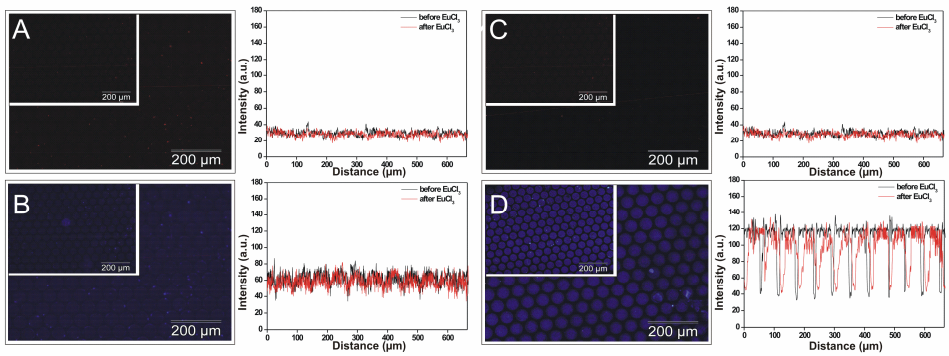

Figure 5.3 Fluorescence microscopy images (884 µm x 666 µm) of 50 µm dots onto a *β*-CD SAM made by µCP: of a mixture of **1** and **4** for 30 min before (insets) and after (main images) immersion in a solution of $EuCl_3$ for 30 min, monitoring Eu^{3+} (A) and antenna (B) emission; of a solution of **2** for 30 min, subsequently, before (insets) and after (main images) immersion in a solution of **3**·Eu^{3+} for 30 min, monitoring Eu^{3+} (C) and antenna (D) emission.

Local emission spectra were recorded to further characterize the patterned surface of **1**·Eu^{3+} and **2** (Figure 5.2b). The emission spectra were selectively collected from both the patterned and nonpatterned areas upon excitation in the UV (step $\mathbf{i_b}$). From the nonpatterned areas, the observed Eu^{3+} emission is faint and can be attributed to inefficient direct UV excitation of **1**·Eu^{3+} alone. However, a significantly higher intensity of Eu^{3+} emission is observed in the **1**·Eu^{3+} **/ 2** patterned area. Clearly the emission of Eu^{3+} is amplified in the area where energy transfer occurred between the naphthalene antenna and the lanthanide complex.

Considering also the fact that twice as much **1**·Eu^{3+} is expected to be present in the nonpatterned area with respect to the printed areas, comparing the intensities at 614 nm, an amplification of a factor of 54 is found between the patterned and nonpatterned areas. To quantify the energy transfer efficiency between naphthalene and the lanthanide complexes, the naphthalene emission lifetimes were determined in the absence and presence of Eu^{3+}.

To obtain sufficient signal in lifetime measurements, a stack of 6 glass slides coated on both sides with a monolayer of **2** or an equimolar mixture of **2** and **1**·Eu^{3+} was sampled at once. The excitation source was a LED emitting at 282 nm at 1 MHz repetition rate. Emitted photons were detected in a narrow wavelength range around the naphthalene emission maximum at 370 nm (slit 10 nm). The emission lifetime from the naphthalene compound on the surface in the absence of the Eu^{3+} could be fitted with a double exponential with one strongly dominating component of τ_1 = 2.3 ns (89% relative amplitude) and a minor component of 7.0 ns (11% relative amplitude) (Figure 5.4). In the presence of **1**·Eu^{3+}, the lifetime of both components significantly dropped to 1.5 ns and 5.3 ns, respectively, while the relative amplitudes were preserved (91% and 9%). From these lifetimes we determined the dominant energy transfer efficiency to be 35% for the major and 25% for the minor component. To exclude any effect from possible energy transfer acceptor saturation due to the very long Eu^{3+} emission lifetime on the recorded decay characteristics, the experiment was repeated using a reduced excitation frequency of 100 kHz. The obtained results were identical to those obtained with 1 MHz excitation.

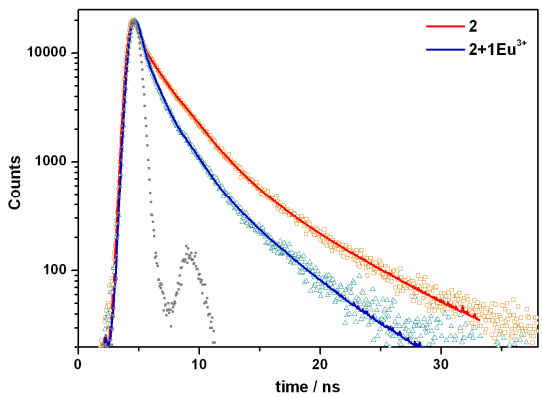

Figure 5.4 Time-resolved fluorescence measurements of **2** alone and of **2** and **1**·Eu^{3+} on a β-CD SAM excited at 282 nm with a 1 MHz LED. The 2.3 ns and 7.0 ns lifetime components were derived from fitting the decay curves of **2**.

To study the stoichiometry of complexation between **2** and **1**·Eu^{3+}, a stepwise procedure (Scheme 5.1, method **ii**) was applied: μCP of solution mixtures of different molar ratios of **1** and **2** was used to generate patterns on the β-CD monolayer, with an empty β-CD monolayer as background for good image contrast and intensity assessment. Directly after printing (step $\mathbf{ii_a}$), the surface was imaged with fluorescence microscopy, followed by immersion in a $EuCl_3$ solution for 30 min (step $\mathbf{ii_b}$) and reimaging (Figure 5.5). The fluorescence intensities of the surface antenna and Eu^{3+} emission were plotted as a function of the molar fraction of antenna **2** (Figure 5.6). Since the printboard ensures that the total immobilized ligand concentration (**1** + **2**) remains constant, this plot fulfills the requirements for a Job plot. This is the first example of the use of a Job plot to study the stoichiometry of binding at a surface.

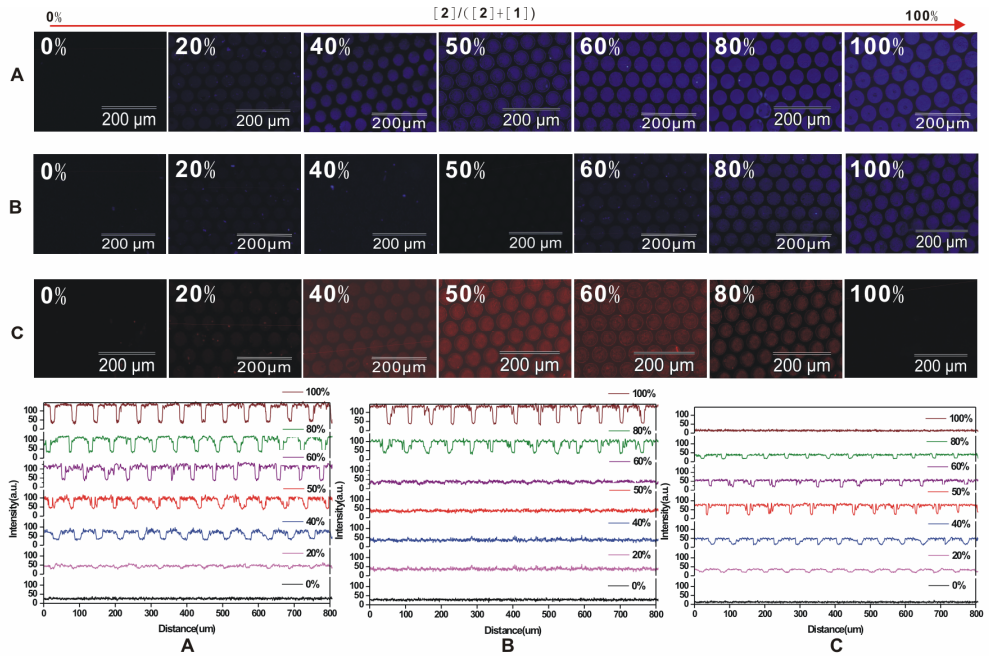

Figure 5.5 Fluorescence microscopy images of 50 µm dots prepared on β-CD monolayers by µCP (30 min) of solution mixtures of different ratios of **1** and **2** (the concentration of **2** varying from 0 %, 20 %, 40 %,50 %,60 %,80 % and 100 %) ($\mathbf{ii_a}$), followed by rinsing with MilliQ water (A), and subsequently immersed in a solution of $EuCl_3$ for 30 min ($\mathbf{ii_b}$) (B, C), monitoring antenna (A, B; **B** filter) and Eu^{3+} emission (C; **R** filter). The percentages of antenna **2** in the mixture of **1** and **2** are given in the images. The intensity profiles (bottom) are also shown before (A) and after (B, C) $EuCl_3$ immersion.

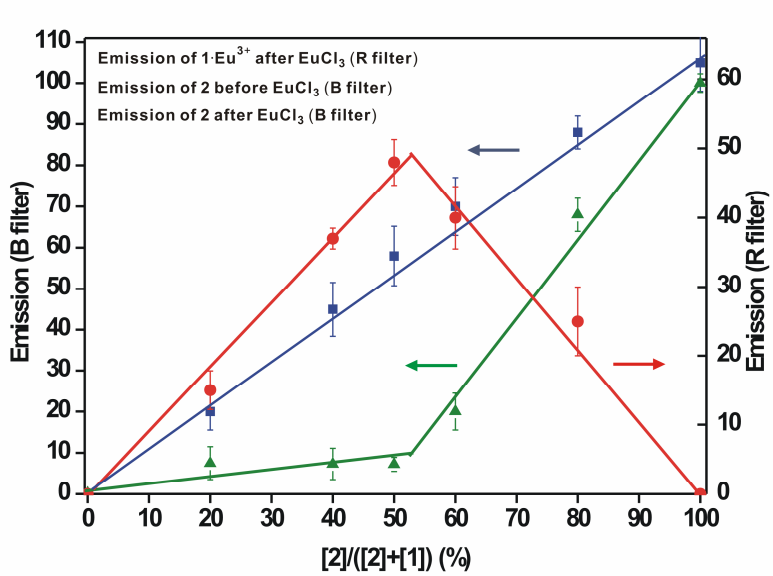

Figure 5.6 Fluorescence intensity of **2** before (blue, squares) and after (green, triangles) immersion in a $EuCl_3$ solution and of Eu^{3+} emission (red, circles) after the solution step, for patterns printed from solutions with varying ratios of **2** and **1**. Lines are presented for fits of the data points from 0-100% (blue line) and from 0-50% and 50-100% separately (green and red lines). The error bars represent a single standard deviation.

The fluorescence intensity of the antenna before complexation with Eu^{3+} increases linearly with the antenna fraction (Figure 5.5A, Figure 5.6), confirming that the ratio of immobilized **1** and **2** is equal to the solution ratio used for printing. The images taken after immersion in the $EuCl_3$ solution show much lower antenna emissions (Figure 5.5B, filter **B**), particularly at antenna fractions of <50%, while strong Eu^{3+} emission (Figure 5.5C, filter **R**) is observed, which shows a maximum at an antenna fraction of 50% (Figure 5.6). These results show (i) quenching of antenna emission in accordance with energy transfer to the Eu^{3+} complex and (ii) optimal sensitized emission at a 1:1 antenna: Eu^{3+}-complex ratio, confirming the stoichiometry of the target complex (Figure 5.1b) to be 1:1. The sharpness of the inflection point in the Job plot indicates the complete formation of the target 1:1 complex. The apparently strong coordination of the carboxylate of **2** to the Eu^{3+} ion of **1**·Eu^{3+} is attributed to the high effective concentration at the surface[9,10] promoting the, now intramolecular, coordinative binding.

A thermodynamic model [25] was employed to simulate the surface Job plot data to check the validity of this method for verifying the stoichiometry of the complex of **1**·Eu^{3+}, **2** and the β-CD monolayer (Figure 5.7). The model can accurately reproduce the line trends observed in the Job plot and thus confirms the validity of the Job plot approach to assess the stoichiometry of a surface assembled complex. The model also shows that the sharp break at a 1:1 ratio of **1**·Eu^{3+} and **2** can only be predicted if the binding constant is $>10^3$ M^{-1}. However, the absolute value of this stability constant is probably influenced by the dry state of the samples in which the fluorescence images were obtained.

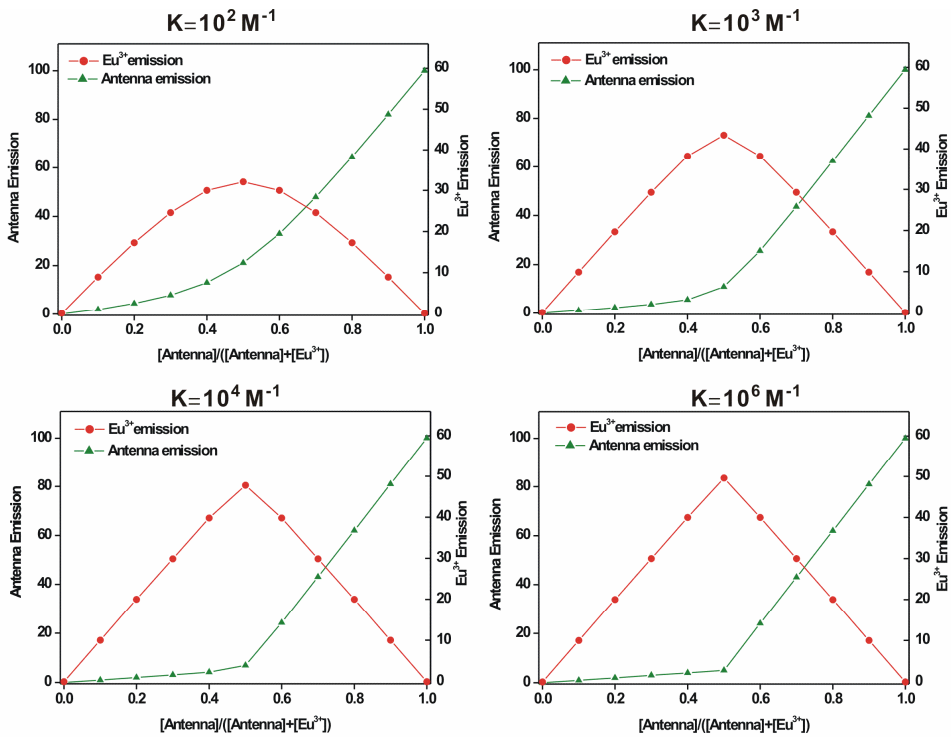

Figure 5.7 Simulated fluorescence intensity data showing the emission of antenna and Eu^{3+} as a function of the ratio of antenna and Eu^{3+}, while varying the binding constant *K* of the carboxylate group of **2** to Eu^{3+} in **1**· Eu^{3+} at the surface.

5.3 Conclusions

This work clearly demonstrates that **1**·Eu^{3+} and the antenna **2** form a 1:1 coordination pair on the *β*-CD SAM. The formation of the target complex is directly indicated by the occurrence of sensitized luminescence. This surface assisted luminescence amplification has potential for developing optical devices or as a sensing platform for biologically relevant anions.[26] The system as a whole represents an example of functional expression, emerging from the combined system of all necessary components.[27] The high specificity of the complex formation is in part attributed to the multivalency of the receptor surface, which is here translated in a higher-level multivalent interface of Eu complexes with vacant coordination sites and antenna molecules with the complementary carboxylate groups. Another crucial factor to drive the system into the direction of the target complex is to encode the necessary information into all individual building blocks. As can be seen here, this information can be limited, while still complex molecular architectures can be achieved.

5.4 Experimental

Materials. For information on the synthesis and characterization of compounds **1**-**4**, the reader is refereed to the work of Deniz Yilmaz.[28]

Substrate and monolayer preparation. Microscope glass slides were used for *β*–cyclodextrin (*β*-CD) monolayer preparation.[29] The substrates were cleaned with piranha solution for 15 min (concentrated H_2SO_4 and 33 % aqueous H_2O_2 in a 3:1 ratio; Caution: piranha should be handled carefully) and rinsed with MilliQ. After drying in a nitrogen stream, the substrates were used immediately for silane monolayer formation. The substrates were enclosed in a low-vacuum desiccator with 0.1 ml of TPEDA, continually pumping for 5 min to create a vapor phase of TPEDA. After overnight incubation, the slides were rinsed with ethanol and dichloromethane to remove any excess of silanes and subsequently dried in a nitrogen stream. The attachment of 1,4-phenylene diisothiocyanate was performed in a 20 mM solution in toluene at 60 ˚C during 2 h. Samples were thoroughly rinsed with toluene and dried in a nitrogen flow. The *β*-CD layer attachment was made during 2 h in an aqueous 0.1 mM *β*-cyclodextrin-heptaamine solution (pH~7) at 60 ˚C. Samples were thoroughly rinsed with water and dried in a nitrogen flow.

Microcontact printing. Patterned silicon substrates were made by photolithography followed by reactive ion etching (RIE) or e-beam lithography. They consisted of gratings of 50 μm dots at 70 μm period with the height of 1 μm. PDMS stamps were prepared by casting a 10:1 (v/v) mixture of poly(dimethylsiloxane) (PDMS) prepolymer and curing agent (Sylgard 184, Dow Corning) against the silicon master. After overnight curing at 60 ºC, the stamps were oxidized by oxygen plasma for 1 min and subsequently inked by dropping an aqueous adsorbate solution onto the stamp. Before printing, the stamps were blown dried in a stream of nitrogen. The stamps were brought into conformal contact with the substrate for 30 min. The stamps were changed for each new print and the same inking procedure was used. After stamp removal, the printed substrates were rinsed with copious amounts of water, blown dry with nitrogen and imaged with fluorescence microscopy.

Printing of 1 and 2 (or 4), followed by $EuCl_3$ immersion. The *β*-CD SAM substrate was printed for 30 min with a stamp inked with an equimolar ratio of **1** and **2** (or **4**) (2 mM each) in saturated *β*-CD in a 3:1 mixture of EtOH/water, followed by rinsing with water and drying in a stream of nitrogen. The printed substrate was immersed in a 4 mM aqueous solution of $EuCl_3$ for 30 min, followed by rinsing and drying in a stream of nitrogen.

Printing of 2, followed by 1·Eu^{3+} (or 3·Eu^{3+}) immersion. The *β*-CD SAM substrate was printed for 30 min with a stamp inked with a solution of **2** in saturated *β*-CD in a 3:1 mixture of EtOH/water, followed by rinsing with water and drying in a stream of nitrogen. The printed substrate was immersed in a 2 mM aqueous solution of **1**·Eu^{3+} (or **3**·Eu^{3+}) for 30 min, followed by rinsing and drying in a stream of nitrogen.

Printing of different ratios of 1 and 2, followed by $EuCl_3$ immersion. The *β*-CD SAM substrate was printed for 30 min with a stamp inked with different molar ratios of **2** and **1** varying from 0%:100%, 20%:80%, 40%:60%, 50%:50%, 60%:40%, 80%:20%, and 100%:0% in a saturated *β*-CD solution in a 3:1 mixture of EtOH/water, followed by rinsing with water and drying in a stream of nitrogen. The printed substrate was immersed in a 4 mM aqueous solution of $EuCl_3$ for 30 min, followed by rinsing and drying in a stream of nitrogen.

Time-resolved fluorescence measurements. Two sets of samples were prepared with or without **1**·Eu^{3+} present. The first sample was printed with a flat stamp inked with 2 mM of **2** for 30 min onto a *β*-CD SAM with saturated *β*-CD in 3:1 EtOH/water. The same procedure was used to prepare substrates with an equimolar ratio of **2** and **1**·Eu^{3+} (2 mM each). In order to enhance the total emission intensity, multiple slides were used in a cuvette during the measurement in air (6 double side printed slides in total). The samples were positioned at 45° orientation relative to the excitation light and the detector. The decay curves at 370 nm for the donor alone (**2**) and in the presence of the acceptor (**1**·Eu^{3+}) were measured upon excitation at 282 nm.

Fluorescence microscopy. Fluorescence microscope images were taken using an Olympus inverted research microscope IX71 equipped with a mercury burner U-RFL-T as light source and a digital Olympus DR70 camera for image acquisition. UV excitation (300 nm $\leq \lambda_{ex} \leq$ 400 nm) and blue emission (410 nm $\leq \lambda_{em} \leq$ 510 nm) was filtered using a Dapi Olympus filter cube. UV excitation (300 nm $\leq \lambda_{ex} \leq$ 400 nm) and red emission (narrow band pass at 615 nm) was filtered using a Olympus filter cube. All fluorescence microscopy images were acquired in air.

Fluorescence spectral microscopy. To record local emission spectra a custom built microscopy setup capable of spectral imaging was used. The sample was illuminated using a mercury lamp and a standard filter cube for UV excitation (excitation 300 nm to 400 nm, detection > 400 nm) via a 100x objective (1.3 NA, Olympus). The local emission was collected by the same objective. The emitted light was imaged via a pinhole and a prism spectrometer onto a cooled CCD camera (Newton EMCCD, Andor). Wavelength calibration was achieved using a calibrated light source (Cal-2000 Mercury Argon Calibration source, Ocean Optics, USA).

Fluorescence lifetime spectrophotometer. Fluorescence lifetimes were determined using a spectrophotometer (FluoroMax4, Horiba Jobin Yvon), equipped with a TCSPC extension and a pulsed 282 nm NanoLED for excitation (all Horiba Jobin Yvon). The recorded data was analyzed using the DAS6 software package of Horiba Jobin Yvon.

Thermodynamic complexation model at interfaces. Complexation of **1**·Eu^{3+} by **2** on a *β*-CD SAM was modeled using a thermodynamic model governed by effective concentration,[25] using a spreadsheet approach. Since each ligand **1** and **2** is bound in a divalent fashion, the maximum coverage of **1**·Eu^{3+} and **2** is only half of the coverage of the *β*-CD SAM. The model employs binding constants for interaction of an adamantyl group to a *β*-CD surface site ($5x10^4$ M^{-1}) and for the 1:1 interaction of the antenna carboxylate group to the Eu^{3+} center (*K*). The latter one is varied to show the effect on the simulated Job plot. The modeled fluorescence intensities are obtained by relating the fractions of unbound and bound antenna **2** and Eu^{3+} complex **1**·Eu^{3+}, assuming arbitrarily set values for the emission of **2**, **1**·Eu^{3+}, and the complex **1**·Eu^{3+}·**2**. The modeled data presented in Figure 5.7 (triangles, green) show that the fraction of unbound **2** at the surface increases after > 50 % of **2** in the printed mixture. The curves start to show a sharp inflection point when $K>10^3$ M^{-1}. There is no significant difference of Eu^{3+} emission (Figure 5.7 circles, red) between the model and the experimental graphs when $K>10^3$ M^{-1}, which means that this *K* value is a lower limit for the complex formation on the *β*-CD SAM. However, since the samples presented in Figure 5.5 were measured in the dry state, the absolute K value is probably unreliable. Due to the fact that the sensitized luminescence is practically absent at 10 μM in solution, the binding constant *K* probably has an upper limit of about 10^4 M^{-1}.

5.5 Acknowledgments

The synthesis part of the work presented in this chapter was performed by Deniz Yilmaz. Christian Blum is acknowledged for performing the local fluorescence emission spectra and lifetimes measurements.

5.6 References

[1] D. N. Reinhoudt, M. Crego-Calama, *Science* **2002**, *295*, 2403.
[2] V. E. Campbell, J. R. Nitschke, *Synlett* **2008**, *2008*, 3077.
[3] C. A. M. Bradley J. Holliday, *Angew. Chem. Int. Ed.* **2001**, *40*, 2022.
[4] J.-M. Lehn, *Proc. Natl. Acad. Sci. U.S.A.* **2002**, *99*, 4763.
[5] J.-M. Lehn, *Chem. Soc. Rev.* **2007**, *36*, 151.
[6] G. M. Whitesides, R. F. Ismagilov, *Science* **1999**, *284*, 89.

[7] R. F. Ludlow, S. Otto, *Chem. Soc. Rev.* **2008**, *37*, 101.
[8] B. C. Gibb, *Nat Chem* **2009**, *1*, 17.
[9] A. Langner, S. L. Tait, N. Lin, C. Rajadurai, M. Ruben, K. Kern, *Proc. Natl. Acad. Sci. U.S.A.* **2007**, *104* 17927.
[10] A. Mulder, J. Huskens, D. N. Reinhoudt, *Org. Biomol. Chem.* **2004**, *2*, 3409.
[11] M. J. W. Ludden, D. N. Reinhoudt, J. Huskens, *Chem. Soc. Rev* **2006**, *35*, 1122.
[12] M. Eigen, *The Hypercycle: A Principle of Natural Self Organization*, Springer-Verlag **1979**.
[13] O. Crespo-Biel, C. W. Lim, B. J. Ravoo, D. N. Reinhoudt, J. Huskens, *J. Am. Chem. Soc.* **2006**, *128*, 17024.
[14] M. L. W. Ludden, A. Mulder, K. Schulze, V. Subramaniam, R. Tampe, J. Huskens, *Chem.Eur.J.* **2008**, *14*, 2044.
[15] C. W. Lim, O. Crespo-Biel, M. C. A. Stuart, D. N. Reinhoudt, J. Huskens, B. J. Ravoo, *Proc. Natl. Acad. Sci. U.S.A.* **2007**, *104*, 6986.
[16] M. F. Hazenkamp, G. Blasse, N. Sabbatini, *J. Phys. Chem.* **1991**, *95*, 783.
[17] G. E. Buonocore, H. Li, B. Marciniak, *Coord. Chem. Rev.* **1990**, *99*, 55.
[18] D. L. Dexter, *J. Chem. Phys.* **1953**, *21*, 836.
[19] J. J. Michels, J. Huskens, D. N. Reinhoudt, *J. Am. Chem. Soc.* **2002**, *124*, 2056.
[20] E. Delgado-Pinar, J. C. Frias, L. J. Jimenez-Borreguero, M. T. Albelda, J. Alarcon, E. Garcia-Espana, *Chem. Commun.* **2007**, 3392.
[21] J. Massue, S. J. Quinn, T. Gunnlaugsson, *J. Am. Chem. Soc.* **2008**, *130*, 6900.
[22] K. L. Ai, B. H. Zhang, L. H. Lu, *Angew. Chem. Int. Ed.* **2009**, *48*, 304.
[23] B. I. Ipe, K. Yoosaf, K. G. Thomas, *J. Am. Chem. Soc.* **2006**, *128*, 1907.
[24] The surface was consecutively imaged by fluorescence microscopy using two different filter sets: one set allows UV excitation and red emission using a narrow bandpass filter centered at 610 nm (**R**, which only collects the emission of Eu^{3+}) and another set allows UV excitation and blue emission (**B**, which only collects the emission of the naphthalene moiety).
[25] J. Huskens, A. Mulder, T. Auletta, C. A. Nijhuis, M. J. W. Ludden, D. N. Reinhoudt, *J. Am. Chem. Soc.* **2004**, *126*, 6784.
[26] J. P. Leonard, C. M. G. dos Santos, S. E. Plush, T. McCabe, T. Gunnlaugsson, *Chem. Commun.* **2007**, 129.
[27] P. Luisi, *Fundam. Chem.* **2002**, *4*, 1572.
[28] S.-H. Hsu, M. D. Yilmaz, C. Blum, V. Subramaniam, D. N. Reinhoudt, A. H. Velders, J. Huskens, *J. Am. Chem. Soc.* **2009**, *131*, 12567.
[29] S. Onclin, A. Mulder, J. Huskens, B. J. Ravoo, D. N. Reinhoudt, *Langmuir* **2004**, *20*, 5460.

Chapter 6

Non-linear Amplification of a Supramolecular Complex at a Multivalent Interface

ABSTRACT. Multivalent binding of a supramolecular complex at a multivalent host surface by combining the orthogonal cyclodextrin-adamantyl (host-guest) and lanthanide-ligand (coordination) interaction motifs is used to monitor molecular binding events by its intrinsic sensitized luminescence. By adding a competing host in solution, the dynamics of the system was varied gradually, where the dependence of surface complex formation on the solution composition was changed from linear to highly nonlinear. A thermodynamic model was used to simulate this nonlinear amplification of complex formation at the CD monolayer in the presence of cyclodextrin by varying the binding constant K_{AE} of the complex and calculation of the surface speciation. The underlying exchange process of the major for the minor component was monitored in time in the presence of different concentrations of cyclodextrin. Pseudo-first-order rate constants were obtained, which depend on the cyclodextrin concentration present on the surface.

---

*Manuscript in preparation: Shu-Han Hsu, Alberto Gomez Casado, M. Deniz Yilmaz, David N. Reinhoudt, Aldrik H. Velders, and Jurriaan Huskens.

6.1 Introduction

Multivalency describes the interaction between multivalent receptors and multivalent ligands. Supramolecular, multivalent interactions are of high interest, since multivalency is one of nature's governing principles in e.g. protein-carbohydrate interactions, cell recognition,[1, 2] as well as a powerful tool for molecular nanostructure fabrication.[3-5] Multivalent interactions at interfaces, e.g., at cell membranes,[6] at lipid membranes,[7, 8] or at self-assembled monolayer (SAM) model systems,[9, 10] are particularly important, since such interfaces, when functionalized with monovalent receptors or ligands can act as multivalent systems.[4] Multivalent binding events have collective properties different from monovalent interactions, which lead to higher binding affinities between the interacting functionalities.

Self-assembly is a spontaneous process to obtain complex and functional molecular architectures from small building blocks.[11] Self-assembly at interfaces is particularly interesting, since the inherent immobilization allows characterization of the molecular-level interaction by single molecule techniques[12] and its potential embedding in a device structure. This provides a unique paradigm to characterize the molecular interaction by the fact that molecules and complexes can be bound to such surfaces, so-called molecular printboards**,** via multivalent interactions.[3, 5]

The used cyclodextrin (CD) based monolayers, serving as a multivalent receptor for multivalent ligands, permit the supramolecular positioning of reversible self-assembled patterns, offering additional benefits regarding control over molecular orientation and stability of binding. The reversible nature of host-guest interactions offers the possibility of self-correction and tunability by changing the conditions, where the immobilized host monolayer allows the variation of environmental conditions, such as competition by a host in solution or change of the polarity of the solution.[5, 13]

Metal-ligand coordination is an effective strategy for strong, directional binding to stabilize designed self-assembled supramolecular architectures.[14, 15] The trivalent cations of several lanthanides and their complexes with organic ligands are known to exhibit characteristic narrow emission line shapes, and relatively long luminescence lifetimes. Because of their sharp, narrow absorption peaks and low absorption coefficients, lanthanide ions are usually excited via energy transfer from an excited organic chromophore (the antenna or sensitizer) that has a much higher absorption coefficient.[16] Previously (see Chapter 5), we

have employed the antenna and the EDTA-Eu^{3+} ligand-based host-guest interactions on the molecular printboard, which spontaneously formed a complex that signals its own correct assembly, by expressing sensitized lanthanide luminescence (Scheme 6.1).[17] The self-correction/self-organization process through host-guest interaction offered by guest-induced competition was reported through the intrinsic signaling property of the sensitized Eu^{3+} emission on the immobilized host monolayer. Such orthogonal motifs like cyclodextrin-adamantyl (host-guest) and lanthanide-ligand (coordination) can lead to higher stoichiometries, increased specificity, and more complex architectures, where the desorption by competition with a host in solution is progressively more difficult due to increasing numbers of interactions.

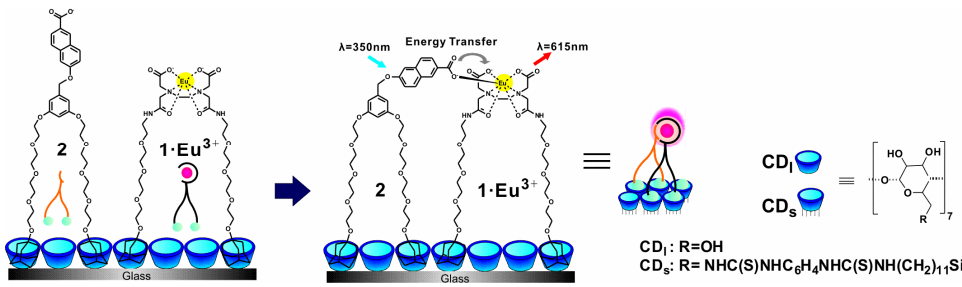

Scheme 6.1 The complexation of **2** and **1**·Eu^{3+} on a CD monolayer and the occurrence of sensitized luminescence upon coordination of **2** to the Eu^{3+} center.

Here, the intrinsic signaling property is used to study a self-assembly-driven amplification process of the complex formation induced by competition-driven ligand exchange on a multivalent surface. The antenna-sensitized Eu^{3+} luminescence at the molecular printboards allows assessment of the stoichiometry of the complex under host-induced binding competition and a quantitative estimation of the complex binding strength. The observed nonlinear amplification of the target complex on the multivalent surface with respect to the solution composition is supported by thermodynamic modeling. Moreover, the kinetics of the ligand exchange process are assessed as well.

6.2 Results and discussion

6.2.1 The system

Five different building blocks were used to study multivalent, orthogonal complexation at a CD monolayer (Scheme 6.1): an EDTA-based ligand **1** for binding a Eu^{3+} ion, the Eu^{3+} ion, a naphthalene-based antenna molecule **2** with a carboxylate group for coordination to the Eu^{3+} ion, cyclodextrin in solution (CD_l), and a cyclodextrin (CD_s) monolayer, which functions as the receptor surface. The EDTA ligand and the antenna molecule are equipped with adamantyl (Ad) groups for noncovalent "anchoring" to the CD monolayers. The CD monolayer is used to immobilize both the sensitizer **2** and the Eu^{3+} complex **1**·Eu^{3+}, thus enforcing the close proximity of the molecules and facilitating sensitized lanthanide luminescence owing to efficient energy transfer.

In Chapter 5, mixtures of **1**·Eu^{3+} and **2** of different compositions were printed onto CD monolayers, showing the formation of **1**·Eu^{3+}·**2** in a linear dependence with the solution concentration of the minor component. The printing process is, however, not compatible with the host-driven competition targeted here.

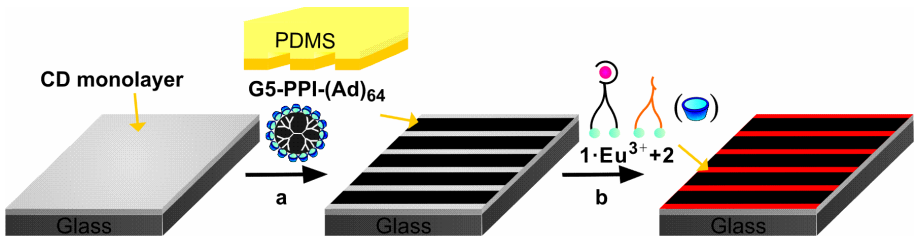

Scheme 6.2 Schematic representation of sample preparation procedures: a) a CD monolayer is patterned with G5-PPI-$(Ad)_{64}$ dendrimers by μCP, b) followed by drop casting a mixture of **1**·Eu^{3+} and **2** with or without CD_l present in solution and equilibration for an hour.

Therefore, microcontact printing (μCP) of G5-PPI-$(Ad)_{64}$ onto the CD monolayers was used to generate surface patterns on the receptor surface.[18] This leaves the unpatterned areas accessible for immobilization of **1**·Eu^{3+} and **2** from solution with or without CD_l present (Scheme 6.2). To study the stoichiometry of complexation between **1**·Eu^{3+} and **2**, solution mixtures of different molar ratios of **1**·Eu^{3+} and **2** were incubated over CD monolayers, with a

G5-PPI-$(Ad)_{64}$ dendrimer-printed pattern as background for good image contrast and quantitative intensity assessment.

The experiments were performed without or with adding CD_l as a competing host (Scheme 6.2). In the former case, filling of the surface is expected to be rapid (Scheme 6.3A). It cannot be followed by exchange, because the divalent ligands are assembled in a kinetically stable fashion.[19, 20] In the latter case, the addition of CD_l, however, can promote the desorption of immobilized molecules, and hence the adsorption of molecules from solution to reach the stable formation of the complex with the highest valency (Scheme 6.3B). The latter provides the thermodynamic driving force for the exchange process.

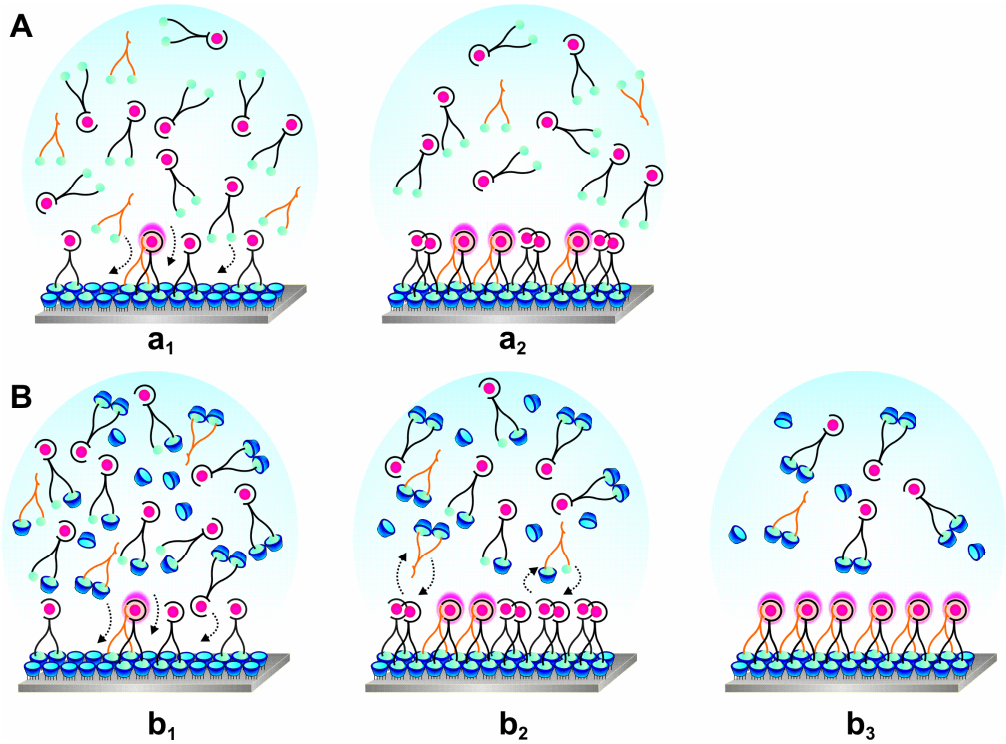

Scheme 6.3 Schematic representation of the assembly procedures of **1**·Eu^{3+} and **2** onto CD monolayers without (top, A) or with (bottom, B) CD_l present in the solution mixtures. (A) By rapid filling of the empty CD_s surface (a_1) in the absence of CD_l; the two different adamantyl-functionalized ligands are assembled on the surface, linearly corresponding to the solution ratio (a_2); (B) after the rapid filling of the empty CD surface (b_1) leading to a filled surface (b_2), the self-organization by dynamic exchange is promoted by the presence of CD_l thus promoting the formation of the stable tetravalent complex (**1**·Eu^{3+}·**2**) under thermodynamic equilibrium (b_3).

6.2.2 Kinetically controlled assembly

An equimolar ratio of **1**·Eu^{3+} and **2** was incubated over a dendrimer-patterned CD monolayer without CD_l present (Scheme 6.3A). The obtained intensity profiles (Figure 6.1) clearly show the **2**-sensitized emission of **1**·Eu^{3+} and thus the formation of **1**·Eu^{3+}·**2**. The intensity after 1 min incubation is identical to that obtained for 1 h incubation and this intensity is comparable to that observed after printing of **1**·Eu^{3+} and **2** (Chapter 5). This demonstrates that the adamantyl-functionalized molecules, **1**·Eu^{3+} and **2** have rapidly immobilized on the host-functionalized surface by host-guest interactions. The filling of the CD surface by the assembly of an equimolar ratio of **1**·Eu^{3+} and **2** in the presence of CD_l is assumed to take place at similar rates.

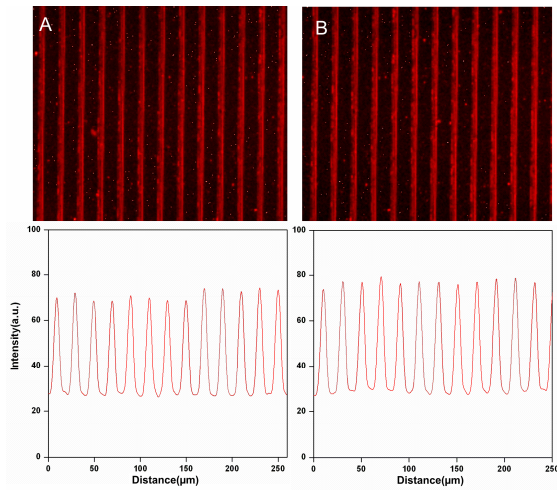

Figure 6.1 Fluorescence microscopy images and corresponding intensity profiles of 10 μm lines prepared by printing G5-PPI-$(Ad)_{64}$ dendrimers on a CD monolayer and incubation with a 50%:50% mixture of **2** and **1**·Eu^{3+} in the absence of CD_l equilibrated for 1 min (A) and 1 h (B).

Solutions of different molar ratios of **1**·Eu^{3+} and **2** without CD_l present (Scheme 6.3A) were prepared in order to study the stoichiometry of the resulting complex and to provide a reference point for the experiments performed under thermodynamic control (see below). Solution mixtures of **1**·Eu^{3+} and **2** were prepared, for which the fraction of **2** was set to 0%, 20%, 40%, 50%, 60%, 80%, and 100%. These solution mixtures were incubated over G5-PPI-$(Ad)_{64}$-printed CD monolayers for 1 h and were imaged by fluorescence microscopy with both filters **R** (Figure 6.2a) and **B** (Figure 6.2b).[21]

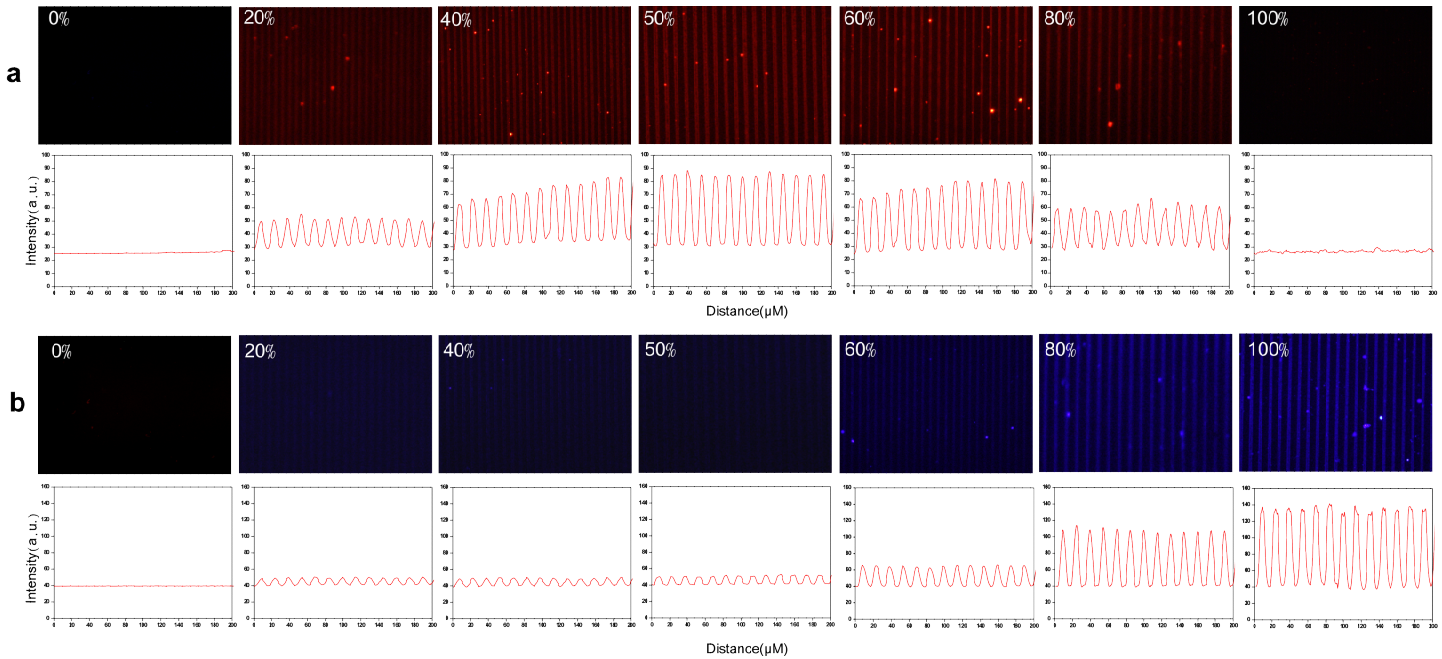

Figure 6.2 Fluorescence microscopy images of 10 μm lines of G5-PPI-$(Ad)_{64}$ dendrimers printed on a CD monolayer and incubated with solution mixtures of different ratios of **1**·Eu^{3+} and **2** in the absence of CD_l, and monitoring the emission of Eu^{3+} (a, filter **R**) and of antenna **2** (b, filter **B**). The percentages of antenna **2** in the mixtures of **1**·Eu^{3+} and **2** are given in the images. The corresponding intensity profiles are also shown.

The fluorescence images and corresponding intensity profiles of **1**·Eu^{3+} (Figure 6.2a) and **2** (Figure 6.2b) as a function of the fraction of **2** in solution show: (i) the quenching of antenna emission is in accordance with energy transfer to the Eu^{3+} and (ii) the optimal sensitized emission occurs at a 1:1 ratio of **1**·Eu^{3+} and **2**. This stoichiometry relation is consistent with the stoichiometry obtained by μCP with different mixtures of **1**·Eu^{3+} and **2** (see Chapter 5). This clearly demonstrates that the assembly of surface species in the absence of CD_l is linearly dependent on the solution composition (Figure 6.3A).

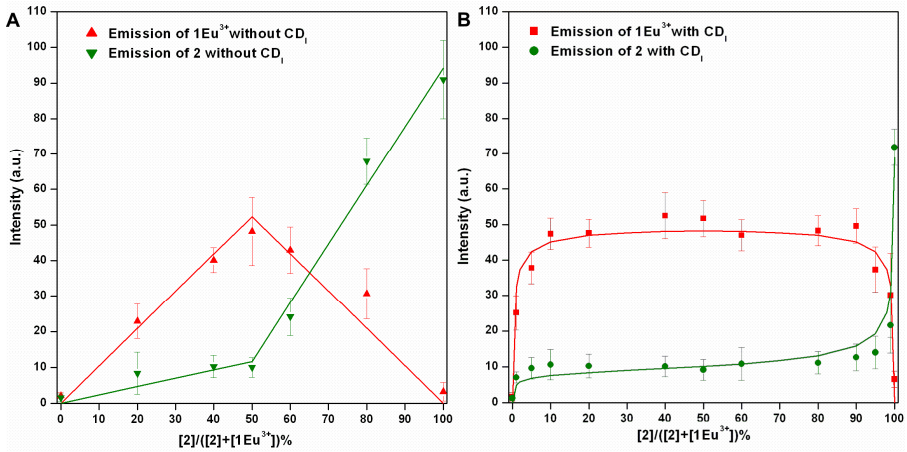

Figure 6.3 Fluorescence intensities of **1**·Eu^{3+} and **2** obtained from solution assembly with different solution mixtures, without (A) and with (B) CD_l present in the different mixtures of **1**·Eu^{3+} and **2**, incubated over G5-PPI-$(Ad)_{64}$-patterned CD monolayers. Emissions of Eu^{3+} (filter **R**) and **2** (filter **B**) were monitored at the same time. Solid curves indicate linear fits (A) and the corresponding fits to the multivalent, sequential binding model (B).

6.2.3 Thermodynamically controlled assembly

Following procedure B in Scheme 6.3, CD monolayers with dendrimer patterns were incubated in solutions of different molar ratios of **1**·Eu^{3+} and **2** in the presence of CD_l in order to study the effect of competition by CD_l on the degree of **1**·Eu^{3+}·**2** formation. Therefore, first, solution mixtures of **1**·Eu^{3+} and **2** were prepared, for which the concentration of **2** was set to 0%, 1%, 5%, 10%, 20%, 40%, 50%, 60%, 80%, 90%, 95%, 99%, and 100% with 200 μM of CD_l present as well. Consecutively, these solution mixtures were incubated over G5-PPI-$(Ad)_{64}$-printed CD monolayers for 1 h and were imaged with fluorescence microscopy with both filters **R** and **B** (Figure 6.4).

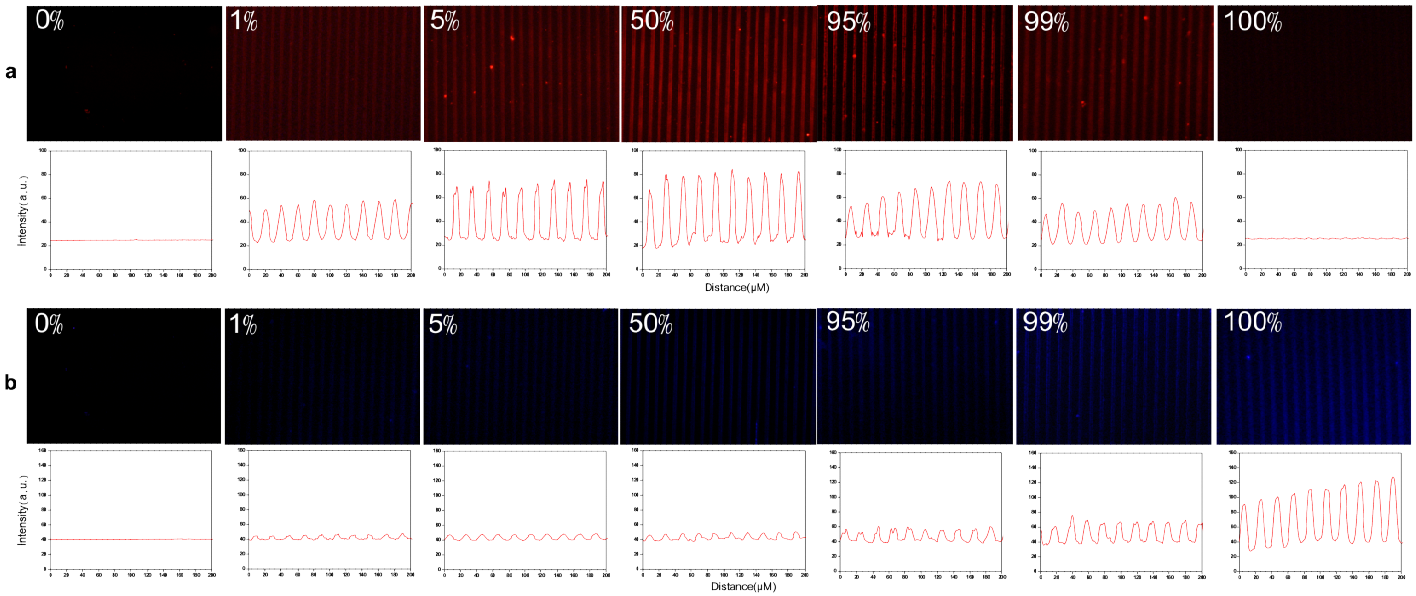

Figure 6.4 Fluorescence microscopy images of 10 μm lines of G5-PPI-$(Ad)_{64}$ printed on a CD monolayer incubated with solution mixtures of different ratios of **1**·Eu^{3+} and **2** with 200 μM CD_l, and monitoring the emission of Eu^{3+} (a, filter **R**) and of **2** (b, filter **B**). The percentages of antenna **2** in the mixtures of **1**·Eu^{3+} and **2** are given in the images. The corresponding intensity profiles are also shown.

By adding 200 μM of CD_l to the solution mixtures of **1**·Eu^{3+} and **2**, the complex formation of **1**·Eu^{3+}·**2** on the surface shows a highly non-linear dependence on the solution ratio (Figure 6.3B). At fractions of **2** in the solution mixtures ranging from 10-90%, the fluorescence intensities of both the Eu^{3+} and the antenna **2** indicate a 1:1 ratio of **1**·Eu^{3+} and **2** at the surface, since these intensities are equal to those obtained for a 1:1 mixture without equilibration (Figure 6.3A). These results infer that the formation of **1**·Eu^{3+}·**2** constitutes a strong thermodynamic driving force for establishing a 1:1 composition at the surface. Kinetically, this equilibrium is established by the competition induced by CD_l, which accelerates desorption of the non-coordinated divalent ligands **1**·Eu^{3+} and **2** and thus promotes exchange of the excess, uncoordinated major component from the surface for the minor component.

For the solution mixtures with fractions of **2** below 10% and above 90%, less Eu^{3+} fluorescence intensity was observed with concomitant variations in the intensity of **2**. These data points indicate the establishment of the equilibrium between the statistically preferred adsorption of the major component vs. the complexation-driven adsorption of the minor component.

6.2.4 Modeling/simulations

To increase the understanding of the nonlinear amplification of **1**·Eu^{3+}·**2** at the CD monolayer in the presence of CD_l under equilibrium conditions, the complex formation of **1**·Eu^{3+}·**2** was modeled by calculating all surface species concentrations and the concomitant fluorescence intensities as a function of the solution composition, while varying the binding constant, K_{AE}, of the coordination of the carboxylate group of 2 to the Eu^{3+} center of **1**·Eu^{3+} (Figure 6.5). The thermodynamic model treats the binding of multivalent ligands to the CD surface as independent binding events, both for inter- and intramolecular binding events (Scheme 6.4). Because each ligand **1**·Eu^{3+} and **2** can bind to the CD monolayer in a divalent fashion, the maximum coverage of **1**·Eu^{3+} and **2** is only half of the coverage of the CD monolayer, where the monovalent binding of ligands is ignored due to their lower association constants towards to CD surface. The model employs binding constants for interaction of an adamantyl group to a CD surface site ($5x10^4$ M^{-1}), and the 1:1 interaction (K_{AE}) of the antenna carboxylate group with the Eu^{3+} center. The intramolecular binding events are associated with an effective

concentration parameter,[22] which is set to be 4-fold lower for the coordination of **2** to **1**·Eu^{3+} than for binding of the divalent ligands to the CD surface, because of the tetravalent nature of the complex. The modeled fluorescence intensities were obtained by relating these to the fractions of unbound and bound **1**·Eu^{3+} and **2**, assuming fixed values for the emission of **2**, **1**·Eu^{3+}, and the complex **1**·Eu^{3+}·**2**. These values were optimized in the procedure.

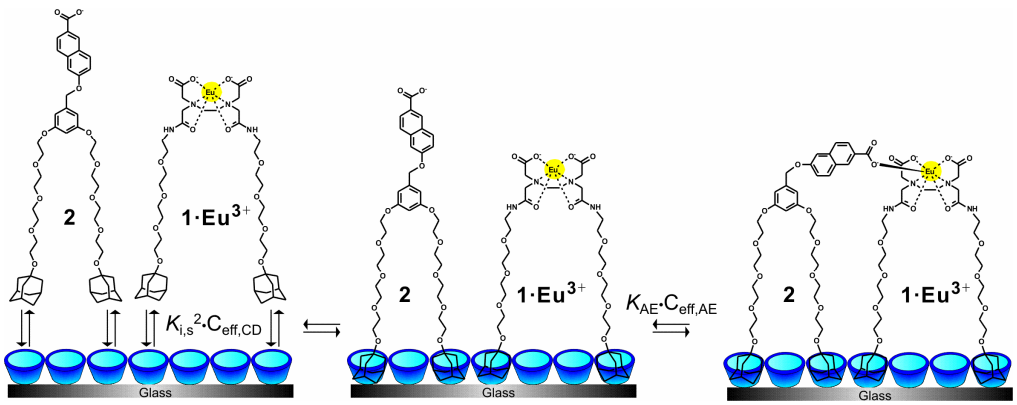

Scheme 6.4 Schematic representation for solution and surface species of **1**·Eu^{3+} and **2** with two sequential binding events at the CD monolayer. Host-guest binding: the multivalent binding of **1**·Eu^{3+} and **2** to the CD monolayer is accompanied with the effective concentration term ($K_{i,s}{}^2C_{eff,CD}$). Complex binding: the association between **1**·Eu^{3+} and **2** is enhanced with the effective concentration term ($K_{i,s}C_{eff,AE}$).

The fluorescence intensity of antenna **2** linearly increases with the fraction of **2** in solution in the absence of binding ($K_{AE} = 0$), indicating that no energy transfer to Eu^{3+} occurred (Figure 6.5a). Upon increase of the binding constant, the antenna emission shows a nonlinear dependence with respect to the solution fraction of **2** because of the simultaneous effects of changing surface composition and fluorescence quenching, both due to the binding of **2** to **1**·Eu^{3+}. The emission intensity at a value of approx. 10 reflects the remaining intensity of **2** after energy transfer to the Eu^{3+} center upon 1:1 complex formation. At higher binding constants, the intensity plateau becomes more flat and more extended, reflecting a 1:1 surface composition of **1**·Eu^{3+} and **2** at this plateau.

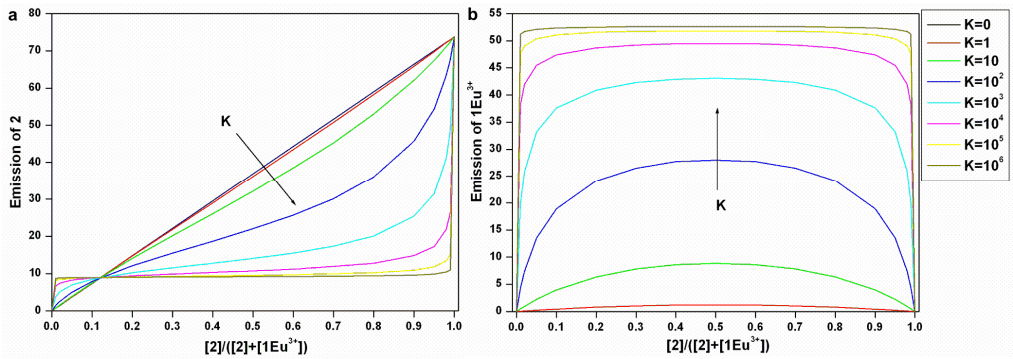

Figure 6.5 Simulated emissions of **2** (a) and of **1**·Eu^{3+}·**2** (b) present at a CD monolayer vs. the solution fraction of **2** as a function of the binding constant K_{AE} of the coordination of the carboxylate group of **2** to **1**·Eu^{3+} at 200 μM CD_l.

The Eu^{3+} emission vs. the solution composition at different binding constants is shown in Figure 6.5b. Overall, the trend of Eu^{3+} emission is similar. Over 90% of maximum Eu^{3+} emission is reached for $K_{AE} > 10^4$ M^{-1}, and the plateau where this maxima intensity is reached widens from a 50%/50% solution composition to more deviating fractions at higher K_{AE} values in accordance with stabilization and thus amplification of the **1**·Eu^{3+}·**2** complex.

Subsequently, the experimental curves at 200 μM CD_l (Figure 6.3B) were fitted to the model. The calculated binding constant $K_{AE} = 6\times10^3$ M^{-1}, which agrees well with the lower limit (10^3 M^{-1}) estimated previously[17] for the assembly to the CD monolayer by μCP.

Figure 6.6A depicts the simulated speciation of the different species present at the CD surface using the thermodynamic model in the presence of CD_l at 200 μM and $K_{AE} = 6\times10^3$ M^{-1}. As can be observed in Figure 6.6A, at very low fractions of **2** in solution, **1**·Eu^{3+} is the predominant species at the surface, as it is also in solution. Upon increase of the solution fraction of **2**, this surface species is rapidly replaced by **1**·Eu^{3+}·**2**. At intermediate fractions between 10% and 90%, **1**·Eu^{3+}·**2** is the major species with a coverage around 90%. Similarly, at high fractions of **2**, antenna **2** becomes the dominant species present at the CD monolayer. At all fractions of **2**, $>$99% of CD_s is involved in host-guest binding.

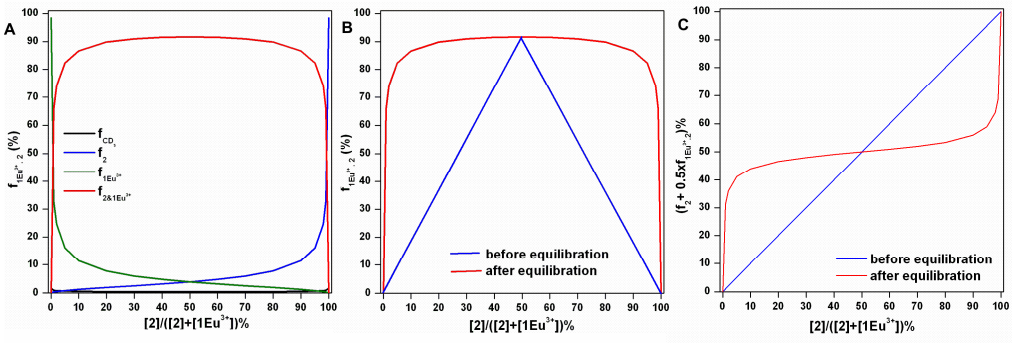

Figure 6.6 (A) Speciation of divalently bound **1**·Eu^{3+}, divalently bound **2**, tetravalently bound **1**·Eu^{3+}·**2** and uncomplexed CD_s present at CD monolayers simulated as a function of the solution fraction of **2** (K_{AE} = 6×10^3 M^{-1}, CD_l = 200 μM). (B) Surface fraction of **1**·Eu^{3+}·**2** vs. the solution fraction of **2** before and after CD equilibration. The curve after equilibration (red) is obtained using the thermodynamic model, while the lines before equilibration (blue) correspond to formation of **1**·Eu^{3+}·**2** from **1**·Eu^{3+}·and **2** assuming that their surface ratio is identical to the solution fraction from which they are assembled. (C) Surface fraction of **2** (including of **2** and **1**·Eu^{3+}·**2**) vs. the solution fraction of **2** before and after CD equilibration.

The surface coverage of **1**·Eu^{3+}·**2** is plotted vs. the solution fraction of **2** in Figure 6.6B as well (red line, Scheme 6.3B, b_3), together with the hypothetical case in which the surface is filled with **1**·Eu^{3+} and **2** in the same ratio as present in solution, but without subsequent ligand exchange (blue line, Scheme 6.3B, b_2). The latter very closely resembles the experimental case in the absence of CD_l (Scheme 6.3A). The comparison of these two graphs (Figure 6.6B) clearly emphasizes the nonlinear amplification of **1**·Eu^{3+}·**2** in case of equilibration, induced by CD_l, driven by complex formation between **1**·Eu^{3+} and **2** (Scheme 6.3B). The total fraction of antenna **2**, including the fraction of noncoordinated **2** and of the fraction complexed in **1**·Eu^{3+}·**2**, is plotted vs. the solution fraction of **2** as shown in Figure 6.6C. Before equilibration, the surface fraction of **2** is equal to the fraction of **2** in solution. After equilibration, the CD_l-driven formation of **1**·Eu^{3+}·**2** results in a strong tendency towards a 50% fraction of **2** on the surface. The plot clearly demonstrates the nonlinear dependence of the surface percentage of **2** on the solution composition.

6.2.5 Exchange kinetics

As shown above, the nonlinear amplification process requires exchange of the major component, present in solution and on the surface after the initial filling of the surface, by the minor one, to drive the surface ratio into the direction of a 1:1 composition. In order to observe this exchange process, it needs to be isolated from the initial filling step. Therefore, an initial immobilization of divalently bound **1**·Eu^{3+} and **2** in the absence of CD_l was followed by an exchange step in the presence of CD_l. As depicted in Scheme 6.5, the CD monolayer was first patterned with G5-PPI-$(Ad)_{64}$ dendrimer and incubated with a solution with 10% of antenna **2** and 90% of **1**·Eu^{3+} without CD_l present for 1 h. After rinsing the sample, the same 10% mixture, but with CD_l present, was incubated over the prefilled surface and the fluorescence intensity was monitored in time.

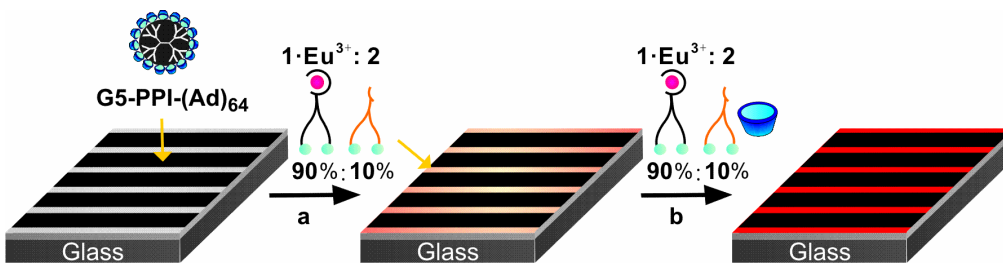

Scheme 6.5 Schematic representation of surface preparation for monitoring the exchange process: a) dendrimer-patterned CD monolayer incubated with a mixture with 10% of antenna **2** and 90% of **1**·Eu^{3+} without CD_l present, b) followed by drop casting the same mixture with CD_l present in solution.

Different concentrations of CD_l present in the 10% solution of antenna **2** were used to observe the kinetic exchange by the complex formation of **1**·Eu^{3+}·**2** promoted by CD_l competition. The kinetic procedure was probed following the intensity increase of Eu^{3+}emission, from the emission of the prefilled surface with 10% of antenna **2** to the complete formation of the target 1:1 complex, which is $>$90% formed after equilibration as shown above.

In the presence of 200 μM of CD_l (Figure 6.7), the exchange process was completed and equilibrated within 30 min (Figure 6.8, red dots). By decreasing the concentration of CD_l, the exchange process was slowed down to reach complete formation of **1**·Eu^{3+}·**2** after 1 h in the presence of 100 μM of CD_l. At even lower concentration (10 μM), the system was equilibrated after 3 h. These observations show that the exchange process of molecular adsorption and desorption onto/from the CD surface is effectively influenced by the presence of CD_l.

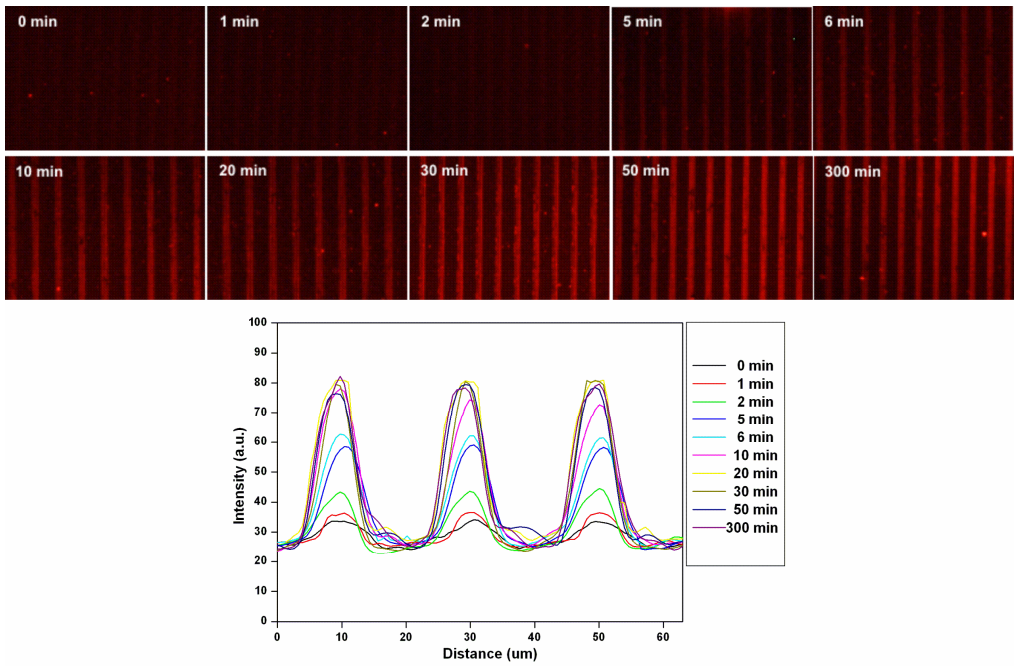

Figure 6.7 a) Fluorescence microscopy images of 10 μm lines of G5-PPI-$(Ad)_{64}$ dendrimers printed on CD monolayers, initially incubated with a mixture of 10% antenna **2** and 90% **1**·Eu^{3+} without CD_l present, followed by drop casting the same mixture with 200 μM CD_l, and monitoring the emission of Eu^{3+} (filter **R**) in time, and (b) the corresponding intensity profiles.

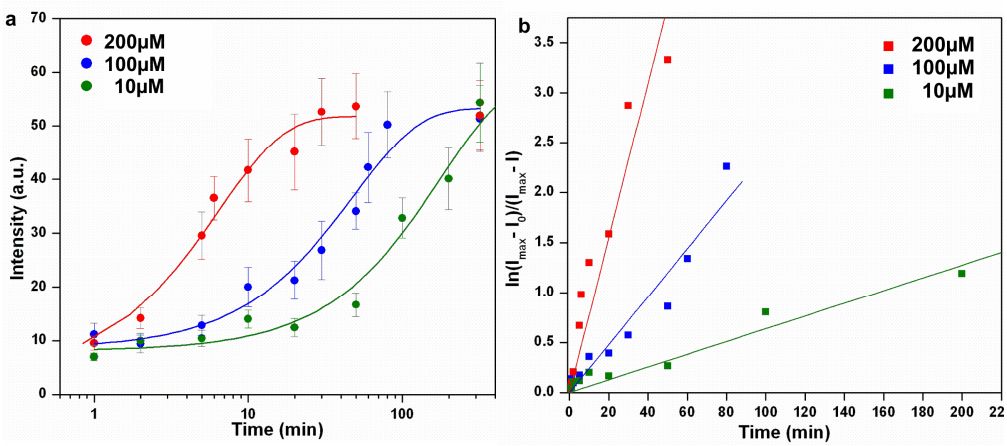

Figure 6.8 a) Monitoring the emission of Eu^{3+} in time by drop casting the mixture of 10% antenna **2** and 90% **1**·Eu^{3+} with 10 μM CD_l, 100 μM CD_l, and 200 μM CD_l onto a surface prefilled in the absence of CD_l. (b) Determination of exchange rate constants at different concentrations of CD_l, where the solid lines present the linear fit to the data points.

The data were plotted in logarithmic format (Figure 6.8b) in order to verify the expected pseudo-first-order kinetics as well as to assess the corresponding rate constants. The linear trends indicate pseudo-first-order kinetics. In the presence of 200 μM of CD_l, the highest rate constant (0.077 min^{-1}) was obtained describing the system is equilibrated efficiently. When the exchange process is equilibrated in the presence of 100 μM of CD_l, the rate constant dropped down to less than half of the value obtained in the presence of 200 μM of CD_l (0.024 min^{-1}), while the rate constant obtained in the presence of 10 μM of CD_l shows the lowest value (0.006 min^{-1}). Therefore, with an increasing concentration of CD_l, the rate of the molecular exchange process apparently increases accordingly, as the rate of equilibrating also increases. Most likely, it indicates that the rate-limiting step of the exchange process is the dissociation of the minor divalent ligand with one Ad group attached to the interface and the other Ad group to a CD_l moiety, since the concentration of this species is expected to increase almost linearly with the concentration of CD_l. However, mass transport issues also play a role. In conclusion, the experiments confirm that (i) an exchange process of the major for the minor ligand is the mechanism of nonlinear amplification, (ii) this process is much slower than the initial surface filling step, and (iii) this exchange process is dependent on competition by the receptor in solution.

6.3 Conclusion

Multivalent interactions at interfaces constitute a complex phenomenon governed by a range of parameters. Here, multivalent binding of a supramolecular complex at a multivalent host surface by combining the orthogonal cyclodextrin host-guest and lanthanide ligand coordination interaction motifs is described and is used to monitor the molecular binding events by its intrinsic luminescence.

We successfully explored the ability to systematically vary multivalency in a controlled manner at interfaces by adding a competing host. The formation of the **1**·Eu^{3+}·**2** complex is observed to be linearly dependent on the solution composition in the absence of cyclodextrin, while strong nonlinear amplification has been observed under the cyclodextrin-promoted thermodynamic equilibrium.

Due to the cyclodextrin-induced competition, the desorption of molecules from the surface is enhanced, promoting assembly of the most stable complex on the CD monolayer with the highest valency under equilibrium. This kinetic self-organized process was also monitored in time in the presence of different cyclodextrin concentrations.

These results revealed new and surprising characteristics of multivalent interactions at interfaces. The model described here gives an insight into how multiple, independent interactions provide a collective selection mechanism, where the molecular-level exchange events can be self-reported and provide the evidence for molecular cooperativity, self-recognition, and self-selection on the surface.

6.4 Experimental

Materials. For information on the synthesis and characterization of the different compounds, the reader is referred to the work of Deniz Yilmaz.[17] MilliQ with a resistivity higher than 18 MΩ·cm was used in all experiments.

Substrate and monolayer preparation. Microscope glass slides were used for cyclodextrin (*β*-CD) monolayer preparation.[23] The substrates were cleaned with piranha solution for 15 min (concentrated H_2SO_4 and 33% aqueous H_2O_2 in a 3:1 ratio; Caution: piranha should be handled carefully) and rinsed with MilliQ. After drying in a nitrogen stream, the substrates were used immediately for silane monolayer formation. The substrates were enclosed in a low-

vacuum desiccator with 0.1 ml of TPEDA, continually pumping for 5 min to create a vapor phase of TPEDA. After overnight incubation, the slides were rinsed with ethanol and dichloromethane to remove any excess of silanes and subsequently dried in a nitrogen stream. The attachment of 1,4-phenylene diisothiocyanate was made in a 20 mM solution in toluene at 60 ˚C during 2 h. Samples were thoroughly rinsed with toluene and dried in a nitrogen flow. The CD layer attachment was made during 2 h in an aqueous 0.1 mM *β*-cyclodextrin-heptaamine solution (pH~7) at 60 ˚C. Samples were thoroughly rinsed with water and dried in a nitrogen flow.

Printing of G5-PPI-$(Ad)_{64}$ dendrimers on CD monolayer, followed by 1·Eu^{3+} and 2 immersion. The CD monolayer substrate was printed for 20 min with a stamp inked with G5-PPI-$(Ad)_{64}$ dendrimers, followed by rinsing with water and drying in a stream of nitrogen. The printed surface was immersed with different molar ratios of **2** and **1** with or without CD_l present. These solution mixtures were incubated over a G5-PPI-$(Ad)_{64}$ dendrimers printed CD monolayer for 1 h, followed by rinsing with water and drying in a stream of nitrogen and imaged with fluorescence microscopy with both filters **R** and **B**.

Exchange process of complex assembly with CD_l present. The G5-PPI-$(Ad)_{64}$ dendrimers printed CD monolayer were first incubated with 10% mixtures of antenna **2** for 1 h, followed by rinsing with water and drying in a stream of nitrogen. The prefilled surface was followed by inking the same mixtures of 10% antenna **2** with adding 10 μM, 100 μM, and 200 μM CD_l, individually, followed by rinsing with water and drying in a stream of nitrogen and imaged in time using filter **R**.

Instrumentation

Fluorescence microscopy. Fluorescence microscope images were taken using an Olympus inverted research microscope IX71 equipped with a mercury burner U-RFL-T as light source and a digital Olympus DR70 camera for image acquisition. UV excitation (300 nm $\leq \lambda_{ex} \leq$ 400 nm) and blue emission (410 nm $\leq \lambda_{em} \leq$ 510 nm) was filtered using a Dapi Olympus filter cube (filter **B**). UV excitation (300 nm $\leq \lambda_{ex} \leq$ 400 nm) and red emission

(narrow band pass at 615 nm) was filtered using a Olympus filter cube (filter **R**). All fluorescence microscopy images were acquired in air.

Modeling. Complexation of **1**·Eu^{3+} by **2** on a CD monolayer was modeled using a thermodynamic model governed by effective concentration, using a spreadsheet approach.[24] Once each ligand **1**·Eu^{3+} and **2** is bound in a divalent fashion, the maximum coverage of **1**·Eu^{3+} and **2** is only half of the coverage of the CD monolayer. The model employs binding constants $K_{i,l}$ and $K_{i,s}$ for interaction of an adamantyl group to a CD site ($5x10^4$ M^{-1}), and the 1:1 (K_{AE}) interaction of the antenna carboxylate group to the Eu^{3+} center. The intramolecular binding events are associated with an effective concentration parameter,[22] which is set to be 4-fold lower (0.025 M^{-1}) for the coordination of **2** to **1**·Eu^{3+} than for binding of the divalent ligands to the CD surface (0.1 M^{-1}), because of the tetravalent nature of the complex. The modeled fluorescence intensities were obtained by relating these to the fractions of unbound and bound **1**·Eu^{3+} and **2**, assuming fixed values for the emission of **2**, **1**·Eu^{3+}, and the complex **1**·Eu^{3+}·**2**. These values are optimized in the procedure.

A general description is given for the divalent binding of the heterotropic supramolecular complex at a multivalent host surface by combing the orthogonal CD host-guest and metal-ion coordination motifs. All species of **1**·Eu^{3+} **(**E), **2** (A), and their complex (AE) due to complexation to CD_l and CD_s are shown in Figure 6.9.

From the coverage calculation[23], the employed concentration of solution species ($[A(CD_l)_2]$ and ($[E(CD_l)_2]$) are always present in large excess compared to surface binding sites (CD_s), so that changes to the solution composition due to surface binding can be ignored. The simplified mass balances for A, E, and CD_S are given by (1), (2), (3), (4) (Figure 6.9). Substitution of the equilibrium constant into the mass balance for $[A]_{tot}$, $[E]_{tot}$, $[CD_s]_{tot}$ provides a set of numerically solvable species with [A],[E], and $[CD_s]$ as the variables. Starting from initial estimates for K_{AE}, this set of equations is solved numerically using the spreadsheet approach. The fractions of surface species are also calculated by dividing each component concentration by the total concentration.

(a)

$$A + CD_l \underset{}{\overset{K_{i,l}}{\rightleftharpoons}} A(CD_l) + CD_l \overset{K_{i,l}}{\rightleftharpoons} A(CD_l)_2$$

$$E + CD_l \overset{K_{i,l}}{\rightleftharpoons} E(CD_l) + CD_l \overset{K_{i,l}}{\rightleftharpoons} E(CD_l)_2$$

$$A + 2\cdot(CD_s) \overset{K_s}{\rightleftharpoons} A(CD_s)_2$$

$$E + 2\cdot(CD_s) \overset{K_s}{\rightleftharpoons} E(CD_s)_2$$

$$A(CD_s)_2 + E(CD_s)_2 \overset{K}{\rightleftharpoons} AE(CD_s)_4$$

$$K_{i,l} = \frac{[A(CD_l)]}{[A]\,[CD_l]} = \frac{[A(CD_l)_2]}{[A(CD_l)]\,[CD_l]} \qquad K_{i,l} = \frac{[E(CD_l)]}{[E]\,[CD_l]} = \frac{[E(CD_l)_2]}{[E(CD_l)]\,[CD_l]}$$

$$K_s = 2K_{i,s}\cdot 1/2K_{i,s}\cdot C_{eff,CD} = K_{i,s}^2\cdot C_{eff,max}\cdot [CD_s]/[CD_s]_{tot} = K_{i,s}^2\cdot C_{eff,max}\cdot f_{CDs}$$

$$f_{CDs} = \frac{[CD_s]}{[CD_s]_{tot}}$$

$$K = K_{AE}\cdot C_{eff,AE}$$

(b)

$$[A]_{tot} = [A] + [A(CD_l)] + [A(CD_l)_2] = [A](1 + K_{i,l}[CD_l](2 + K_{i,l}[CD_l])) \quad (1)$$

$$[E]_{tot} = [E] + [E(CD_l)] + [E(CD_l)_2] = [E](1 + K_{i,l}[CD_l](2 + K_{i,l}[CD_l])) \quad (2)$$

$$[CD_s]_{tot} = [CD_s] + 2[A(CD_s)_2] + 2[E(CD_s)_2] + 4[AE(CD_s)_4] \quad (3)$$

$$1 = f_{CDs}(1 + 2\cdot[A]\cdot K_{i,s}^2\cdot C_{eff,max}\cdot f_{CDs} + 2\cdot[E]\cdot K_{i,s}^2 C_{eff,max}\cdot f_{CDs} + 4\cdot K_{AE}\cdot C_{eff,AE}\cdot K_{i,s}^4\cdot C_{eff,max}^2\cdot[A][E]\cdot f_{CDs}^3) \quad (4)$$

Figure 6.9 (a) Equilibria for all species of antenna **2** (A), europium complex **1**·Eu^{3+} (E) and its complex (AE) in the presence of CD_l and CD_s and (b) simplified mass balances for A, E and CD_S.

6.5 Acknowledgements

Deniz Yilmaz is acknowledged for the synthesis of the molecules, **1**·Eu^{3+} and **2**. Prof. Jurriaan Huskens and Alberto Casado are gratefully acknowledged for the model design.

6.6 References

[1] M. Mammen, S. K. Choi, G. M. Whitesides, *Angew. Chem. Int. Ed.* **1998**, *37*, 2755.
[2] L. L. Kiessling, J. E. Gestwicki, L. E. Strong, *Angew. Chem. Int. Ed.* **2006**, *45*, 2348.
[3] A. Mulder, J. Huskens, D. N. Reinhoudt, *Org. Biomol. Chem.* **2004**, *2*, 3409.
[4] J. Huskens, *Curr. Opin. Chem. Biol.* **2006**, *10*, 537.
[5] M. J. W. Ludden, D. N. Reinhoudt, J. Huskens, *Chem. Soc. Rev.* **2006**, *35*, 1122.
[6] J. E. Gestwicki, L. L. Kiessling, *Nature* **2002**, *415*, 81.
[7] M. L. Pisarchick, N. L. Thompson, *Biophys. J.* **1990**, *57*, A292.
[8] E. L. Doyle, C. A. Hunter, H. C. Phillips, S. J. Webb, N. H. Williams, *J. Am. Chem. Soc.* **2003**, *125*, 4593.
[9] N. Horan, L. Yan, H. Isobe, G. M. Whitesides, D. Kahne, *Proc. Natl. Acad. Sci. U.S.A.* **1999**, *96*, 11782.
[10] S. J. Metallo, R. S. Kane, R. E. Holmlin, G. M. Whitesides, *J. Am. Chem. Soc.* **2003**, *125*, 4534.
[11] D. N. Reinhoudt, M. Crego-Calama, *Science* **2002**, *295*, 2403.
[12] A. Langner, S. L. Tait, N. Lin, C. Rajadurai, M. Ruben, K. Kern, *Proc. Natl. Acad. Sci. U.S.A.* **2007**, *104*, 17927.
[13] A. Mulder, S. Onclin, M. Peter, J. P. Hoogenboom, H. Beijleveld, J. ter Maat, M. F. Garcia-Parajo, B. J. Ravoo, J. Huskens, N. F. van Hulst, D. N. Reinhoudt, *Small* **2005**, *1*, 242.
[14] Y. Michito, K. K. Jeremy, F. Makoto, *Angew. Chem. Int. Ed.* **2009**, *48*, 3418.
[15] M. Fujita, *Chem. Soc. Rev.* **1998**, *27*, 417.
[16] G. E. Buonocore, H. Li, B. Marciniak, *Coord. Chem. Rev.* **1990**, *99*, 55.
[17] S. H. Hsu, M. D. Yilmaz, C. Blum, V. Subramaniam, D. N. Reinhoudt, A. H. Velders, J. Huskens, *J. Am. Chem. Soc.* **2009**, *131*, 12567.
[18] S. Onclin, J. Huskens, B. J. Ravoo, D. N. Reinhoudt, *Small* **2005**, *1*, 852.
[19] A. Mulder, T. Auletta, A. Sartori, S. Del Ciotto, A. Casnati, R. Ungaro, J. Huskens, D. N. Reinhoudt, *J. Am. Chem. Soc.* **2004**, *126*, 6627.
[20] T. Auletta, B. Dordi, A. Mulder, A. Sartori, S. Onclin, C. M. Bruinink, M. Peter, C. A. Nijhuis, H. Beijleveld, H. Schonherr, G. J. Vancso, A. Casnati, R. Ungaro, B. J. Ravoo, J. Huskens, D. N. Reinhoudt, *Angew. Chem. Int. Ed.* **2004**, *43*, 369.
[21] The surface was consecutively imaged by fluorescence microscopy using two different filter sets: one set allows UV excitation and red emission using a narrow bandpass filter centered at 610 nm (**R**, which only collects the emission of Eu^{3+}) and another set allows UV excitation and blue emission (**B**, which only collects the emission of the naphthalene moiety).
[22] J. Huskens, A. Mulder, T. Auletta, C. A. Nijhuis, M. J. W. Ludden, D. N. Reinhoudt, *J. Am. Chem. Soc.* **2004**, *126*, 6784.
[23] S. Onclin, A. Mulder, J. Huskens, B. J. Ravoo, D. N. Reinhoudt, *Langmuir* **2004**, *20*, 5460.

[24] J. Huskens, H. Van Bekkum, J. A. Peters, *Comp. Chem.* **1995**, *19*, 409.

Chapter 7

Edge Lithography using Multivalent Interactions

ABSTRACT. This chapter describes preliminary experiments for the fabrication of submicrometer-scale molecular patterns of the antenna-lanthanide complex introduced in Chapters 5 and 6. Fabrication of nanoscale patterns is achieved by supramolecular microcontact printing of an antenna molecule having two adamantyl groups for host-guest interactions, and consecutive filling of the non-patterned areas with the Eu^{3+}-EDTA complex, also functionalized with two adamantyl groups for host-guest interactions. Multivalent interactions on the cyclodextrin (CD) surface are used to enhance the selective formation and isolation of the self-reporting lanthanide-antenna complex at the boundary of both pattern areas. Molecules divalently interacting with the host surface (*i.e.* the antenna ligand and the Eu^{3+}-EDTA complex) are not inert against washing steps with competing host molecules (CD) in solution, whereas the tetravalently interacting lanthanide-antenna complex, formed at the boundaries, has an enhanced kinetic and thermodynamic stability. Fluorescence and atomic force microscopy measurements have been used to monitor the three-step procedure and prove the formation of 150 nm wide line patterns of the tetravalent lanthanide-antenna complex starting from a micrometer-sized PDMS stamp in the printing step. This work shows that the concept of multivalency can be used to fabricate nanosize features with microsize tools.

---

*Manuscript in preparation: Shu-Han Hsu, M. Deniz Yilmaz, David N. Reinhoudt, Jurriaan Huskens and Aldrik H. Velders.

7.1 Introduction

Multivalency concerns the interactions between multivalent receptors and multivalent ligands. Multivalent interactions are of interest, since multivalency is one of nature's governing principles in *e.g.* protein-carbohydrate interactions and cell recognition,[1, 2] and has proven to be a powerful tool for the fabrication of molecular nanostructures.[3-5] Multivalent interactions at interfaces, *e.g.*, at cell membranes,[2] at lipid membranes,[6, 7] or at self-assembled monolayer (SAM) model systems,[8-10] are particularly important, since such interfaces, when functionalized with monovalent receptors or ligands can act as multivalent systems.[4] Multivalent binding events have collective properties different from monovalent interactions, which lead to higher binding affinities between the interacting species. The strength of the binding of multivalent molecules can be accurately tuned by varying the supramolecular chemistry of the host-guest system and by varying the number of noncovalent interactions.

Miniaturization, for example in the semiconductor industry, has led to a variety of techniques for nanofabrication. Edge lithography is a collection of techniques that aims for the edges of an original micropattern to become the features of the final pattern. Thus, nanofeatures can be obtained along a predefined pattern.[11, 12]

The concept of molecular printboards, which are monolayers of receptor molecules (e.g. cyclodextrins), is suited for studying the host-guest binding of multivalent guests at interfaces.[3, 4] The adamantyl-functionalized antenna and EDTA-Eu^{3+} motifs introduced in Chapter 5 have been exploited to investigate host-guest interactions on the molecular printboards; the supramolecular complex signals its own correct assembly by expressing sensitized lanthanide luminescence.[13] The orthogonal recognition motif of cyclodextrin host-guest and lanthanide-ligand coordination can lead to more complex and higher-valent architectures. When such complexes with a higher valency, here tetravalent, are immobilized on the cyclodextrin surface, their desorption from the surface becomes more difficult, leading to non-linear amplification of complex formation, as described in Chapter 6. Even upon incubation with solutions containing competing host molecules, the multivalent complexes firmly bind to the surface due to the high number of interacting sites.

Here, the controlled nanoscale fabrication of nanostructures of the tetravalent adamantyl-functionalized lanthanide-antenna complexes is presented. The complexes form along the boundaries of antenna and EDTA-Eu^{3+} pattern areas, created by a microcontact

printing (μCP) step followed by an incubation step (see Scheme 7.1). A subsequent washing step removes divalently bound molecules and leaves the tetravalently immobilized lanthanide-antenna complex. The intrinsic signaling property of the antenna-sensitized Eu^{3+} luminescence was used to study and prove the formation of the supramolecular tetravalent complex on the surface, while the dimensions of the submicrometer patterns were characterized by AFM.

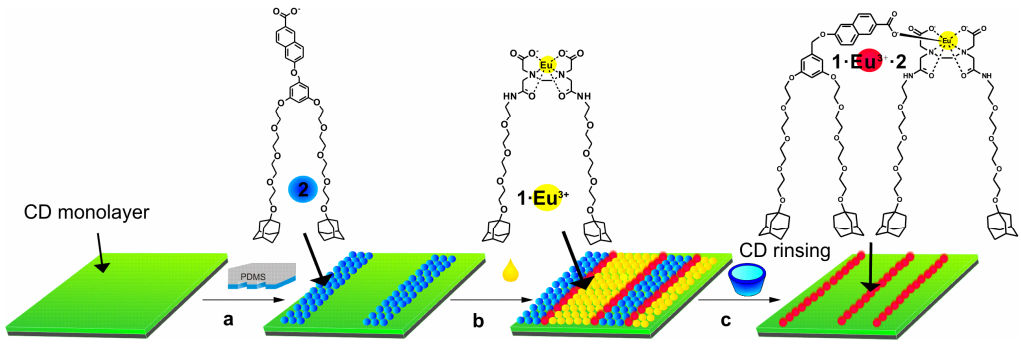

Scheme 7.1 Schematic illustration of preparation of the backfilled monolayers and the resulting structures at the edges. (a) μCP of antenna **2** (blue) on a CD monolayer; (b) incubation with **1**·Eu^{3+} (yellow); and rinsing with a CD solution leaving tetravalently immobilized **1**·Eu^{3+}·**2** patterns (red).

7.2 Results and discussion

Four different building blocks were used to study the multivalent, orthogonal complexation: an EDTA-based ligand **1** for binding Eu^{3+} ion, the Eu^{3+} ion, a naphthalene-based antenna **2** with a carboxylate group for coordination to the Eu^{3+} ion, and CD monolayers. The EDTA ligand and the antenna molecule are equipped with adamantyl (Ad) groups for noncovalent anchoring to the CD monolayers. The CD monolayer is used to immobilize both the sensitizer **2** and the Eu^{3+} complex **1**·Eu^{3+}, thus enforcing the close proximity of the molecules and facilitating sensitized lanthanide luminescence owing to efficient energy transfer.

Submicrometer patterns of tetravalent lanthanide-antenna complexes were prepared in a three-step procedure (Scheme 7.1). Supramolecular μCP[14] of the sensitizer **2** onto the CD monolayer was used to generate surface patterns on the receptor surface (Scheme 7.1, step a).[15] This leaves the unpatterned areas accessible for immobilization of **1**·Eu^{3+} from solution (Scheme 7.1, step b). The backfilled surface was consecutively rinsed with a CD solution (Scheme 7.1, step c), and the resulting patterns were visualized with fluorescence microscopy as well as by AFM.

Scheme 7.2 shows an idealized, 1-dimensional, side-view of the molecular interactions of **1**·Eu^{3+} and **2** occurring on a CD monolayer, as described in the three-step procedure in Scheme 7.1, leading to the formation of a supramolecular complex along the intermixing boundary areas of the two components. The resulting surfaces from all three steps were imaged by fluorescence microscopy using two different filter sets: one set allowing UV excitation and red emission using a narrow bandpass filter centered at 610 nm (**R**, which mainly collects the emission of Eu^{3+}) and another set allowing UV excitation and blue emission (**B**, which only collects the emission of the naphthalene moiety).

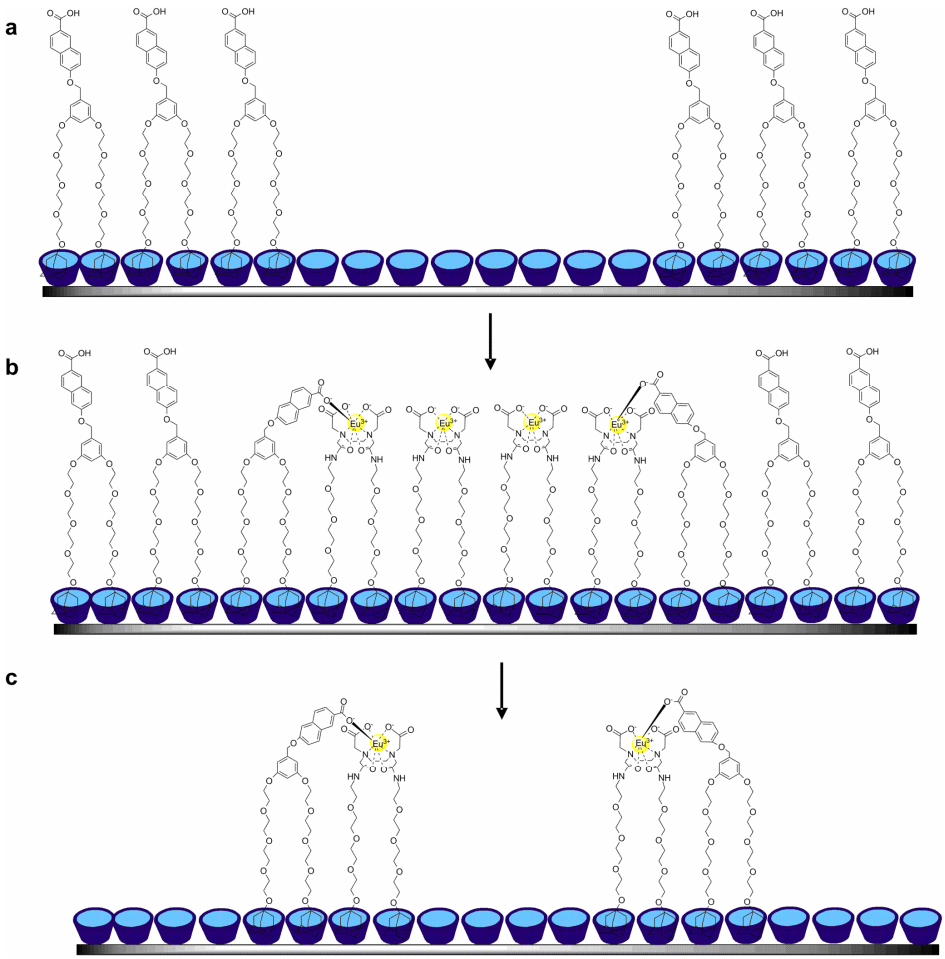

Scheme 7.2 Edge complexation procedure: (a) the local immobilization of **2** on a CD monolayer by μCP, (b) backfilled by **1**·Eu^{3+}, and the formation of nanostructures of the tetravalent complex, **1**·Eu^{3+}·**2**, along the intermixing boundary; and (c) removal of divalent components (**1**·Eu^{3+}·and **2**) by rinsing with CD.

In the first step, (Schemes 7.1 and 7.2, step a), antenna **2** was patterned on a CD monolayer by supramolecular μCP with an inked PDMS stamp, and the sample was rinsed with MilliQ water. A fluorescence image was taken with filter **B** and a pattern was observed corresponding to 5 μm lines of **2** (Figure 7.1a). Weak intensity profiles were also observed with filter **R**, which is equipped with a narrow band pass filter at 615 nm, and are due to the tail of the emission band of the antenna. AFM imaging also revealed that the antenna **2** was transferred to the CD monolayer and surface patterns with an average height difference of ~ 1.7 nm relative to the CD monolayer are seen (Figure 7.2a). The width of the line patterns is ~5 μm, which corresponds to the profile features of the stamp.

In the second step (Schemes 7.1 and 7.2, step b), the substrate was incubated with a solution of **1**·Eu^{3+}, rinsed with MilliQ water, and imaged with fluorescence microscopy. With filter **B**, a similar image was observed as obtained after step a. Most importantly, the edges of the patterns show significantly enhanced Eu^{3+} luminescence (filter **B**) compared to the centers of the **1**·Eu^{3+} areas, indicating the occurrence of sensitized luminescence of the edges, due to the formation of the luminescent europium(III)-antenna complex, **1**·Eu^{3+}·**2**. AFM measurements showed no difference in the height image, as expected for a fully covered surface, while the same area demonstrates a clear pattern in the phase image (Figure 7.2b), due to the different contrast of the antenna to the europium(III)-EDTA complex.

Finally, in the third step, the sample was extensively rinsed with a 10 mM cyclodextrin solution (Schemes 7.1 and 7.2, step c). Fluorescence profiles (Figure 7.1c) showed protrusions along the edges of the patterns both with filter **B** (very weak) and filter **R** (intense). Similar background intensities at filter **B** in the printed and backfilled areas indicated the complete removal of divalently bound **2**, and the observed emission of edge line is attributed to **2** bound to **1**·Eu^{3+}. Moreover, at filter **R**, similar background intensities in the printed and backfilled areas were also observed due to the removal of **2**. The edge lines maintained the same intensity compared with the profiles observed at step b, indicating that the complexes of **1**·Eu^{3+}·**2** are not removed because of their enhanced stability. Also AFM topography measurements showed a clear line pattern corresponding to the edge of the stamp profile (5 and 10 μm spacing) with an average height of ~ 1.5 nm and width of ~ 150 nm (Figure 7.2c). The height of the line patterns seems higher than can be expected for the complex. This may be attributed to some residual PDMS.

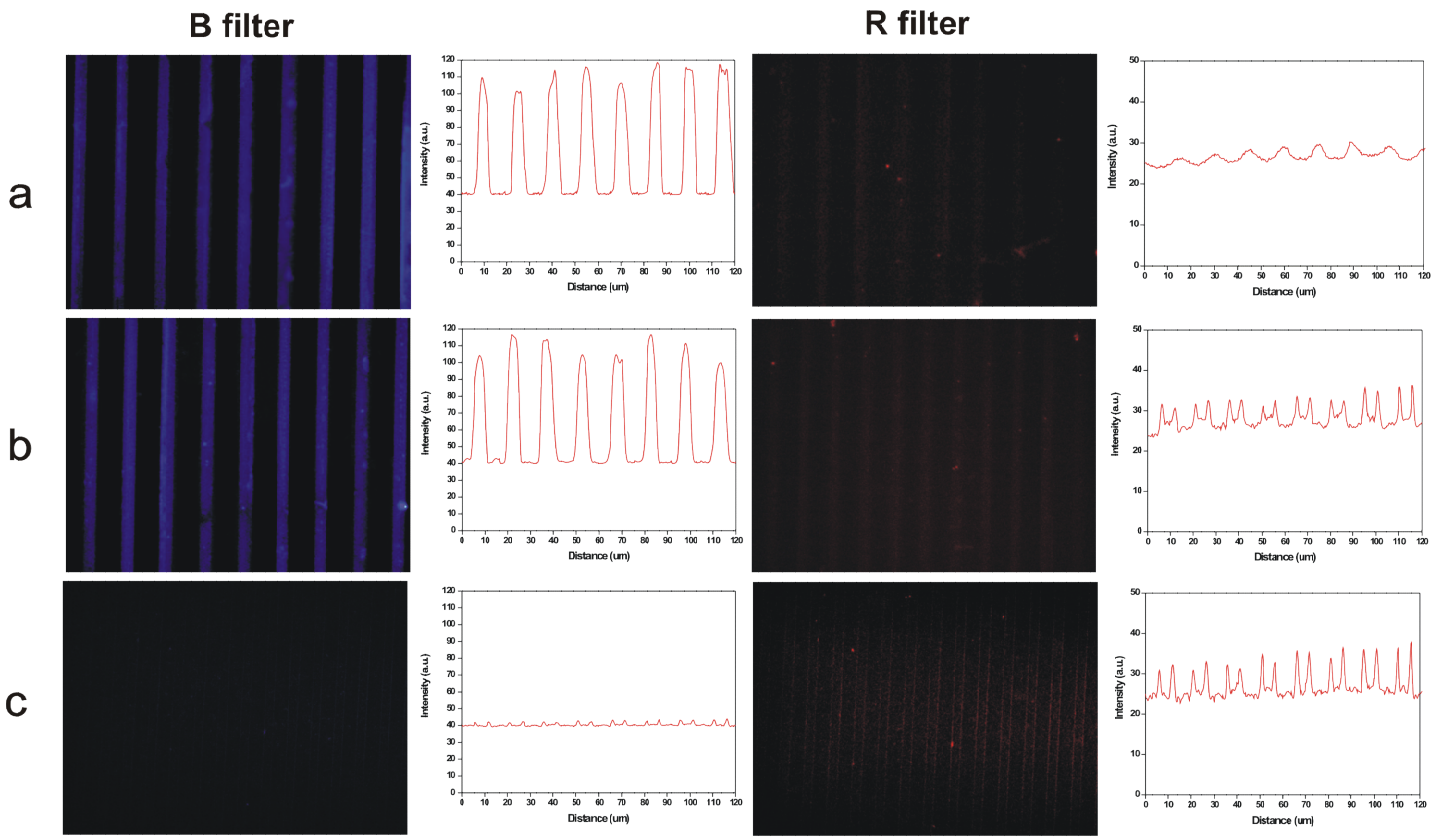

Figure 7.1 Fluorescence microscopy images and corresponding intensity profiles of 5 μm lines prepared by (a) printing **2** on a CD monolayer (Scheme 7.2a) and (b) incubation with **1**·Eu^{3+} (Scheme 7.2b), and (c) rinsing with CD solution (Scheme 7.2c). The samples were studied by monitoring emission of antenna **2** (filter **B**) and of **1**·Eu^{3+} (filter **R**). Scan areas are 120 μm x 90 μm.

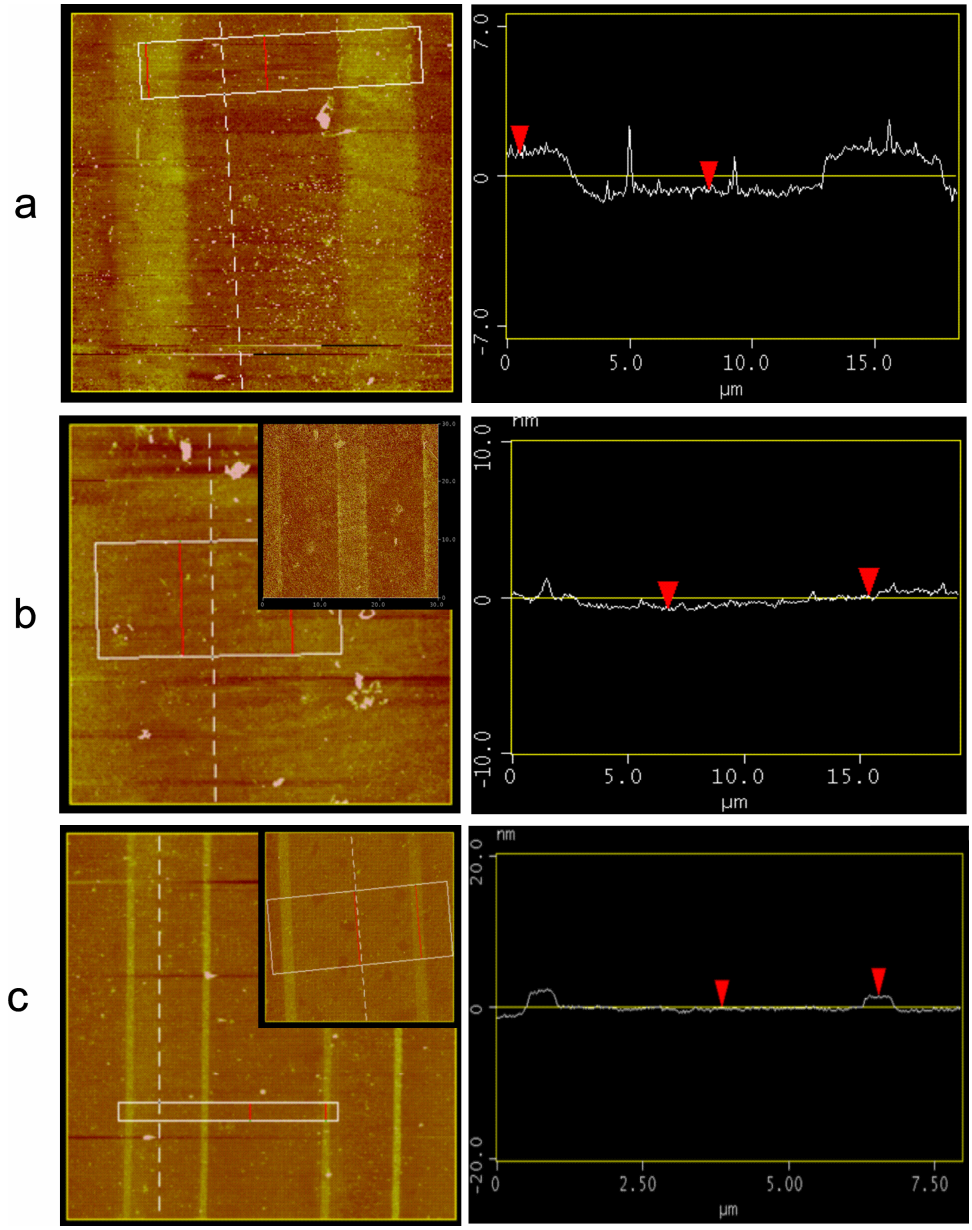

Figure 7.2 AFM height images of (a) micropatterns of **2** on a CD monolayer (average height difference ~ 1.7 nm and average width ~ 5 µm), (b) incubation with **1**·Eu^{3+}. The inset shows the phase image of the same area (average height difference ~ 0.5 nm), and (c) rinsing with a CD solution. The inset shows the areas with higher magnification (average height difference ~ 1.5 nm and average width ~ 150 nm). AFM image scan size is 30 µm × 30 µm.

In an attempt to correlate the observed fluorescence intensities (Figure 7.1) to coverage, the following can be considered. The antenna intensity in the line areas of **2** is about 70 a.u. (arbitrary unit) (filter **B**, after subtraction of the background). In an area with 50% antenna and 50% **1**·Eu^{3+}, a decrease of this intensity is expected, with a factor 2 to incorporate the coverage change from 100% to 50%, and about a factor 4 for the energy transfer from **2** to **1**·Eu^{3+} occurring in the complexed state (see Chapter 5). This would lead to an expected intensity of about 9 a.u. for micrometer-wide lines. Since the diffraction limit of optical microscopy is about 500 nm, 150 nm-wide lines (as observed here by AFM), densely packed with **1**·Eu^{3+}·**2**, are therefore expected to show up in fluorescence microscopy images as lines with an intensity of about 3 a.u. This is within error equal to what is observed in Figure 7.1. Similarly, a Eu^{3+} intensity (filter **R**) of about 12 a.u. is expected for the nanolines, which is not far off from the ~8-10 a.u. observed in Figure 7.1. More work is needed to correlate the fluorescence intensities to surface coverages and pattern sizes.

The orthogonal cyclodextrin-adamantyl (host-guest) and lanthanide-ligand (coordination) interaction motifs have been used to monitor the molecular binding events as described in Chapters 5 and 6. Here, the same system is used to manipulate the stability of individual entities on the surface through addition of competing host molecules in solution. Therefore, the surface composition can be tuned from molecules with divalent interacting sites, by supramolecular microcontact printing and/or incubation, to tetravalent interacting sites, by washing away the lower-valent entities. A relatively simple and straightforward three-step procedure consisting of supramolecular μCP, incubation and washing, hence resulted in the formation of nanometer-sized structures with an enhanced stability functionality along the edges of a predefined pattern.

7.3 Conclusions and outlook

In this chapter, a simple and elegant example of edge lithography to fabricate molecular nanoscale patterns by microscale techniques is presented, governed by multivalency. Molecules divalently interacting with the host surface (*i.e.* the antenna ligand and the Eu^{3+}-EDTA complex) are not inert against washing steps with competing host molecules (CD) in solution, while the tetravalently interacting entities (i.e. the lanthanide-antenna complex) formed at the boundary areas have an enhanced stability on the cyclodextrin surface.

More work is needed to explain the feature height and to systematically vary the CD concentration during the rinsing step. The obtained line width can possibly narrowed down further, but the resolution and sensitivity of the current fluorescence microscopy setup become limiting. Creative designs of new self-reporting systems and manipulation of the optical properties of the sensitized complex in combination with high resolution microscopy (e.g. near-field scanning optical microscopy) could be useful to improve the sensitivity of observations of the nanostructures on the surfaces.

Complementary research is envisioned to further improve control over the surface composition as a strategy for preparation of functional surfaces sensing. The approach presented here could serve as a platform for the fabrication of nanostructures in a simple and fast way using micrometer scale tools.

7.4 Experimental

Materials. For information on the synthesis and characterization of the different componds, the reader is referred to the work of Deniz Yilmaz.[13] MilliQ with a resistivity higher than 18 MΩ·cm was used in all experiments.

Substrate and monolayer preparation. Microscope glass slides were used for (*β*-CD) cyclodextrin monolayer preparation. The substrates were cleaned with piranha solution for 15 min (concentrated H_2SO_4 and 33% aqueous H_2O_2 in a 3:1 ratio; caution: piranha should be handled carefully) and rinsed with MilliQ. After drying in a nitrogen stream, the substrates were used immediately for silanized monolayer formation. The substrates were enclosed in a low-vacuum desiccator with 0.1 ml of TPEDA, continually pumping for 5 min to create a vapor phase of TPEDA. After overnight incubation, the slides were rinsed with ethanol and dichloromethane to remove any excess of silanes and subsequently dried in a nitrogen stream. The attachment of 1,4-phenylene diisothiocyanate was made in a 20 mM solution in toluene at 60 ˚C during 2 h. Samples were thoroughly rinsed with toluene and dried in a nitrogen flow. The CD layer attachment was made during 2 h in an aqueous 0.1 mM *β*-cyclodextrin-heptaamine solution (pH~7) at 60 ˚C. Samples were thoroughly rinsed with water and dried in a nitrogen flow.

Microcontact printing. Stamps were prepared by casting a 10:1 (v/v) mixture of poly(dimethylsiloxane) and curing agent (Sylgard 184, Dow Corning) against a silicon master. After overnight curing at 60 ºC, the stamps were oxidized by oxygen plasma for 1 min and subsequently inked by dropping aqueous adsorbate solution onto the stamp.

Printing of 2 on a CD monolayer (Scheme 7.1a). The CD SAM substrate was printed for 30 min with a oxidized stamp inked with a solution of **2** (2 mM) in saturated CD in a 3:1 mixture of EtOH/water, followed by rinsing with water and drying in a stream of nitrogen.

Immersion in 1·Eu^{3+} (Scheme 7.1b). The printed substrate was immersed in a 2 mM aqueous solution of **1**·Eu^{3+} for 10 min, followed by rinsing with MilliQ water and drying in a stream of nitrogen.

Rinsing with CD solution (Scheme 7.1c). The backfilled sample was thoroughly rinsed with aqueous 10 mM cyclodextrin and dryed in a stream of nitrogen.

Fluorescence microscopy. Fluorescence microscope images were taken using an Olympus inverted research microscope IX71 equipped with a mercury burner U-RFL-T as light source and a digital Olympus DR70 camera for image acquisition. UV excitation (300 nm $\leq \lambda_{ex} \leq$ 400 nm) and blue emission (410 nm $\leq \lambda_{em} \leq$ 510 nm) was filtered using a Dapi Olympus filter cube (**B** filter). UV excitation (300 nm $\leq \lambda_{ex} \leq$ 400 nm) and red emission (narrow band pass at 615 nm) was filtered using a Olympus filter cube (**R** filter). All fluorescence microscopy images were acquired in air.

Atomic force microscopy (AFM). AFM experiments were carried out with a NanoScope IIIa Multimode AFM (Digital Instruments, Veeco Metrology Group, USA) in tapping mode with a J-scanner. AFM imaging was performed at ambient conditions.

7.5 References

[1] M. Mammen, S. K. Choi, G. M. Whitesides, *Angew. Chem. Int. Ed.* **1998**, *37*, 2755.
[2] L. L. Kiessling, J. E. Gestwicki, L. E. Strong, *Angew. Chem. Int. Ed.* **2006**, *45*, 2348.
[3] A. Mulder, J. Huskens, D. N. Reinhoudt, *Org. Biomol. Chem.* **2004**, *2*, 3409.

[4] M. J. W. Ludden, D. N. Reinhoudt, J. Huskens, *Chem. Soc. Rev.* **2006**, *35*, 1122.
[5] J. Huskens, *Curr. Opin. Chem. Biol.* **2006**, *10*, 537.
[6] M. L. Pisarchick, N. L. Thompson, *Biophys. J.* **1990**, *57*, A292.
[7] E. L. Doyle, C. A. Hunter, H. C. Phillips, S. J. Webb, N. H. Williams, *J. Am. Chem. Soc.* **2003**, *125*, 4593.
[8] N. Horan, L. Yan, H. Isobe, G. M. Whitesides, D. Kahne, *Proc. Natl. Acad. Sci. U.S.A.* **1999**, *96*, 11782.
[9] S. J. Metallo, R. S. Kane, R. E. Holmlin, G. M. Whitesides, *J. Am. Chem. Soc.* **2003**, *125*, 4534.
[10] K. D. Schierbaum, T. Weiss, E. U. Thoden van Velzen, J. F. J. Engbersen, D. N. Reinhoudt, W. Goepel, *Science* **1994**, 1413.
[11] J. Haneveld, E. Berenschot, P. Maury, H. Jansen *J. Micromech. Microeng.* **2006**, *16*, S24.
[12] D. E. Prober, M. D. Feuer, N. Giordano, *Appl. Phys. Lett.* **1980**, *37*, 94.
[13] S. H. Hsu, M. D. Yilmaz, C. Blum, V. Subramaniam, D. N. Reinhoudt, A. H. Velders, J. Huskens, *J. Am. Chem. Soc.* **2009**, *131*, 12567.
[14] T. Auletta, B. Dordi, A. Mulder, A. Sartori, S. Onclin, C. M. Bruinink, M. Peter, C. A. Nijhuis, H. Beijleveld, H. Schonherr, G. J. Vancso, A. Casnati, R. Ungaro, B. J. Ravoo, J. Huskens, D. N. Reinhoudt, *Angew. Chem. Int. Ed.* **2004**, *43*, 369.
[15] S. Onclin, J. Huskens, B. J. Ravoo, D. N. Reinhoudt, *Small* **2005**, *1*, 852.

Chapter 8

Fabrication of Quantum Dot Structures at Interfaces using Multivalent Supramolecular Interactions

ABSTRACT. Well-defined patterns of Quantum Dots (QDs) functionalized with cyclodextrin (CD QDs) were obtained using supramolecular interactions. Two different methods were used: (i) immobilization of the CD QDs from solution onto CD monolayer surfaces patterned with adamantyl-terminated dendrimers (G2-PPI-$(Ad)_8$), and (ii) immobilization via direct microcontact printing of CD QDs onto a monolayer of G2-PPI-$(Ad)_8$ dendrimer. The microstructures of CD QDs show a high stability attributed to surface enhanced multivalent interactions between the cyclodextrins at the CD QD surface and adamantyl groups at the G2-PPI-$(Ad)_8$ dendrimer periphery. The molecular recognition functionality of the individual quantum dots was shown capable to form host-guest complexes with other molecules of interest at available (CD) binding cavities. Ferrocenyl-functionalized molecules as well as adamantyl-functionalized lissamine rhodamine dyes were systematically introduced onto the quantum dot surfaces by cross patterning demonstrating the photophysical interaction by photo-induced charge transfer and by fluorescence resonant energy transfer (FRET).

---

* Part of this chapter has been published in: Denis Dorokhin, Shu-Han Hsu, Nikodem Tomczak, David N. Reinhoudt, Jurriaan Huskens, Aldrik H. Velders, Julius Vancso, *ACS Nano.* **2009**, *4*, 137-142; and part is in preparation for publication with Dorokhin, Denis Dorokhin, Shu-Han Hsu, Nikodem Tomczak, David N. Reinhoudt, Jurriaan Huskens, Aldrik H. Velders, Julius Vancso.

8.1 Introduction

An important line of research in nanotechnology is the generation of functional molecular assemblies.[1] For the construction of molecule-based functional devices, the development of methods for integrating molecular components into well-ordered assemblies with a well-defined supramolecular architecture is needed.[2-4] Such devices require control of molecular orientation and organization at the nanometer scale, hence it is important to study and develop methods for the controlled assembly of multicomponent nanostructures.[5]

It has only been recently recognized that surfaces, in particular those functionalized with molecular recognition units, e.g. like the so-called molecular printboards, offer additional benefits regarding control over molecular orientation, footprint, stability of binding, and suppression of nonspecific interactions.[6, 7] Such β-cyclodextrin (CD) monolayers on silicon surfaces have been prepared onto which positioning of thermodynamically and kinetically stable assemblies of multivalent systems, e.g. dendrimers, can be reached.[8, 9] It has been shown that an adamantyl-terminated dendrimer binds to CD surfaces, leaving multiple guest groups exposed to the solution available for consecutive complexation of hosts from solution.[9]

In this chapter, the preparation of patterned surfaces is described that have been used to pattern microstructures of quantum dots through supramolecular interactions. Two methods to create patterns of these supramolecular assemblies are compared, both based on multivalent supramolecular host-guest interactions between adamantyl-modified functionalities and cyclodextrin-modified quantum dots (CD QDs). The aim of this study was to chemically direct the assembly of functionalized quantum dots onto a patterned substrate to obtain microscale architectures. Such micro-arrays of quantum dots (QD) on a surface allow us to further demonstrate the application for luminescence sensing with ferrocenyl functionalized dendrimers,[10] and fluorescence resonance energy transfer (FRET) between lissamine rhodamine dyes and quantum dots.

8.2 Results and discussion

To create supramolecularly assembled patterns of quantum dots, functionalization of the quantum dot surface is required. This is necessary for providing relevant and selective interactions between the respective surface pattern components and quantum dots. Accordingly,

multivalent host-guest complexation chemistry in aqueous solution was chosen to provide stable, well-ordered structures. In this study, two commercially available carboxylate-functionalized CdSe/ZnS QDs were used, with the first absorption peaks at 580 and 595 nm, and corresponding maxima of the emission at 597 and 608 nm, respectively.[10] The carboxylic acid groups on the surface of the QDs stabilize the nanoparticles in aqueous media and provide functionality for covalent binding of amine-terminated cyclodextrin molecules (Scheme 8.1).

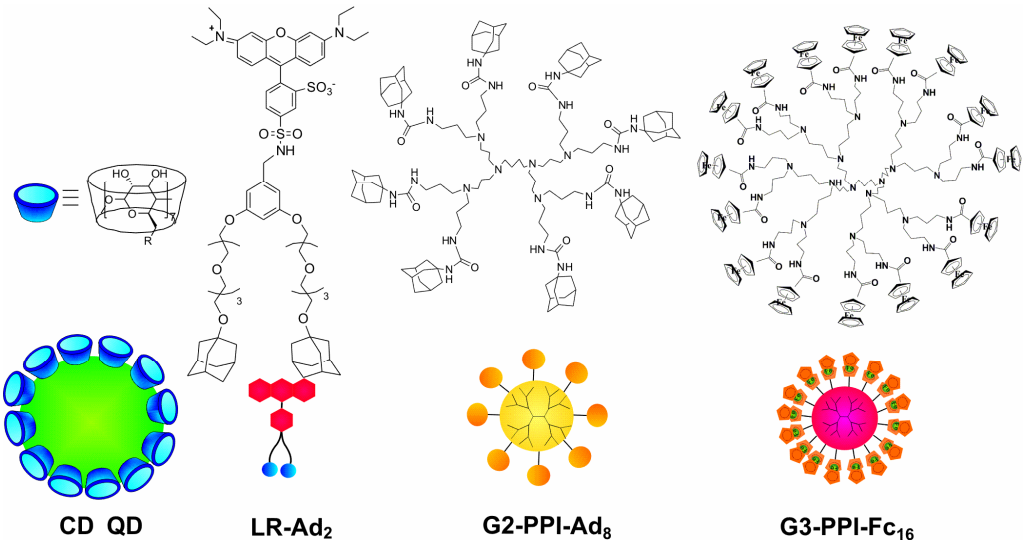

Scheme 8.1 From left to right: chemical structure of a cyclodextrin-functionalized quantum dot (CD QD), the adamantyl-terminated dendrimer (G2-PPI-Ad_8), the ferrocenyl-functionalized dendrimer (G3-PPI-Fc_{16}), and adamantyl-functionalized lissamine rhodamine dye (LR-Ad_2).

Two different methods for the supramolecular microstructure fabrication with CD QDs were explored and were compared for uniformity and homogeneity (Scheme 8.2). The first method uses a sequential process through the self-assembly of adamantyl-functionalized dendrimer patterns and cyclodextrin-functionalized quantum dots immobilized from solution; the second method utilizes a direct transfer printing of CD QDs to monolayers fully modified with adamantyl-functionalized dendrimers.

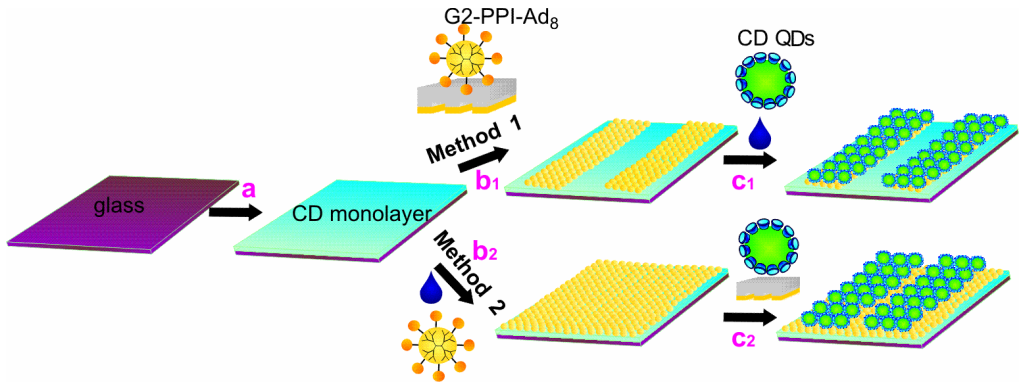

Scheme 8.2 Schematic illustration of quantum dots (CD QDs) immobilization with two different procedures (methods 1 and 2). (a) CD monolayer formation. (b_1) μCP of G2-PPI-Ad_8 over CD monolayer. (c_1) Incubation with CD QDs. (b_2) Incubation with G2-PPI-Ad_8 on CD monolayer. (c_2) Direct μCP of CD QDs on G2-PPI-Ad_8 functionalized surface.

In the first approach described above, the concept of selective deposition on chemically patterned surfaces as a template for quantum dot immobilization through host-guest interactions is used. A pattern of adamantyl-terminated dendrimers (G2-PPI-Ad_8) on a CD monolayer is formed by μCP (Scheme 8.2 b_1). Adamantyl-terminated dendrimers are insoluble in water, but by complexation of the adamantyl endgroups by slight excess of cyclodextrin and by the protonation of the dendrimer core, they are soluble in aqueous solution at pH = 2.[11] By using supramolecular μCP, the G2-PPI-Ad_8 were transferred from the stamp to the CD monolayer, and immobilized by supramolecular interaction, as well as the enhanced multivalency from the surface immobilization. Owing to the high number of functional units on the periphery of the G2-PPI-Ad_8 dendrimers, besides binding multivalently to the CD monolayer, additional unbound adamantyl group are exposed to the solution, which are available for consecutive complexation with other hosts.[12] CD QDs bearing surface-immobilized cyclodextrin can therefore bind to the G2-PPI-Ad_8 patterned surface through host guest recognition from solution. The attachment of CD QDs to the G2-PPI-Ad_8 layer was performed by simply casting a solution of CD QDs onto the dendrimer patterned surface (Scheme 8.2 c_1). Immobilization of CD QDs is highly selective to the G2-PPI-Ad_8 pattern, while leaving a background of CD monolayer in the non-patterned area.

The fluorescence emission from the CD QDs pattern obtained by method 1 is shown in Figure 8.1A. The 10 µm fluorescent lines and 5 µm spacing correspond to the spacing on the PDMS stamp used to pattern the G2-PPI-Ad_8 on the CD monolayer previously. This result indicates that the CD QDs bound to the substrate selectively to the areas where the G2-PPI-Ad_8 molecules were previously printed. The average height of the pattern measured by AFM (Figure 8.1B) is equal to ~10 nm, which corresponds approximately to the total height of the G2-PPI-Ad_8 and CD QDs layers. Additionally, there are no quantum dots observed between the dendrimer patterns, which prove unequivocally that the CD QDs do not attach directly to the CD monolayer. The defects in the CD QDs pattern, as visualized by AFM, may be related to a lower coverage of adamantyl-terminated dendrimers on the CD monolayer from incomplete supramolecular µCP.

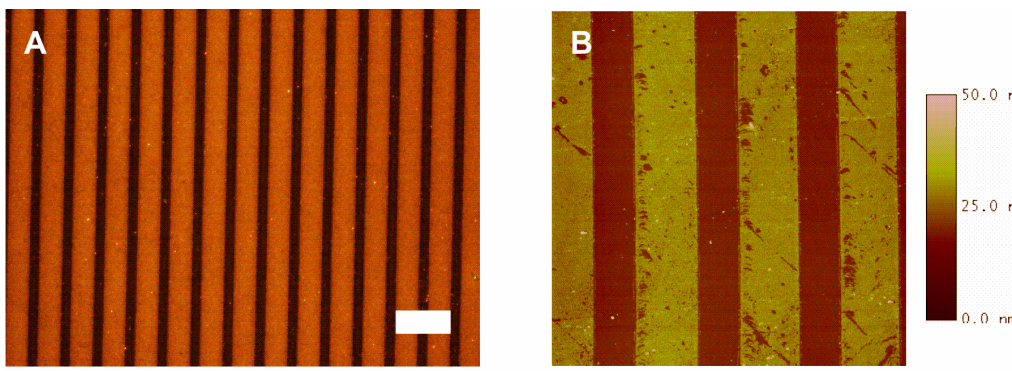

Figure 8.1 Fluorescence (A) and AFM height images (B) of micropatterns of CD QDs on a glass substrates obtained by drop casting the QDs on microcontact printed G2-PPI-Ad_8 dendrimers. The scale bar is 25 µm. AFM image scan size is 50×50 µm.

The second method, direct printing of CD QDs, was performed on the monolayer fully functionalized with G2-PPI-Ad_8. The CD monolayer was therefore first immersed in a 10 mM solution of G2-PPI-Ad_8 for 10 min (Scheme 8.2 b_2), followed by rinsing with MilliQ water and drying in a nitrogen stream. After drying, an oxidized PDMS stamp inked with CD QDs was brought into conformal contact with the G2-PPI-Ad_8 functionalized substrate for 10 min (Scheme 8.2 c_2). Following stamp removal, the unbound CD QDs were rinsed off with a PBS buffer. The fluorescence image of the resulting pattern is shown in Figure 8.2A (5 µm lines and 10 µm spacing on the PDMS stamp).

The height of the CD QDs patterns, as obtained from the AFM image (Figure 8.2B) is equal to ~6 nm, in good agreement with the estimated size of the CD QDs conjugate. Similar to the first method, the fluorescence and AFM imaging revealed that there are no QDs present in the space between the patterns. This means that there is no substantial diffusion of the CD QDs across the G2-PPI-Ad_8 functionalized surface after μCP.

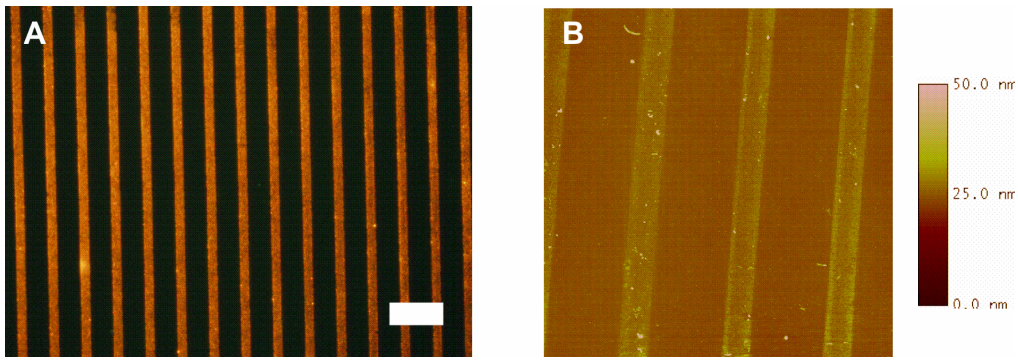

Figure 8.2 Fluorescence (A) and AFM height images (B) of CD QDs patterns on a glass substrate obtained by microcontact printing of the CD QDs onto a fully G2-PPI-Ad_8 functionalized surface. The scale bar is 25 μm. AFM image scan size is 50×50 μm.

To further investigate the recognition functionality of immobilized CD QDs, two different substrates were introduced: ferrocenyl-terminated dendrimers (G3-PPI-Fc_{16}) and lissamine rhodamine labeled with two adamantyl molecules (LR-Ad_2) (Scheme 8.3). The formation of specific host-guest complexes on the surface of CD QDs can modulate the emission of the quantum dots. The ferrocenyl-terminated dendrimer (G3-PPI-Fc_{16}) was chosen for the quenching effect of ferrocene when in close proximity to the quantum dots surface.[13, 14] The lissamine rhodamine was selected as a possible energy transfer acceptor for the immobilized quantum dots.

For subsequent experiments the patterns were prepared *via* the first method using the chemically directed assembly of functionalized quantum dots onto G2-PPI-Ad_8 patterns, because of free cyclodextrin sites are capable of binding of ferrocenyl-terminated dendrimers. Subsequently, ferrocenyl-terminated dendrimers or adamantyl-labeled lissamine rhodamine were introduced by cross printing over the CD QDs patterns obtained previously (Scheme 8.3). The resulting cross-patterns were characterized by fluorescence and AFM microscopy.

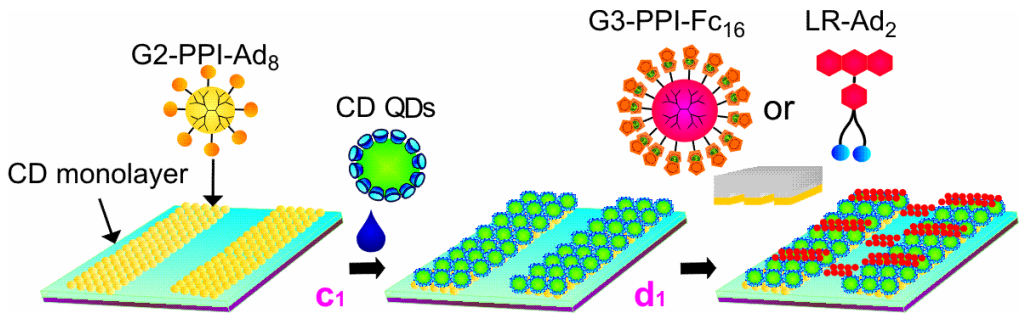

Scheme 8.3 Schematic illustration of cross pattern fabrication. Method 1 (Scheme 8.2) was used (c_1) by incubating CD QDs over a G2-PPI-Ad_8 printed CD monolayer, and (d_1) followed by cross printing of G3-PPI-Fc_{16} or (LR-Ad_2) over the CD QDs patterns.

G3-PPI-Fc_{16} dendrimers were solubilized in water at low pH in the presence of cyclodextrins and multiple numbers of ferrocene functionalities at the dendrimer periphery should provide for a stable multivalent attachment to the CD QDs pattern.

An AFM topography height image of the cross-printed sample is shown in Figure 8.3. There are four areas with different heights corresponding to the (**I**) primary CD monolayer, (**II**) G2-PPI-Ad_8 dendrimers with CD QDs on top, (**III**) G3-PPI-Fc_{16} dendrimers on CD monolayer, and (**IV**) G3-PPI-Fc_{16} dendrimers printed on top of the CD QDs/G2-PPI-Ad_8 layer. The height differences with respect to region **I** are equal to ~10 nm (**II**), ~3 nm (**III**), and ~13 nm (**IV**). The difference between regions **I** and **III** approximately corresponds to the estimated height of the G3-PPI-Fc_{16} dendrimers. Accordingly, G3-PPI-Fc_{16} dendrimers result the height difference between regions **IV** and **II**. These results indicate the success of G3-PPI-Fc_{16} transfer by supramolecular μCP, and in particular, there was no lift-off of the quantum dots upon contact with the stamp. Therefore, a hybrid multilayer structure of quantum dots and dendrimers was successfully obtained through the multivalent binding between the respective components.

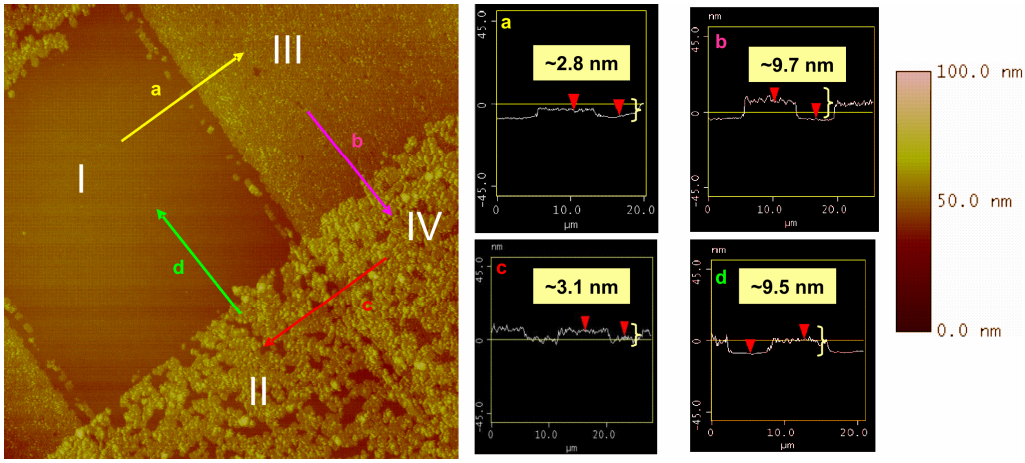

Figure 8.3 AFM height image of the crossed patterns. Surface of (I) CD monolayer, (II) G2-PPI-Ad_8 dendrimers with CD QDs on a CD monolayer, (III) G3-PPI-Fc_{16} dendrimers on a CD monolayer, (IV) G3-PPI-Fc_{16} dendrimers printed on top of the CD QDs/G2-PPI-Ad_8 layer. Scan size is 10×10 µm. Arrows indicate the cross section between (a) CD monolayer and G3-PPI-Fc_{16} on a CD monolayer; (b) G3-PPI-Fc_{16} on a CD monolayer and G3-PPI-Fc_{16} dendrimers printed on top of the CD QDs/G2-PPI-Ad_8 layer; (c) G3-PPI-Fc_{16} dendrimers printed on top of the CD QDs/G2-PPI-Ad_8 layer and G2-PPI-Ad_8 dendrimers with CD QDs on a CD monolayer; and (d) G2-PPI-Ad_8 dendrimers with CD QDs on CD monolayer and CD monolayer.

Figure 8.4 shows a fluorescence image of the CD QDs pattern cross-printed with G3-PPI-Fc_{16} dendrimers. In the areas where G3-PPI-Fc_{16} dendrimers are in contact with CD QDs the luminescence of the CD QDs is visibly decreased while CD QDs are still luminescent in the non-contacted areas. The quenching effect observed in the fluorescence image is due to the formation of host-guest complexes between the ferrocenyl groups of G3-PPI-Fc_{16} and the cyclodextrin hosts at the CD QDs surface. Modulation of the quantum dots optical properties in the multilayer structures is therefore demonstrated and it represents a proof-of-concept for sensing of interesting target molecules.

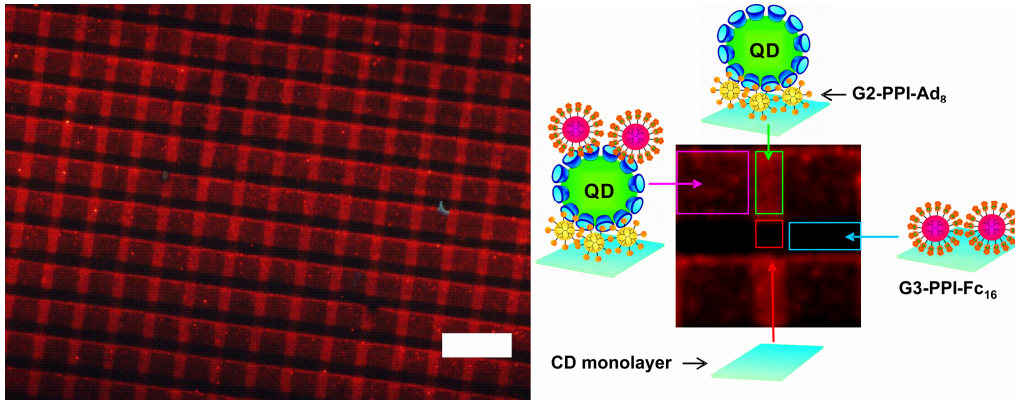

Figure 8.4 Fluorescence image of a CD QDs pattern cross-printed with G3-PPI-Fc_{16} dendrimers. The scale bar is 30 μm. The enlarged image indicates the functionality of the corresponding area individually.

Another microstructure composing of a potential energy transfer pair, was prepared in a similar method as described in Scheme 8.3, by cross printing the adamantyl-labeled lissamine rhodamine (LR-Ad_2) over the CD QDs pattern. The guest molecule, a lissamine rhodamine chromophore, functionalized with two adamantyl groups is known to bind to the cyclodextrins via divalent host-guest interactions. This structure allows a systematic study of FRET between quantum dots (donors) and the lissamine rhodamine dyes (acceptor) using fluorescence microscopy.

Figure 8.5 shows fluorescence images after printing the LR-Ad_2 chromophores perpendicularly across the CD QDs pattern. The filter sets were specially chosen for imaging patterns separately: where only CD QDs were excited and their emission was collected (Figure 8.5A), or only LR-Ad_2 chromophores were excited and the emission was collected (Figure 8.5B), and only CD QDs were excited, while only the emission of the LR-Ad_2 chromophores could be observed (Figure 8.5C). The fluorescence image in Figure 8.5B clearly shows that LR-Ad_2 was printed perpendicularly to the CD QDs pattern. Evidence for FRET in the structure is clearly obtained by examining the obtained images with a decrease of quantum dot luminescence (Figures 8.5A) and concomitant appearance of the emission of the lissamine rhodamine dye in the same areas (Figures 8.5C). A characteristic pattern of small red squares is visible in Figure 8.5C from the emission of the lissamine rhodamine dye showing that FRET only takes place where both the donor and acceptor are present.

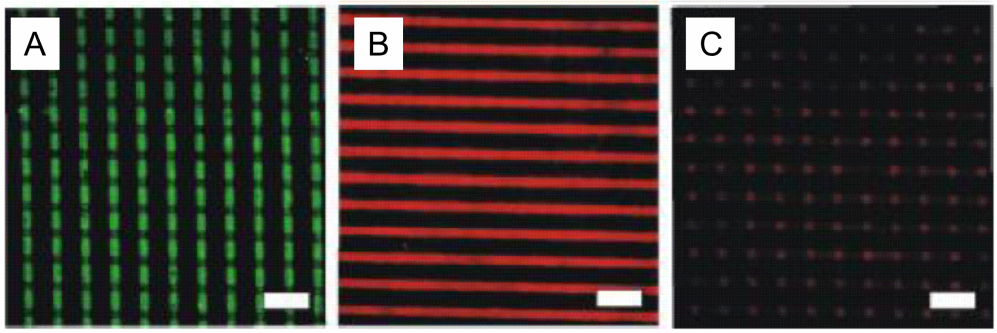

Figure 8.5 Fluorescence images of CD QDs patterns cross-printed with LR-Ad_2. Images were recorded with the following filter sets: (A) 300 nm ≤ λ_{ex} ≤ 400 nm, λ_{em} ≥ 420 nm; (B) λ_{ex} = 510-550 nm, λ_{em} ≥ 590 nm and (C)) 300 nm ≤ λ_{ex} ≤ 400 nm, λ_{em} ≥ 615 nm. The scale bars are 25 μm.

8.3 Conclusions

This chapter describes two different methods for the immobilization of water-soluble cyclodextrin-functionalized quantum dots on surfaces based on multivalent supramolecular interactions. The stable and ordered microstructures of quantum dots were used to study the photophysical properties in a systematic way. The molecular recognition functionality (i.e. empty cyclodextrin on the quantum dots surface exposed to the solution) of the individual quantum dots can be exploited for further assembly of complementary guest molecules. In particular, the luminescence of quantum dots was modulated by introducing ferrocenyl-functionalized dendrimers by cross-printing on a CD QDs pattern. Concomitantly, the FRET process between immobilized quantum dots and lissamine rhodamine dyes was also successfully demonstrated using the same strategy. Such stable, ordered supramolecular microstructures with recognition properties can potentially be engineered as sensing platforms for the detection of complementary compounds.

8.4 Experimental

Materials. For information on the synthesis and characterization of cyclodextrin-modified quantum dots the reader is refered to the work of Denis Dorokhin.[10] Ferrocenyl-terminated poly(propylene imine) (G_3-PPI-Fc_{16}) dendrimers, lissamine rhodamine divalent adamantyl

(LR-Ad_2), and adamantyl-terminated poly(propylene imine) (G_2-PPI-Ad_8) dendrimers were synthesized according to previously reported procedures.[9, 11] For all experiments, MilliQ water with a resistivity higher than 18 MΩ·cm was used.

Substrate and monolayer preparation. Microscope glass slides were used for cyclodextrin monolayer preparation. The substrates were cleaned with piranha solution for 15 min (concentrated H_2SO_4 and 33% aqueous H_2O_2 in a 3:1 ratio; Caution: piranha should be handled carefully) and rinsed with MilliQ water. After drying in a nitrogen stream, the substrates were used immediately for silanized monolayer formation. The substrates were enclosed in a low-vacuum desiccator with 0.1 ml of TPEDA, and the desiccator was continually pumping for 5 min to create a vapor phase of TPEDA. After overnight incubation, the slides were rinsed with ethanol and dichloromethane to remove any excess of silanes and subsequently dried in a nitrogen stream. The attachment of 1,4-phenylene diisothiocyanate was made in a 20 mM solution in toluene at 60 ˚C during 2 h. Samples were thoroughly rinsed with toluene and dried in a nitrogen flow. The *β*-CD layer attachment was made during 2 h in an aqueous 0.1 mM *β*-cyclodextrin-heptamine solution (pH~7) at 60 ˚C. Samples were thoroughly rinsed with water and dried in a nitrogen flow.

Microcontact printing of G2-PPI-Ad_8 , G3-PPI-Fc_{16} and LR-Ad_2.. PDMS stamps were prepared by casting a 10:1 (v/v) mixture of poly(dimethylsiloxane) (PDMS) prepolymer and curing agent (Sylgard 184, Dow Corning) against a silicon master. After overnight curing at 60 ºC, the stamps were oxidized by oxygen plasma for 1 min and subsequently inked by dropping aqueous adsorbate solutions of G2-PPI-Ad_8, G3-PPI-Fc_{16} or LR-Ad_2 onto the stamp. Before printing, the stamps were blown dried in a stream of nitrogen. The stamps were brought into conformal contact with the substrate for 10 min. The stamps were changed for each new print and the same inking procedure was used. After stamp removal, the printed substrates were rinsed with copious amounts of water, blown dry with nitrogen and imaged with fluorescence microscopy.

Immobilization of CD QDs onto functionalized glass slides. Immobilization of CD QDs on the glass surface was performed by casting 100 μL of a 10^{-6} M CD QDs solution on a

previously modified CD monolayer patterned with G2-PPI-Ad_8 for 10 min. The substrate was rinsed with a PBS buffer and dried under N_2.

Immobilization of G3-PPI-Fc_{16} and LR-Ad_2 onto QD-functionalized glass slides. The G2-PPI-Ad_8 pattern on CD monolayer were incubated with CD QDs for 10 mins, rinsed with a PBS buffer and dried under N_2. The substrate was further cross-printed with G3-PPI-Fc_{16} or LR-Ad_2 accordingly for 10 min, followed by PBS buffer rinsing and dried under N_2.

Fluorescence Microscopy. Fluorescence microscope images were taken using an Olympus inverted research microscope IX71 equipped with a mercury burner U-RFL-T as light source and a digital Olympus DR70 camera for image acquisition. UV excitation (300 nm $\leq \lambda_{ex} \leq$ 400 nm) and blue emission (420 nm $\leq \lambda_{em}$) was filtered using a Dapi Olympus filter cube. UV excitation (300 nm $\leq \lambda_{ex} \leq$ 400 nm) and red emission (narrow band pass at 615 nm) was filtered using a Olympus filter cube. Green excitation (510 nm $\leq \lambda_{ex} \leq$ 550 nm) and red emission ($\lambda_{em} \geq$ 590 nm) was filtered using a Olympus filter cube. All fluorescence microscopy images were acquired in air.

Atomic force microscopy (AFM). AFM experiments were carried out with a NanoScope IIIa Multimode AFM (Digital Instruments, Veeco Metrology Group, USA) in tapping mode with a J-scanner. AFM imaging was performed at ambient conditions.

8.5 Acknowledgements

Denis Dorokhin is thanked for providing cyclodextrin-functionalized quantum dots and adamantyl-terminated poly(propylene imine) (G_2-PPI-Ad_8) dendrimers.

8.6 References

[1] A. N. Parikh, B. Liedberg, S. V. Atre, M. Ho, D. L. Allara, *J. Phys. Chem.* **1995**, *99*, 9996.

[2] J. -M. Lehn, *Supramolecular Chemistry*, VCH Press, New York, U.S.A., **1995**.

[3] C. A. Nijhuis, B. J. Ravoo, J. Huskens, D. N. Reinhoudt, *Coord. Chem. Rev.* **2007**, *251*, 1761.
[4] K. Sachin, C.-C. Mercedes, N. R. David, *ChemPhysChem* **2008**, *9*, 20.
[5] B. D. Ana, M.-M. Ramón, S. Félix, H. Katrin, R. Knut, *Angew. Chem. Int. Ed.* **2006**, *45*, 5924.
[6] S. Onclin, A. Mulder, J. Huskens, B. J. Ravoo, D. N. Reinhoudt, *Langmuir* **2004**, *20*, 5460.
[7] M. J. W. Ludden, D. N. Reinhoudt, J. Huskens, *Chem. Soc. Rev.* **2006**, *35*, 1122.
[8] O. Crespo-Biel, B. Dordi, D. N. Reinhoudt, J. Huskens, *J. Am. Chem. Soc.* **2005**, *127*, 7594.
[9] C. A. Nijhuis, J. Huskens, D. N. Reinhoudt, *J. Am. Chem. Soc.* **2004**, *126*, 12266.
[10] D. Dorokhin, S.-H. Hsu, N. Tomczak, D. N. Reinhoudt, J. Huskens, A. H. Velders, G. J. Vancso, *ACS Nano* **2009**, *4*, 137.
[11] J. J. Michels, M. W. P. L. Baars, E. W. Meijer, J. Huskens, D. N. Reinhoudt, *Chem. Soc., Perkin. Trans.* **2000**, 1914.
[12] V. Mahalingam, S. Onclin, M. Peter, B. J. Ravoo, J. Huskens, D. N. Reinhoudt, *Langmuir* **2004**, *20*, 11756.
[13] D. Dorokhin, N. Tomczak, A. H. Velders, D. N. Reinhoudt, G. J. Vancso, *J. Phys. Chem. C.* **2009**, *113*, 18676.
[14] D. Dorokhin, N. Tomczak, M. Y. Han, D. N. Reinhoudt, A. H. Velders, G. J. Vancso, *ACS Nano* **2009**, *3*, 661.

Summary

Molecular nanostructures are important in the emerging field of nanoscience, because of the tunability of the properties of these structures. Nanostructures based on molecular interactions can be manipulated by selectively modifying specific functional groups while leaving the rest of the structures unchanged. Immobilization of molecules on a surface is required for many applications. Therefore, to achieve a suitable nanostructure one must consider not only interactions between the molecules themselves, but also between the molecules and the surface. These collective interactions play an important role for the functional design of the systems.

This thesis describes the use of covalent reactions and noncovalent interactions at interfaces, interacting vertically or laterally, for the construction of molecular assemblies. With the use of such molecular interactions, several functional molecules have been employed as the building blocks for nanostructures.

Chapter 1 provides a general introduction to this thesis. Chapter 2 reviews the recent studies on lateral molecular interactions at interfaces. Different molecular nanostructures held together at interfaces by covalent and noncovalent interactions are discussed, both on metal and oxide surfaces.

Chapter 3 describes the preparation of an imidazolide monolayer, amine layers-activated with *N*,*N*-carbonyldiimidazole (CDI). The successful immobilization of imidazolide monolayers was clearly shown by contact angle measurements, X-ray photoelectron spectroscopy, and grazing-angle infrared spectroscopy. The reactivity of the imidazolide monolayers was studied by reaction with amino-, carboxyl- and hydroxyl-containing dyes. Fluorescent images were observed respectively to the formation of urethane, amide or carbamate covalent bonds. The remaining surface activity of the imidazolide monolayers was demonstrated by consecutively introducing different functional molecules on the same surface. The imidazolide monolayers described in this chapter serve as useful “platforms”, which can be utilized to anchor a variety of functional groups by microcontact printing and open many possibilities for surface patterning.

By using the imidazolide monolayer described in Chapter 3, in chapter 4 the preparation of coumarin-terminated monolayers were described and fully characterized. Orthogonal surfaces were obtained combining alkyne and cyclodextrin patterns on the same surface. The selectivity and specificity of the orthogonally functionalized alkyne-βCD surface have been demonstrated by sequential and one-step printing procedures with different azide and bis-adamantyl-functionalized dyes. Therefore, the orthogonal surface was successfully prepared and it was shown that it is accessible for different chemical functionalities via covalent reactions or noncovalent interactions.

Chapter 5 introduces the multivalent binding of a supramolecular complex at a host surface by combining the orthogonal cyclodextrin host-guest and lanthanide-ligand coordination motifs. These motifs have been used to monitor molecular coordination events by sensitized Eu^{3+} luminescence. First, local emission spectra of the immobilized complex, composed of **1**·Eu^{3+} and the antenna **2,** demonstrated the occurrence of sensitized Eu^{3+} luminescence and thus qualitatively confirmed complex formation. Furthermore, the energy transfer efficiency between the naphthalene units and the lanthanide complex was quantified to be 35% by time-resolved fluorescence measurements. By examining the sensitized luminescence of the surface-immobilized complex from different solution ratios, the target complex on the β-CD SAM has a 1:1 stoichiometry as deduced from the first example of a Job plot at the surface.

Chapter 6 continues the study described in Chapter 5. The same lanthanide complex was used to study the dependence of complex formation at the interface on the solution composition under kinetic and thermodynamic control. The transition from kinetic to thermodynamic control was achieved by the addition of a competing host in solution. The formation of the **1**·Eu^{3+}·**2** complex is shown to be linearly dependent on the solution composition in the absence of cyclodextrin, while a strongly nonlinear amplification is observed under the cyclodextrin-promoted thermodynamic equilibrium. Due to the cyclodextrin-induced competition, the desorption of molecules from the surface is enhanced, promoting assembly of the most stable complex on the CD monolayer with the highest valency under equilibrium. A thermodynamic model was developed to simulate this nonlinear amplification of complex formation at the CD monolayer. The binding constant K_{AE} of the complex was determined as well as the surface speciation. Moreover, the kinetics of the self-

organization process was monitored in time in the presence of different concentrations of cyclodextrin, which allowed the estimation of the corresponding reaction rate constants. The model described here provides insight into how multiple, independent interactions provide a collective selection mechanism, where the molecular-level exchange events are self-reporting.

In Chapter 7 provides a preliminary experiment for the fabrication of submicrometer-scale molecular patterns of the antenna-lanthanide complex introduced in Chapters 5 and 6. Fluorescence and AFM measurements show that fabrication of nanoscale patterns is achieved by supramolecular microcontact printing of an antenna molecule, incubated with a lanthanide ligand, and followed by cyclodextrin washing. The further development to manipulate the sensitivity of the system is also discussed.

In Chapter 8, microstructures of quantum dots were prepared at interfaces via supramolecular interactions. Two different methods for the immobilization of cyclodextrin-functionalized quantum dots on surfaces were used. Fluorescence images demonstrated the successful immobilization of cyclodextrin-modified quantum dots, while AFM measurements showed the homogeneity of the resulting structures of quantum dots. The recognition functionality of the quantum dots was exploited by introducing ferrocenyl-functionalized dendrimers on cyclodextrin-modified quantum dot patterns, where the luminescence of the quantum dots was visibly decreased in the contact area, while they were still luminescent in the non-contact areas. Using the same methods, the energy transfer process between immobilized quantum dots and lissamine rhodamine dyes was clearly demonstrated. Such microstructures with recognition properties can potentially be engineered as sensing platforms for the detection of molecules at the interface.

The results presented in this thesis illustrate the versatility of the combined molecular interactions, covalent and noncovalent, in creating functional micro-/nanostructures at interfaces. Reactive monolayers serve as bottom-up platforms to introduce different functionalities via covalent attachment, while the orthogonal functionalities on the surface open the possibility to immobilize target molecules via complementary covalent or noncovalent interactions. Different supramolecular assemblies on surfaces demonstrate that different nanostructures can be obtained by combining the specificity and stability of multiple supramolecular interactions. Such systems allow the exploration of intermolecular processes, e.g. energy transfer or electron transfer. The fundamental understanding of the molecular

interactions in self-assembled nanostructures at interfaces opens new approaches in the design of more advanced nanofabrication schemes.

Samenvatting

Moleculaire nanostructuren spelen een belangrijke rol in het opkomende onderzoeksveld van de nanowetenschappen, met name vanwege de mogelijkheid tot het nauwkeurig kunnen afstellen van de eigenschappen van deze structuren. Nanostructuren waarvan de stabiliteit gebaseerd is op moleculaire interacties kunnen gemanipuleerd worden door selectief speciale functionele groepen te beïnvloeden, maar tegelijkertijd de overige onderdelen van de structuren onveranderd te laten. Voor veel toepassingen is het een vereiste om moleculen te immobiliseren op oppervlakken. Om geschikte nanostructuren aan oppervlakken te krijgen moet men niet alleen interacties tussen moleculen zelf, maar ook tussen moleculen en de oppervlakken in acht nemen. De gezamenlijke interacties spelen een belangrijke rol in het ontwerpen van dit soort systemen.

Dit proefschrift beschrijft het gebruik van covalente en niet-covalente interacties aan oppervlakken, met verticale en laterale wisselwerkingen, met als doel de constructie van moleculaire assemblages. Gebruik makend van zulke moleculaire interacties zijn verschillende functionele moleculen ontworpen als bouwstenen voor nanostructuren.

Hoofdstuk 1 geeft een algemene inleiding tot dit proefschrift. Hoofdstuk 2 geeft een overzicht van recente studies aan laterale interacties aan oppervlakken. Verschillende nanostructuren bijeengehouden aan (metaal- en oxide-)oppervlakken door covalente en niet-covalente interacties worden bediscussieerd.

Hoofdstuk 3 beschrijft het maken van imidazolide-monolagen, dat zijn amine-monolagen die geactiveerd zijn met *N,N*-carbonyldiimidazool (CDI). De succesvolle bereiding van imidazolide-monolagen is aangetoond met contacthoek-metingen, Röntgen-fotoelektronspectroscopie en infraroodspectroscopie. De reactiviteit van de imidazolide-monolagen is bestudeerd in reacties met amino-, carboxyl- en hydroxylgroep-bevattende kleurstoffen, en overeenkomstige fluorescentieplaatjes zijn verkregen onder vorming van, respectievelijk, covalente urethaan-, amide- of carbamidebindingen. Het reactief blijven van de imidazolide-monolagen is aangetoond met de opeenvolgende reacties van verschillende functionele moleculen op het oppervlak. De in dit hoofdstuk beschreven imidazolide-

monolagen vormen een nuttig platform dat gebruikt kan worden om een variëteit aan functionele groepen te verankeren door middel van microcontactdruk (μCP), en biedt zo nieuwe mogelijkheden voor oppervlaktepatronering.

Voortbordurend op de imidazolide-monolagen beschreven in hoofdstuk 3, is in hoofdstuk 4 het maken van coumarine-gefunctionaliseerde monolagen beschreven. Zogenaamde orthogonale oppervlakken zijn verkregen door alkyn- en cyclodextrine- (CD-) patronen te combineren op één en het hetzelfde oppervlak. De selectiviteit en specificiteit van het orthogonaal gefunctionaliseerde alkyn-CD oppervlak zijn bewezen met sequentiële en 1-staps stempelprocedures, met verschillende azide-, respectievelijk, adamantyl-gefunctionaliseerde kleurstoffen. De orthogonale oppervlakken zijn succesvol verkregen en blijken toegankelijk te zijn voor verschillende chemische functionaliteiten via covalente of niet-covalente interacties.

In hoofdstuk 5 is de multivalente binding van een supramoleculair complex aan een receptor-oppervlak geïntroduceerd, waarbij orthogonale cyclodextrine gast-gastheer en lanthanide-ligand coördinatie-interacties worden gecombineerd. Deze bouwstenen zijn gebruikt om de moleculaire coördinatie te bestuderen met behulp van gesensitiseerde Eu^{3+}-luminescentie. Ten eerste, locale emissie spectra van een verankerde verbinding, bestaande uit **1**.Eu^{3+} en antenne **2**, tonen de gesensitiseerde Eu^{3+}-emissie aan, en bevestigen daarmee de complex-vorming op een kwalitatieve manier. De energie-overdrachtsefficiëntie tussen de naftaleen-antenne en het lanthanide-complex is bepaald (35%) met tijdopgeloste fluorescentiemetingen. Door het bestuderen van de gesensitiseerde luminescentie van het oppervlakte-verankerde complex, uitgaande van verschillende verhoudingen van de bouwstenen in oplossing, blijkt de doelverbinding op de CD-monolaag een 1:1-stoichiometrie te hebben, zoals afgeleid aan de hand van dit eerste voorbeeld van een 'Job-plot' aan een oppervlak.

Hoofdstuk 6 gaat verder met de studie beschreven in hoofdstuk 5. Hetzelfde lanthanide-ligand-antenne-complex is gebruikt om de afhankelijkheid van de complexvorming aan oppervlakken te bestuderen als functie van de samenstelling in oplossing, onder kinetische en thermodynamische controle. Het onderscheid tussen kinetische en thermodynamische controle is verkregen door het toevoegen van een competitieve gastheer (CD) in de oplossing.

De vorming van het complex blijkt lineair afhankelijk te zijn van de samenstelling in oplossing in afwezigheid van cyclodextrine, terwijl een sterke niet-lineaire complexvorming is gezien onder omstandigheden van cyclodextrine –gestimuleerd thermodynamisch evenwicht. Door de cyclodextrine-geïnduceerde competitie wordt de desorptie van moleculen van het oppervlakte gestimuleerd, en wordt de assemblage van het meest stabiele complex, met de hoogste valentie, onder evenwichtscondities bevoordeeld. Een thermodynamisch model is ontwikkeld om deze niet-lineaire versterking van complexvorming op de CD-monolaag te simuleren. De bindingsconstante K_{AE} is bepaald alsook de oppervlaktevulling met de verschillende componenten. Verder is ook de kinetiek bekeken van het zelforganiserende proces in aanwezigheid van verschillende concentraties cyclodextrine, wat tot een schatting van de overeenkomstige snelheidsconstantes heeft geleid. Het model dat hier is beschreven geeft inzicht in hoe meerdere, onafhankelijke interacties tot een collectief selectiemechanisme leiden waarbij de moleculaire uitwisselingsgebeurtenissen zelf-signalerend zijn.

Hoofdstuk 7 beschrijft de eerste experimenten voor de fabricage van submicrometerschaal moleculaire patronen van het lanthanide-ligand-antenne-complex beschreven in hoofdstukken 5 en 6. Fluorescentie en AFM-metingen laten zien dat nanoschaal-patronen kunnen worden gemaakt, beginnend met supramoleculair μCP van de antennemoleculen, gevolgd door incubatie met het lanthanide-ligand-complex en wassen met cyclodextrine. De ontwikkelingen om de gevoeligheid van het systeem verder te manipuleren zijn ook bediscussieerd.

In hoofdstuk 8 worden microstructuren van ‘quantum dots’ (QDs) beschreven, geassembleerd aan oppervlakken door middel van supramoleculaire interacties. Twee verschillende methoden voor het immobiliseren van cyclodextrine-gefunctionaliseerde quantum dots (CD-QDs) zijn gebruikt. Fluorescentieplaatjes laten de succesvolle verankering zien van CD-QDs, terwijl AFM-metingen de homogeniteit van de resulterende QD-structuren laten zien. De herkenningsfunctionaliteit van de CD-QDs is verder gebruikt door ferroceen-gefunctionaliseerde dendrimeren te introduceren, waarbij de luminescentie van de QDs zichtbaar is verminderd in de contactgebieden terwijl ze luminescent zijn gebleven in de gebieden waar geen ferroceen-QD-interacties zijn. Dezelfde methodologie gebruikend is de energie-overdracht tussen geïmmobiliseerde QDs en lissamine-rhodamine-kleurstoffen

aangetoond. Dit soort microstructuren kunnen in principe worden ontwikkeld tot een sensorplatform voor de detectie van moleculen aan oppervlakken.

De resultaten die in dit proefschrift staan beschreven illustreren het potentieel van de gecombineerde niet-covalente en covalente interacties voor het maken van functionele micro/nanostructuren aan oppervlakken. Reactieve oppervlakken dienen als 'bottom-up'-platform om verschillende functionaliteiten te introduceren door middel van covalente reacties, terwijl orthogonale functionaliteiten aan het oppervlak de mogelijkheid geven om moleculen via complementaire covalente of niet-covalente interacties vast te zetten. Supramoleculaire assemblages aan oppervlakken bewijzen hoe verschillende nanostructuren kunnen worden verkregen door het combineren van meerdere specifieke en stabiele supramoleculaire interacties. Met dit soort systemen kunnen intermoleculaire processen in zelfassemblerende nanostructuren bestudeerd worden, zoals energie- en elektronenoverdracht. Het fundamentele begrip van moleculaire interacties in zelfassemblerende nanostructuren aan oppervlakken opent nieuwe wegen voor meer geavanceerde nanofabricage-strategieën.

Acknowledgement

During these four years, many people have supported me, listened to me and encouraged me. Here I would like to show my gratitude to all of you.

Thanks to my promoter, David. Since my project is the last project you wrote, you gave me a lot of attention to reach your dream! You trusted me that I can complete the thesis on time and guided me to write a literature review properly. Although you gave me a difficult task before handing in the thesis, we still squeezed out one more extra chapter. I remember when I struggled with organic synthesis in my first year and felt frustrated, you told me that "we don't want to turn a physicist to a bad chemist but instead we want to make a use of your expertise". Hope what I have already presented here is not disappointing you.

Jurriaan, I still think that it is my good luck to have you as my promoter. I appreciate that you can always think rationally and clearly. I enjoyed the moments when you taught me how to build my own model based on your famous simulation systems. I like the way that you guided me to write the papers: making sure I understand the messages and proposing your suggestions to me. Such a high respect from a supervisor is what I enjoy most. Hopefully, you will remember me, the Miss Holidays!

"PhD is the process from this point to another point, there is several ways to reach…," our dear Papa, Aldrik, said. You told me that Phd is not about publications, but it is to develop as a scientist who can think independently and responsibly. As a daily supervisor, you seem like a friend to us. I cannot count how many nights you did not have a goodnight kiss to your angels, just because you wanted to stay with us and cheered us up. Thank you that you were always there for me even after two *mothers* left subsequently.

Mercedes, thank you for choosing me to be your PhD student even after I wrote you back a letter saying "I am not a chemist". You spent time teaching me how to search articles and help me to prepare molecules during my first year. It is nice to see a small girl (like me) full of energy!

I do not know how many PhD students you had experienced so far but, for sure, you are a part of my memory. I would like to thank: Wim, thank you for reading my thesis and

giving me valuable comments. Pascal, it is nice to have you as an enthusiastic person in the lab, and thank you for trying to convince the English embassy that I am not a terrorist! Richard, how amazing is that you can share knowledge about everything, especially, for wine and beer. I cannot image the lab running without you. Marcel, it is most difficult for me to talk to you since our words must travel a particularly long distance among the others. I will remember your greeting style to me: "Madam". Without you, Tieme, how can I deal with all the official documents? It is very annoying, isn't it? Bianca, I admire you can handle the work and kids very well as a good mother!

After struggling to be a chemist for half year, Laura, your coming, gave me the light and direction. It is not easy to understand you and to feel the same rhythm between us. I cried in front of my fume hood and you told me, "This is life!" After tears, I know how to listen to you. It was not easy time for you, but one thing I want let you know is that you are always my first mother here! Thank you for hosting us in Zaragoza, although I could not talk to your father but I could feel his most warm smile. Like we prayed for your job in the church, I really wish you enjoy your life now! Another little girl, Elisabetta, with such a strong mind, always insisted on your beliefs without hesitating. There was a period of time when we looked for each other to have lunch together, to swim together, and to watch movies together. You taught me how to see the world with sympathy, and you also showed me how to have an elegant lifestyle. Only few seconds, I made up my mind to join your Christmas celebration in Bari. I cannot forget the warm atmosphere at Christmas afternoon; we all sat beside the stove and opened the gifts, a nice set of bag and scarf from your mother. Your father, a history professor, shared many stories by pointing out my country, "Formosa" in the map, and treated me like a daughter by removing the fishbones for me. How nice I had you here to share many days and I will keep the memory of them with me. My dear stepmother, Arancha, your arrival survived me from fighting alone with chemistry. We were always the last ones to turn off the light in the lab. You strive to be the best for most of things; therefore, I always saw your tears under such pressure. You always treat everyone sincerely, and that is why there are always so many people surrounding you. Girl, trust yourself, you will get what you want from the effort you paid! Dear Deniz, I always said without you I could not finish my PhD. You were appointed to help me with molecular design. We worked together like the best team: you explained me patiently what was going on in the flask, and I showed you how "difficult" it was to blow dry

the glass slides. We always dreamed together for new ideas; and the moment to open the microscopy shutter took our breath away. You accompanied me to cycle home and discussed the facing problems together. Would you keep the promise that "you will always be ready to receive my compound ordering!" Alberto, as the only two physicists in the lab, we have the same kind of stubbornness and cannot avoid arguing. According to you, you are a special Spanish with different tastes: no car, no buying house…everything is extraordinary. You are always kind to follow my request to sit down when you talked to me, then I could feel the equal height between us. I still remember when you carefully added the pillow under the bike seats; I still remember the moment when you shared with me your feeling about the love; and I knew this big boy actually have a soft mind! When will it be the next time we could play soccer together?

Jordi, as most handsome boy in the lab (with chicken hair style), I am really pleased to have you as my paraninf. You have taken actions to show considerations for the earth. After you returned from Africa, you told us the story that the children can design their own toys out of trash. Definitely, you teach me to satisfy what we have and inspired me to think that there is nothing impossible if you want! As volunteer in Madagascar this summer, what shocking stories will you bring back? Because of your nice suggestion, Xing Yi, I started working on weekends. We shared the Chinese corner (according to Mirko) together. You even made a plan for me when to start writing my thesis, and shared with me your well-organized schedule. I really wonder how far you can fly and how high you can reach. Because of you, I cannot see any limitations of female's ability in the scientific field, because you are always well-prepared! As you figured out in America, there are nice research institutes in Taiwan as well (with nice Taiwanese), so I will wait for you and In Yee visiting. When you came for interview, you wore a high hat, held a pipe in the mouth and dressed a long black coat. Therefore, we have the Sherlock Holmes in the lab, Albert. Although you laughed at my poor knowledge about chemistry, you never stopped to help me to purify, extract, and analyze the compounds. We recorded the speech you made and the diagram of PhD life you sketched on the fume hood window at that afternoon. With your love to chemistry, I believe you can achieve your dream.

Jealemy, you are always full of energy for life, and you know clearly what you want. I still remember the conversation we had in Lunteren; you told me that "just follow your heart!" I learnt from you to do what I want, and express what I feel. Kim, I thought you were my

opponent when we had our interviews together. We wrote our literature report at the same period, and I was really scared to talk to you due to your prefect Australian English. You are the one who always looks the positive side of things and know how to enjoy the life (Do you ever feel tired?). Duan, as a senior, you are always ready to help me. With your encouragement, I joined the student association and had the chance to "show off" myself. You always led the group in an organized way; therefore, we had a great success in all the activities. When we had holidays in Greece, I realized how emotional you are and how much tolerance you have. What lucky thing for me to have you as a guide lighting the way! Wish you satisfy every choice you make from now on. Huaping, we competed on our Chinese calligraphic skills, memorizing Chinese poems and historical knowledge. Do you still remember our discussion in the train back from Greece? You told me about your childhood in your wonderland, and how you reached your position today. I saw a man with a strong determination, but still holding a sensitive heart. When can we have this kind of touched conversation again? Chien Ching, for a while, we were the only two Taiwanese in the University of Twente. It was you who showed me around the city tasting the herring, singing in the chorus. I still remember when we singed our Taiwanese song, "plumb blossom", at the theater in Bulgaria. All the audience was quiet and moved and we were proud to represent and introduce our country! Thank you to let me realize how wonderful I still have my grandparents waiting at home! Yiping, you were always ready to supply my requests of masters and delivered them with high quality in an efficienct way. It was a nice period to join the Piranha club with you, although I am not a good student to learn your nice turn in the swimming pool! Girl, wish you hold your happiness tightly.

Raluca, thank for the fresh homemade juice at home before Jordi kidnapped you from us! I still remember your calling "Dinner is ready!" when I tried to survive my fish in the aquarium. I saw the fresh Lasagne at the table and I felt being at home. Let's wish we have something interesting out of our collaborations and you will not feel disappointed. Francesca, it is not easy to find another girl to have the same height as me here (although you did not admitt it!). You always keep yourself learning from the new things and required the best outcome out of it. We both experienced the last writing periods together and hope we can overcome it successfully together. Lanti, I always need to slow down myself and feel myself more elegant when I talk to you. You shared with me the happiness to welcome a new life. You made me understand that science is not everything, and you made me jealous of the love you have. What

else needs a girl more than that? Pieter, we burned the midnight oil together for Duan's movie. It is a great thing that we could collaborate with each other easily in such limited time. Thank you for your understanding my approaching deadline. A special German girl like you, Carmen, always wears a sunshine smile. We got the chance to work together during your project assignment, and we had so many funs together. Just because you heard my fish were swimming in a small vase, you brought me a nice aquarium next day!

Alessandro, I was surprised when they put you beside my desk without any notice. How many interesting things we figured out in such routinary life: you washed my dirty glassware, prepared the PDMS stamps for me, and what was important, you kept my bench clean! Without you being around, the lab is too quiet! Because I know you are busy for your tomato DNA extraction in Parma! Although you arrived lately, Anna, I felt something in common between us. I saw myself in you when you tried to adjust yourself to the new environment. It is not easy, right? I believe you can manage this without anymore tears. Melanie, we are always in the same team doing the sport. How amazing to see a girl passing the soccer without hesitation. Dae June, it is a pity you can not share with me the nice things here, and I just wish you feel satisfied what you have now. I know what I will miss most in the early morning or the end of the working day is the "good morning/goodbye, Shu Han!" from you, Mudassir. Joost and Clemens, you both are an annoying couple during my lunch time. But when I saw your face in our garden, you were my heroes to save us from being frozen without heater. Hopefully, next time I will not find my video recorder on sale in the Marktplatz. Carlo, my dear housemates in Javastraat, thank you for all the Italian cuisine you prepared during my busy writing period. I enjoyed every Saturday brunch, and for sure I will miss the best Parmigiano Reggiano cheese in the world! Peter, they always say most wise people are quiet, therefore, I think I need to learn from you! Sven, with all the confidence you have, I think PhD is an easy task for you. There are so many people here to create the nice atmosphere, and that is the reason I don't feel lonely being away from home: Rick (thank you for always picking me up for the squash match night),Vijay, Ocktay, Dennis, Janet, Roberto, Tom, Miguel, Mirko (I miss the arguments with you!), Victoria, Ignacio, and Martine.

Xiaoying, it has been really nice to have you as my best friends here. What a destiny, we have the same birthday and then we will also celebrate our achievement together. Just like I told you all the time, you gave me a feeling like being at home. I will treasure all our girl talk

and the memories we shared. Wish you will satisfy what you have now and hold the happiness you will find soon! Jincy, an elegant India girl that is always ready for new things. From you, I felt the insistent to be a female scientist! Thank you for all the culture exchange we had, especially when I got the chance to wear your beautiful Sari.

For my friends from Sweden: Nat, Hina, and Fawad, finally we all managed to obtain our doctor degree in the Netherlands. I still remembered several nights we struggled together for our master theses in Sweden, and what is the next target for us?

Tar, without your understanding, I can't complete my dream here. Thank your waiting for me in Taiwan for four years. Now we will pursue our dream together side by side. Thanks to your family to accept our situation and support me like own family. I promise this year I will learn your language and communicate with them by myself.

爺爺奶奶，如果沒有你們當年的一席話: "去看看這個世界，去追求我們這一代，身爲女孩不敢想的夢吧!" 您們的孫女怎能飛的好遠，看的好廣! 親愛的爸爸媽媽，每一次的機場別離，轉身向你們揮手，知道自己又得孤單面對，只因你們給的家庭溫暖太多太多，只能抱著你們塞下的娃娃訴說心事! 你們，一直指引著我，在我哭著說要放棄時，只溫和的告訴我:再試一次，好嗎? 只因有你們的成全，今天我才能站在台上；只因有你們的溫暖，我知道自己是最幸福的女孩! 齊齊，中中，謝謝你們代替姐姐這六年來陪在他們身邊，這一次，我們又可以擠在爸爸的休旅車後座，打打鬧鬧的旅行，這一次，不想再錯過你們生命中所有重要的時刻! 姐姐我要回家了!

About the Author

Shu Han Hsu was born on the 3th of October 1982, in HsinChu, Taiwan. She obtained her Bachelor degree of Material Science and Engineering, 2nd Class Honors from the National Tsing-Hua University, Taiwan in the year of 2005. In 2004, she set up the exchange master program between National Tsing-Hua University, Taiwan and Linkoping University (LITH), Sweden. In October 2005, she received the degree of Master of Science in the master's program in "Material Physics and Nanotechnology", with research project entitled: "Layer-by-Layer Assembly of Gold Nanoparticles on Silicon Substrates" under the supervision of Professor Bo. Liedberg. From February 2006, she was a PhD candidate under the supervision of Prof. David N. Reinhoudt, Prof. Jurriaan Huskens, and Dr. Aldrik. Velders, in the Supramolecular Chemistry and Technology (SMCT) and Molecular Nanofabrication (MNF) groups at the University of Twente, the Netherlands, on the project of molecular assembly at interfaces. The results of her research are described in this thesis.